

# Design of a Bio-Impedance Analyzer and Tissue Phantom for Prevention of Pressure Ulcers

A Major Qualifying Project proposal to be submitted to the faculty of Worcester Polytechnic  
Institute in partial fulfillment of the requirements for the Degree of Bachelor of Science

By:

Sanjay Batchu

---

*Sanjay Batchu*

Konstantinos Tako

---

*Konstantinos Tako*

Submitted to:

---

Professor Yitzhak Mendelson, Advisor, Biomedical Engineering

# Table of Contents

Abstract .....	1
Authorship .....	2
Acknowledgements .....	3
Executive Summary .....	4
1 Introduction .....	6
1.1 Pressure Ulcer Problem .....	6
2 Literature Review .....	8
2.1 Pressure Ulcers .....	8
2.1.1 Formation of Pressure Ulcers .....	8
2.1.2 Promoting Factors of Pressure Ulcers .....	10
2.1.3 Areas at High Risk of Developing Pressure Ulcers .....	10
2.1.4 Stages of Pressure Ulcer Progression .....	11
2.1.5 Current Pressure Ulcer Management Techniques .....	14
2.2 Status of Pressure Ulcer Prevention Devices .....	15
2.2.1 Current Products on the Marketplace .....	15
2.2.2 Pressure Ulcer Prevention Methods in Development .....	18
2.2.3 Bioimpedance .....	19
3 Project Approach .....	22
3.1 Initial Client Statement .....	22
3.2 Technical Design Requirements .....	22
3.3 Revised Client Statement .....	23
3.4 Management Process .....	23
4 Existing Bioimpedance Analyzer .....	25
4.1 Operation of the Existing Bioimpedance Device .....	25
4.2 Safety of the Device .....	27
5 Design Modifications of the Existing Bioimpedance Analyzer and Validation .....	28
5.1 Design Improvements .....	28
5.1.1 Impedance Measurement Capabilities .....	28
5.1.2 Noise Reduction .....	30
5.1.3 Automatic Switching of Modes .....	31

5.2	Final Design Validation .....	32
5.2.1	Testing using Resistors .....	32
5.2.2	Testing using Resistors and Capacitors.....	32
5.2.3	Testing using the simplified Hayden Model .....	33
5.2.4	Systematic Error Investigation.....	35
5.2.5	Testing Results using Resistors.....	35
5.2.6	Testing Results using Resistors and Capacitors.....	37
5.2.7	Testing Results using the simplified Hayden Model .....	38
5.2.8	Results of Systematic Error Investigation.....	40
5.2.9	Statistical Significance Analysis .....	43
5.2.10	Summary of Testing Results .....	45
5.2.11	Limitations of Testing using Electrical Components.....	46
6	Tissue Phantom Selection .....	47
6.1	Analysis of Wants and Needs .....	47
6.2	Methods for Preliminary Material Testing.....	49
6.2.1	Preliminary Impedance Testing of Phantom Materials.....	51
6.2.2	Current Depth Testing.....	53
6.2.3	Electrode Spacing and Type Test.....	54
6.2.4	Human Impedance Data Collection .....	55
6.3	Preliminary Results of Impedance Testing .....	56
6.3.1	Qualitative Analysis of Preliminary Impedance Testing Results.....	56
6.3.2	Quantitative Analysis of Preliminary Impedance Testing Results.....	57
6.3.3	Results of Electrode Spacing Testing .....	64
7	Experimental Design – Post Material Selection.....	65
7.1	Pressure Ulcer Simulation.....	65
7.1.1	Saline Sensitivity Test.....	66
7.1.2	Potato Tissue Moisture Drying Test .....	66
7.2	Results of Pressure Ulcer Simulation Testing.....	67
7.2.1	Results of Saline Sensitivity Testing.....	67
7.2.2	Results of Potato Tissue Drying Experiment .....	69
7.3	Ethical Concerns, Health and Safety Issues .....	74
7.4	Manufacturability, Sustainability, and Environmental Impact .....	74
7.5	Societal and Political Impacts .....	74

8	Conclusions and Recommendations .....	75
	References.....	76
	Appendices.....	A-1
	Appendix A: Preliminary Impedance Testing Data.....	A-1
	Potato Impedance Data .....	A-4
	Cucumber Data .....	A-5
	Appendix B: Post-Material Selection Experiments .....	B-1
	Pressure Ulcer Simulation Experiment.....	B-1
	Appendix C: Potato Drying Experiment.....	C-1
	Potato Sample I.....	C-1
	Potato Sample II.....	C-5
	Potato Sample III .....	C-9
	Appendix D: MATLAB Code .....	D-1
	MATLAB code to load data.....	D-1
	MATLAB code to plot Bioimpedance Device data.....	D-3
	MATLAB code to plot Keysight Impedance Analyzer data.....	D-12
	Appendix E: Arduino Code.....	E-1
	Arduino Code for one mode programming.....	E-1
	Arduino Code for Automatic Switching of Modes .....	E-8

# List of Figures

Figure 1: Common body positions that are at high risk for pressure ulcer development .....	11
Figure 2: Stage I Pressure Ulcer [6].....	11
Figure 3: Stage II Pressure Ulcer [6]. .....	12
Figure 4: Stage III Pressure Ulcer [6].....	12
Figure 5: Stage IV Pressure Ulcer [6].....	13
Figure 6: Unstageable Pressure Ulcer [6]. .....	14
Figure 7: Deep Tissue Injury [6].....	14
Figure 8: The WellSense M.A.P System [8].....	16
Figure 9: The Leaf Healthcare Patch [10]/. ....	17
Figure 10: Difference in tissue strain amongst healthy and unhealthy tissue as shown in figures C and D [11] .....	18
Figure 11: Current propagation through cells according to frequency [16] .....	20
Figure 12: Simplified Hayden Model [21].....	20
Figure 13: Project Approach Diagram.....	24
Figure 14: Electrical Circuit Diagram of the Existing Bioimpedance Device.....	25
Figure 15: High frequency noise present in low amplitude sinusoidal signal .....	30
Figure 16: Signal without noise .....	30
Figure 17: Inverting amplifier with switches to control gain .....	31
Figure 18: Resistor and Capacitor in parallel configuration.....	32
Figure 19: Impedance measurement error using a 249.5k $\Omega$ resistor .....	36
Figure 20: Phase angle measurement error using a 249.5k $\Omega$ resistor.....	36
Figure 21: Impedance and phase angle of both theoretical calculations and bioimpedance device measurements using 100k $\Omega$ resistor and 100pF capacitor in parallel .....	37
Figure 22: Impedance and phase angle measurement error using 100k $\Omega$ resistor and 100pF capacitor in parallel.....	38
Figure 23: Impedance and phase angle of both theoretical calculations and bioimpedance device measurements.....	39
Figure 24: Percent Impedance Measurement Error .....	39
Figure 25: Phase angle measurement error.....	40
Figure 26: Impedance error using the AD5933 only to measure a 1.8k $\Omega$ resistor .....	40
Figure 27: Phase angle error using the AD5933 only to measure a 1.8k $\Omega$ resistor.....	41
Figure 28: Impedance error using the AD5933 and the inverting amplifier to measure a 1.8k $\Omega$ resistor.....	41
Figure 29: Phase angle error using the AD5933 and the inverting amplifier to measure a 1.8k $\Omega$ resistor.....	42
Figure 30: Impedance error using the AD5933, the inverting amplifier and the TIA to measure a 1.8k $\Omega$ resistor.....	42

Figure 31: Phase angle error using the AD5933, the inverting amplifier and the TIA to measure a 1.8k $\Omega$ resistor.....	43
Figure 32: Setup for the Preliminary Impedance Measurement Test .....	52
Figure 33: Bologna Current Depth Test Diagram.....	54
Figure 34: Diagram of electrode spacing testing .....	55
Figure 35: Setup Used for Gathering Human Impedance Data .....	56
Figure 36: Impedance of cucumber .....	58
Figure 37: Phase Angle of Cucumber.....	58
Figure 38: Impedance of apple .....	59
Figure 39: Phase Angle of Apples .....	60
Figure 40: Impedance measurement of potato.....	61
Figure 41: Phase Angle of Potato .....	61
Figure 42: Human forearm skin and modified potato impedances for RMS calculation .....	63
Figure 43: Impedance measurements for different electrode separation distances (2cm to 10cm) .....	64
Figure 44: Setup for the pressure ulcer simulation experiment .....	66
Figure 45: Impedances in a simulated pressure ulcer potato .....	67
Figure 46: Impedance measurements of potato at 3cm and 5 cm (solid lines and dashed lines respectively).....	68
Figure 47: Impedance measurements of potato at saline increments of 0.05mL.....	68
Figure 48: Impedance measurements of potato at different times of drying naturally .....	69
Figure 49: Impedance measurements of potato at different times of drying under hottest level..	70
Figure A-1: Apple Impedance Graph from 5 kHz to 100 kHz at 3CM Separation Distance	A-1
Figure A-2: Apple Impedance Graph from 5 kHz to 100 kHz at 5CM Separation Distance	A-2
Figure A-3: Impedance of Peeled Apple at 3CM Electrode Separation	A-3
Figure A-4: Impedance of Peeled Apple at 5CM Electrode Separation	A-3
Figure A-5: Impedance of Potato at 5cm Separation Distance	A-4
Figure A-6: Impedance of Peeled Potato at 3cm Separation Distance	A-4
Figure A-7: Impedance of Peeled Potato at 5cm Separation Distance	A-5
Figure A-8: Impedance of Cucumber at 3cm Separation Distance	A-5
Figure A-9: Impedance of Cucumber at 5cm Separation Distance	A-6
Figure A-10: Impedance of Peeled Cucumber at 3cm Separation Distance	A-6
Figure A-11: Impedance of Peeled Cucumber at 5cm Separation Distance	A-7

Figure B-1: Progression from Control to Stage I Pressure Ulcer Simulation in Potato I	B-1
Figure B-2: Progression from Stage I to Stage II Pressure Ulcer Simulation in Potato I	B-2
Figure B-3: Progression from Stage III to Stage III Pressure Ulcer Simulation in Potato I	B-3
Figure B-4: Progression from Stage III to Stage IV Pressure Ulcer Simulation in Potato I	B-4
Figure B-5: Progression from Control to Stage I Pressure Ulcer Simulation in Potato Sample II	B-5
Figure B-6: Progression from Stage I to Stage II Pressure Ulcer Simulation in Potato Sample II	B-6
Figure B-7: Progression from Stage II to Stage III Pressure Ulcer Simulation in Potato Sample II	B-7
Figure B-8: Progression from Stage III to Stage IV Pressure Ulcer Simulation in Potato Sample II	B-8
Figure C-1: Control Measurement of Potato Drying Sample I	C-1
Figure C-2: Lowest Heat Setting for Potato I	C-2
Figure C-3: Medium Heat Setting for Potato I	C-3
Figure C-4: High Heat Setting for Potato I	C-4
Figure C-5: Control Measurement of Potato Drying Sample II	C-5
Figure C-6: Low Heat Setting for Potato II	C-6
Figure C-7: Medium Heat Setting for Potato II	C-7
Figure C-8: High Heat Setting for Potato II	C-8
Figure C-9: Control Measurement of Potato Drying Sample III	C-9
Figure C-10: Low Heat Setting for Potato III	C-10
Figure C-11: Medium Heat Setting for Potato III	C-11
Figure C-12: High Heat Setting for Potato III	C-12

# List of Tables

Table 1: Impedance measurement range for the initial design.	27
Table 2: Impedance measurement range for the final design.	29
Table 3: Mean and Coefficient of Variation (CV) of measurements using a 249.5k $\Omega$ resistor at selected frequencies.	44
Table 4: Mean and Coefficient of Variation (CV) of measurements using 100k $\Omega$ resistor and 100pF capacitor in parallel at selected frequencies.	44
Table 5: Mean and Coefficient of Variation (CV) of measurements using the simplified Hayden model at selected frequencies.	44
Table 6: Results for all the tests that were performed.	45
Table 7: Tissue Phantom Weighted Wants.	49
Table 8: Summary of Materials and Tests Performed.	50
Table 9: Parameters for the E4990A Impedance Analyzer.	52
Table 10: Results of Preliminary Impedance Test.	57
Table 11: Statistical Analysis of Cucumber Samples.	59
Table 12: Statistical Analysis of Apple Impedance Measurements.	60
Table 13: Statistical Analysis of Potato Impedance Measurements.	62
Table 14: Root Mean Squared Error of tissue phantom impedances and human impedances.	63
Table 15: Average and Coefficient of Variance (CV) for Control Group.	70
Table 16: Average and Coefficient of Variance (CV) for Highest Heat Level Group.	71
Table 17: The Weight Loss of Each Potato and the Average in the Control Group.	72
Table 18: The Weight Loss of Each Potato Sample and the Average in the Highest Heat Group.	73

# List of Abbreviations

CV	Coefficient of Variation
FDA	Food and Drug Administration
M.A.P.	Monitor Alert Protect
MQP	Major Qualifying Project
SEM	Sub Epidermal Moisture
TIA	Transimpedance Amplifier
WPI	Worcester Polytechnic Institute

# **Abstract**

There is a significant need for a device that can detect the early presence of pressure ulcers in order to reduce the costs and time spent on taking care of patients that are at high risk for pressure ulcer development. This MQP describes a pressure ulcer detection device that is based on the use of bioimpedance. In order to test the efficacy of the device, a tissue phantom material was needed to reduce testing costs and optimize specific device parameters. In order to accomplish this task different potential phantom materials were investigated and tested to determine which specific material would be able to replicate the electrical response of human skin across a wide range of frequencies. Potatoes were able to replicate a similar bioimpedance response to that of humans and were modified to simulate a pressure ulcer.

# Authorship

Chapter 1 .....	Sanjay Batchu
Chapter 2 .....	All
Chapter 3 .....	Sanjay Batchu
Chapter 4 .....	Konstantinos Tako
Chapter 5 .....	Konstantinos Tako
Chapter 6 .....	All
Chapter 7 .....	Sanjay Batchu
Chapter 8.....	Konstantinos Tako

# Acknowledgements

This project would not be possible without the guidance of all the people who have helped us during the entire academic year. We would like to thank our advisor, Professor Yitzhak Mendelson, PhD for his constructive comments and feedback throughout the entire MQP process. We would also like to thank our advisor, Professor John McNeill, PhD for giving us guidance on the development of the bioimpedance device. We would also like to extend our gratitude to Joshua Harvey who played a significant role in our progress throughout the entire year and helped us understand the major electrical components of this project and we would like to extend our gratitude for his help. We would also like to thank Dr. Raymond Dunn, MD and the entire team in the plastic surgery department at UMASS for giving us significant insight on the clinical problems of pressure ulcers.

# Executive Summary

Pressure ulcers are localized injuries to tissues that occur in patients with limited mobility and usually occur in hospital settings. These injuries usually develop in areas of the body that are close to bony prominences as a result of prolonged pressure on certain areas of the body. The prolonged pressure can lead to a compression of blood vessels and thus restrict blood flow which deprives the affected area of oxygen and nutrients which causes cell death. Approximately 1 million patients are diagnosed with pressure ulcers annually thus there is a significant need for a device for early detection and prevention of pressure ulcers.

Due to the fact that late stages of pressure ulcers can cost hospitals over 100 thousand dollars, hospitals have maintained some practices such as moving patients into different positions every 2 hours which is very time consuming and inefficient. In addition to moving patients, hospitals use different scales such as the Braden scale which aim to classify ulcers once they are present on the body in order to prioritize the hospital's response. However, these scales may be inaccurate for certain patients if they have darker pigmentation which can obscure some of the visual cues associated with pressure ulcers such as redness or inflammation. In addition, to these processes there are new products on the market that aim to improve the compliance of patient turning, but do not address the problem of continuous monitoring of patients for pressure ulcer risk factors.

In order to address the problems with current hospital practices and current products on the market, the team used bioimpedance as a measuring tool of water content underneath the skin. Prior research has shown that this can be used as a tool to detect areas of the body where pressure ulcers may form. Since, a pre-existing bioimpedance analyzer was designed by Joshua Harvey, a PhD student, the purpose of the MQP was to improve the design and accuracy of the pre-existing bioimpedance analyzer and also select an appropriate material that could be used as a tissue phantom which can aid in the testing and optimization of the bioimpedance analyzer.

In order to address the selection process of the tissue phantom material, the team decided to focus on materials that have analogous electrical properties to human tissue and are structurally stable so that electrodes and other recording devices can be supported. The group conducted a literature review on tissue phantoms and chose materials that have been used in prior impedance studies or have a history of use in medical device testing. After a list of materials to be tested was

selected the materials were tested using an impedance analyzer across a wide frequency range spanning 5 kHz to 100 kHz in order to examine if their impedance response would be analogous to human tissues. Once a preliminary test was conducted, the materials were qualitatively and quantitatively analyzed via MATLAB to see which one had the closest response to that of humans.

Potatoes were found to have an impedance response most similar to that of humans and further testing was conducted to determine whether they could be used to simulate pressure ulcer conditions. In addition, further testing was conducted to measure key characteristics of the existing impedance analyzer such as its ability to detect changes in fluid levels. Finally, a test was conducted on potato tissue to study its impedance response across a range of moisture levels and temperature range to examine whether the potato could properly simulate the physiological process of pressure ulcers in humans.

After conducting tests on a potato, it was deemed that it would serve as an adequate tissue ulcer phantom for the testing and optimization of the existing bioimpedance analyzer. In addition, it was also found that the potato could simulate the physiological conditions that occur during a pressure ulcer in humans. Therefore, it was concluded that potatoes can be used as tissue phantoms for human skin and provided insight on how water content affects the impedance measurements on human skin.

# 1 Introduction

The purpose of this chapter is to introduce the pressure ulcer problem as well as the overall purpose of this Major Qualifying Project.

## 1.1 *Pressure Ulcer Problem*

Pressure ulcers are localized injuries to skin and underlying tissue that form due to bony prominences in the body pressing against the skin. During a pressure ulcer, tissue necrosis occurs due to lack of oxygen and nutrients in the area as a result of restricted blood flow which consequently leads to open sores. These open sores can become infected and if not treated, lead to death. In the United States, 2.5 million people develop pressure related injuries annually, and over 60,000 of these occurrences relate in death of the patient.[1] In addition to leading to death, pressure ulcers cost the average patient \$150,000 if the condition is not treated early and cost the overall health care system \$11 Billion annually.[1] With the severity of patient deaths and costs to the healthcare system there is an imminent need to discover a new system that prevents pressure ulcers and the resulting conditions associated with them.

Hospitals today are aware of the problems associated with pressure ulcers and have instigated certain prevention practices to avoid the occurrence of pressure ulcers. The current established practice involves a nurse physically repositioning the patient every two hours in order to relieve pressure from key areas of the body that are prone to pressure ulcers.[2] However, this process is very time consuming and cumbersome thus reducing its efficacy in protecting at-risk patients from developing pressure ulcers. Hospitals are also using different grading scales and guidelines that have been developed over the years to identify high risk patients for pressure ulcer development and to assess the severity of a pressure injury. However, the main problem with these scales is that they are not accurate in patients with darker skin tones as early pressure ulcer signs such as redness may not be immediately visible.

In order to alleviate the problems associated with the current medical practices, various companies have developed medical devices that aim to either detect or prevent pressure ulcers. These devices range from handheld scanners to full bed pressure relief systems that incorporate air cushions and pumps to alleviate pressure to affected or high-risk areas of the body. Handheld scanners, although useful, still rely on nursing staff going through patients to take measurements without alerting when a pressure ulcer is forming. In contrast, while full bed systems enable remote

monitoring and pressure mapping, they are extremely expensive and are neither available nor affordable to everyone.

This project aimed in the development of a low cost, wearable device that is capable of detecting pressure ulcers at an early stage of their formation. This way nursing staff can be alerted and preventative measures can be utilized early in the formation of a pressure injury while at the same time reducing the time that is spent by turning over patients that are not at risk of a pressure injury. Additionally, this project aimed in the selection of a medium that had similar electrical impedance characteristics to human skin and which would be modified to simulate the formation of a pressure ulcer.

## 2 Literature Review

### 2.1 *Pressure Ulcers*

Pressure ulcers also known as bedsores or decubitus ulcers, occur as a result of localized damage to the skin and subcutaneous tissue as a result of prolonged pressure over bony areas of the body. In addition to pressure, shear forces and friction forces on weakened skin can also cause pressure ulcers to form on a patient's skin.

Pressure ulcers are a significant problem in the healthcare industry and negatively affect both patients and caregivers on a global scale. In recent years, it has been found that up to 15% of acute patients develop pressure ulcers during their stay at hospitals. In addition, the incidence rate for pressure ulcer development has increased by approximately 60% in the same time period. Along with the deep physiological pain experienced by bed-bound patients, who are most prone to this type of injury, there are steep financial costs associated with pressure ulcers. It is said that that a typical healthcare provider incurs an average cost of \$48,000 for a pressure ulcer occurrence which amounts to a national outlay of almost \$11 Billion [1]. Every year approximately 2.5 million patients obtain hospital acquired pressure ulcers which cause over 60,000 deaths per year. As pressure ulcers obtained in hospital cases are more severe they can cost the hospital upwards of \$150,000 per patient in addition to other legal settlement costs for malpractice cases [1]. As evidenced by the statistics shown above, pressure ulcers play a significant role in the increase in healthcare costs in the United States.

#### 2.1.1 *Formation of Pressure Ulcers*

The main cause for the formation of pressure ulcers is prolonged pressure between areas of the body close to bony prominences and an external surface such as a bed or wheelchair. The excessive pressure imposed on certain low-fat areas of the body such as the heels or behind the neck cause blood vessels in the area to become occluded and thus oxygen and nutrients to the cells are made unavailable causing cell death. If the pressure is sustained for a long period of time and left unchanged prolonged cell death will eventually lead to tissue necrosis, apoptosis and ulceration.

Necrosis is a form of cell injury which leads to premature cell death in living tissue and is caused by external factors to the cells, such as infection, toxins, or trauma. During necrosis, cell membrane integrity is lost and a release of products of cell death into the extracellular space is initiated which leads to an inflammatory response. During inflammation, leukocytes and nearby phagocytes are attracted in order to eliminate cell death by phagocytosis which however causes damage to healthy surrounding tissues due to microbial damaging substances that are released in the process. This inhibits the healing process which results in a build-up of dead tissue and cells which needs to be removed surgically, a procedure known as debridement [3].

In contrast to necrosis, apoptosis is a highly regulated process that can be initiated through one of two pathways, the intrinsic pathway and the extrinsic pathway. In the intrinsic pathway cells kill themselves after sensing cell stress which includes extremes of temperature, exposure to toxins, and mechanical damage. In the extrinsic pathway cells kill themselves as a response to signals that are released from other cells. Both pathways induce cell death and excessive apoptosis causes atrophy [4].

Although prolonged pressure is the primary cause of pressure ulcers, shear and friction forces also play a large role in pressure ulcer formation. Shear forces often occur as a result of friction and result in pressure ulcers due to the fact that the skin stays in place even when the body glides across a surface such as a bed. When the subcutaneous tissue underneath the skin remains in place, any movement of the outside will result in a differential movement of muscle tissue and blood vessels causing them to tear open and reduce blood flow which causes ischemia. In addition to shear forces, friction forces may exacerbate underlying pressure ulcer conditions due to the fact that they cause the stratum corneum of the patient to be lost. When this layer is lost, the resulting breach of the epidermis leads to infection of the site.

Finally, excessive moisture in patients from sweat, urine, and feces can induce pressure ulcers by macerating the surface of the skin. Weakened skin leads to blisters and skin breakdown over a period of time causing progression in ulcer severity. In addition, the excessive moisture will weaken the strength of the outermost skin layer and allows the patient to be more susceptible to damage from excess pressure, shear, and friction [5].

### ***2.1.2 Promoting Factors of Pressure Ulcers***

There are numerous factors that influence the formation of pressure ulcers in patients. Each patient is different but there are some essential risk factors that lead to pressure ulcer. Some of these risk factors include, impaired mobility, age, impaired neurological function, inadequate nutrition, anemia, and previous edemas.

Impaired mobility is a major risk in pressure ulcer development because the body usually moves into different positions at night to relieve pressure on any one area of the body. If this process is impaired in a paralyzed patient, the body will fail to move into different positions and the area will become ischemic due to a lack of oxygen and nutrients.

Patients who are of advanced age are usually more prone to pressure ulcers because their skin is weaker due to lack of collagen. In addition, these patients usually have fragile blood vessels and have low body fat content which both reduce the ability of the individual to reduce pressure.

The human body usually autonomously makes postural adjustments when in one specific position using feedback from the autonomous nervous system. If a patient is neurologically impaired and cannot feel pain, this feedback system is harmed and thus the patient may not change posture causing conditions for pressure ulcer formation.

In addition to neurological factors, nutrition can also play a role in increasing the risk of developing pressure ulcers. For example, patients who are lacking nitrogen face an increased risk of tissue damage and a delay in the healing process. Hemoglobin is used to indicate nutritional status and if one has poor quality hemoglobin tissue necrosis associated with extended pressure will be exacerbated as the blood will carry less oxygen.

Finally, patients with prior health issues such as edemas also face higher risk of developing pressure ulcers. The excess interstitial fluid associated with edemas presses against blood vessels and occludes blood flow which causes deoxygenation of tissue and results in ischemia.

### ***2.1.3 Areas at High Risk of Developing Pressure Ulcers***

When investigating the process by which pressure ulcers form, it is important to understand that certain areas of the body are more prone to pressure ulcers than others. The fundamental idea behind a pressure ulcer is that factors such as pressure, and shear forces cause blood flow to

become restricted due to damage of the capillaries. It is evident that areas of the body that are near bony prominences can reach localized pressures as high as 34 mm/Hg and cause capillary damage.

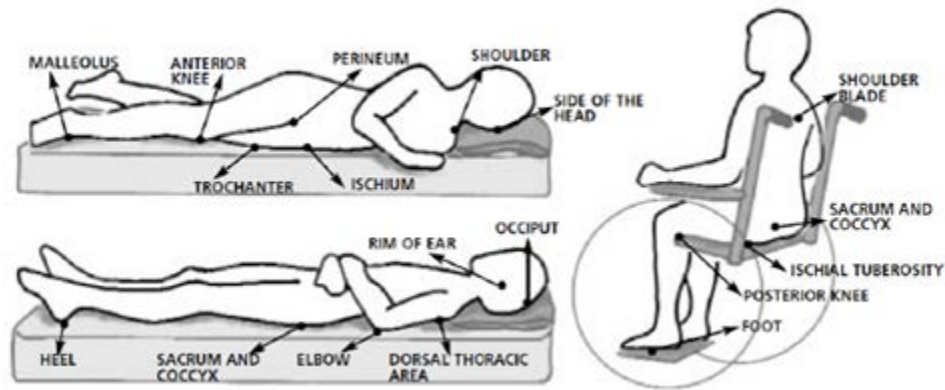


Figure 1: Common body positions that are at high risk for pressure ulcer development

#### 2.1.4 Stages of Pressure Ulcer Progression

Currently, pressure ulcers are mainly assessed visually and can be classified in six different stages. Stage I pressure ulcers, shown in Figure 2, are called Non-Blanchable Erythema and usually consist of skin that is intact but is not blanchable, and areas that can be softer or stiffer than the surrounding area [6].

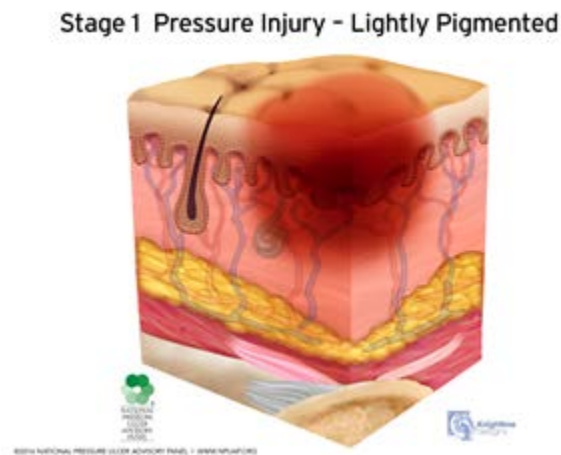
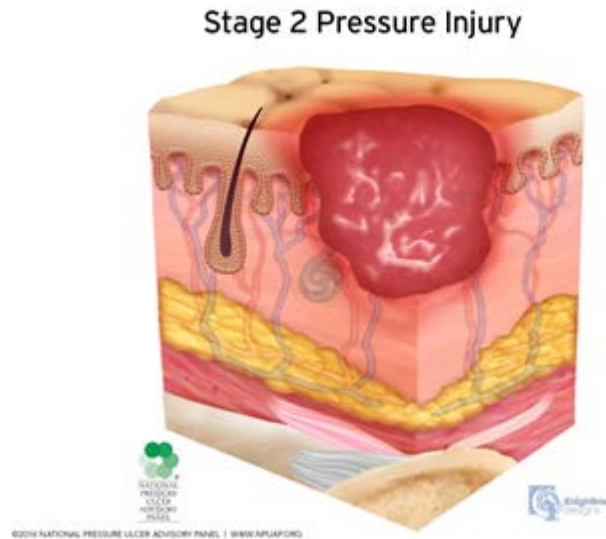


Figure 2: Stage I Pressure Ulcer [6].

If the pressure ulcer is not treated or progresses into a Stage II, as shown in Figure 3, partial loss of dermis occurs and a gap forms that can be potentially filled with some fluid which forms a blister. Usually Stage II ulcers can appear somewhat shiny without any bruising [6].



*Figure 3: Stage II Pressure Ulcer [6].*

Stage III and IV pressure ulcers are much more serious than the earlier stages and patients who experience these usually need long term care in order to recover. Stage III ulcers, shown in Figure 4, are extremely dangerous as there is full tissue loss and there is a possibility of seeing subcutaneous adipose tissue. In addition, there can be undermining and tunneling underneath the skin in these types of ulcers [6].

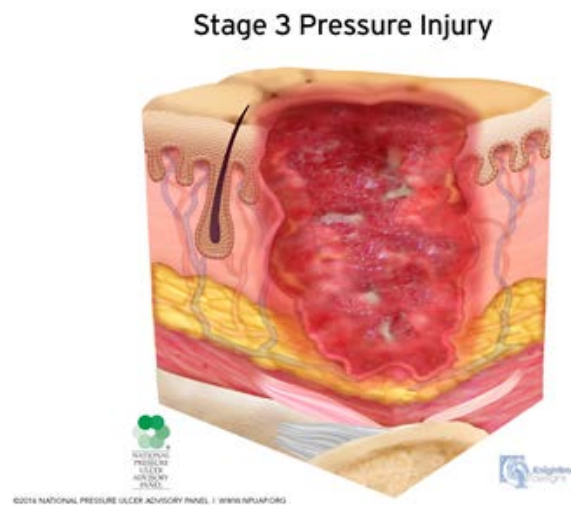


*Figure 4: Stage III Pressure Ulcer [6].*

Stage IV pressure ulcer, as shown in Figure 5, is the most serious stage for pressure ulcers and can lead to significant damage to the patient. In Stage IV, the ulcer has caused full tissue loss and the tendon or muscle are usually visible. In addition, Stage IV ulcers can extend deeper into muscles or tendons while presenting ischemic tissue called eschar, which is dead tissue emitted from the skin [6].

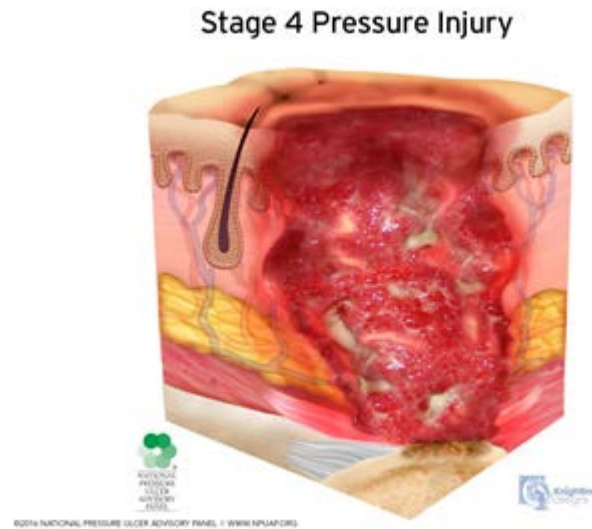


*Figure 5: Stage IV Pressure Ulcer [6].*

Besides the four main stages, pressure ulcers can also be classified as Unstageable, shown in Figure 6, or as a Deep Tissue Injury (DTI) with unknown depth, shown in Figure 7. Unstageable pressure ulcers usually have full tissue loss but cannot be staged as the depth of the ulcer cannot be measured due to the excessive amount of dead tissue (slough or eschar). In contrast, a DTI has a thin covering of intact skin but can be colored extremely red or pink due to soft tissue damage underneath [6].

### Unstageable Pressure Injury - Slough and Eschar

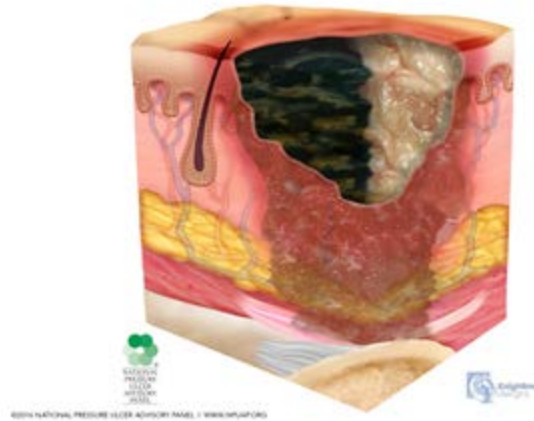


Figure 6: Unstageable Pressure Ulcer [6].

### Deep Tissue Pressure Injury

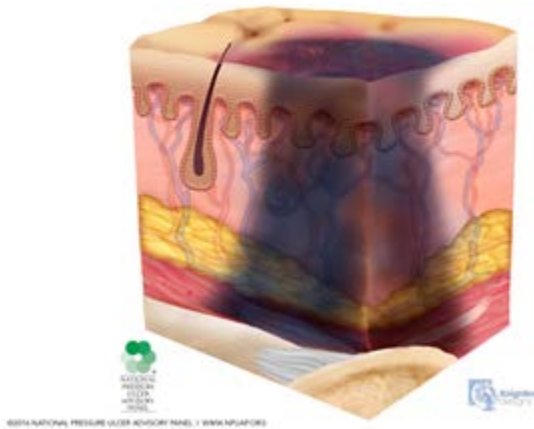


Figure 7: Deep Tissue Injury [6].

#### 2.1.5 Current Pressure Ulcer Management Techniques

Maintaining proper skin condition is essential to preventing the occurrence of pressure ulcers as skin that is too wet leads to increased maceration while skin that is too dry can rub against bed sheets or other surfaces and lead to more damage. In order to prevent such damage, caregivers use barrier ointments or pastes that can be used to protect the skin [2]. Immobilized patients may have incontinence which be a risk to pressure ulcer formation. In such cases, it is important to keep the area free of any urine or fecal matter as that may intensify the pressure ulcer [2].

Lastly, the best method that can be used to manage pressure ulcers is to offload as much pressure as possible from high risk areas of the body. The clinical standard to achieve this is to reduce the patient every two hours as well as use pillows to cushion risk prone areas [2]. By following these practices, it is possible for high risk patients to prevent pressure ulcers

## ***2.2 Status of Pressure Ulcer Prevention Devices***

Pressure ulcers are not a new problem in hospitals and health care facilities. Currently, there are some solutions on the market that have been created that attempt to solve the problem. There are some devices that are in use today to measure various parameters that can determine the occurrence of pressure ulcers, yet they all have some major limitations. The bigger systems include bed-based solutions that can be effective yet are extremely expensive and leave the patient constrained to a limited space. Other systems require user intervention and cannot be used autonomously which makes them more difficult for the nursing staff to use effectively. With these limitations, it is important to be able to create a device that is wearable, mobile, clinically effective and inexpensive. This device would immensely assist caregivers in preventing pressure ulcers by alerting them as early as possible.

### ***2.2.1 Current Products on the Marketplace***

There are three main devices that can be used to detect pressure ulcers before they become prevalent on the body. There is a device created by Well Sense which is called the M.A.P System with MAP being an acronym for Monitor, Alert, and Protect [7]. This system promises to create a pressure map of the body in relation to the body and shows areas of high pressure in color detail. However, there are some key issues with this system that can be improved such as the fact that the caregiver has to travel to the patient in order to see the visual pressure map. In addition, the system measures pressure relative to the bed so even though when a patient relocates an affected area, the system will show less pressure but there still might be pressure effects on the patient. Time is also an important determinant in the creation of pressure ulcers and this system cannot detect a time profile to areas of increased pressure. Finally, a system like this, is usually very expensive and still requires nursing staff to turn the patient as it is not able to detect pressure ulcers early but only acts as a compliance device. Costs for the WellSense system are not available publicly. However, similar systems that use air circulation to control the skin microclimate may cost upwards of

\$15,000 dollars which is not feasible for every patient in a healthcare setting. Figure 8 shows the WellSense M.A.P System.



*Figure 8: The WellSense M.A.P System [8].*

Another device that currently exists is the SEM, or Sub-Epidermal Moisture, Scanner by Bruin Biometrics which measures the subepidermal moisture of areas that are at risk for developing pressure ulcers. The system consists of a handheld device that is comprised of two electrodes which determines the impedance of skin as current is passed between the two electrodes. [9]. This device allows for the detection of pressure ulcers in situations where visual assessments could not, as SEM values are claimed to be a good non-visual metric to measure conditions that may lead to pressure ulcers. However, there are some limitations to this device as it needs to be placed on the suspected area by a caregiver. In addition, in its current state the device has some variability in results based on the training of the person using the device as different levels of force applied when taking a measurement affect the SEM result.

After examining both mat-based and SEM based systems it is evident that there has been progress made in the detection of pressure ulcers, yet there is a need to design a device that can wirelessly transmit data to a central location and can detect pressure ulcers using some of the factors mentioned previously.

Finally, there is a patch based system developed by Leaf Healthcare that consists of an accelerometer encased in a wearable patch that is placed on a patient in order to measure motion [24]. The purpose of this patch, shown in Figure 9, is to use the tracked motion data and alert the central nursing patient the last time the patient has been turned which ended up resulting in increased compliance of the most common pressure ulcer prevention method which is the repositioning of patients at risk of pressure ulcers every two hours. Leaf Healthcare states that this device has reduced the incidence rate of hospital acquired pressure ulcers by 85 percent and has improved the rate at which patients are repositioned on time to almost 98 percent. Although these figures are excellent news in the pressure ulcer community, the Leaf Healthcare patch does not measure the main instigator of pressure ulcers which is prolonged pressure but rather simply measures compliance to the nursing staff.



*Figure 9: The Leaf Healthcare Patch [10]/.*

Although the SEM scanner, M.A.P system and Leaf Healthcare patch all aim to prevent pressure ulcers, there is still a need for an inexpensive pressure ulcer prevention device that can provide continuous monitoring, and diagnose pressure ulcers early in their formation so that they can be treated more effectively.

### 2.2.2 Pressure Ulcer Prevention Methods in Development

Due to the financial implications of pressure ulcers on the overall health system, there is still a systemic need for a device or methodology that can detect the presence of pressure ulcers before they present with symptoms. There are three main methods currently being pursued that show some promise in pressure ulcer prevention. These methods include A-Mode Ultrasound Elastography, optical sensors to detect blood flow, and bioimpedance.

Ultrasound Elastography is an imaging technique that provides local information on the mechanical properties of biological tissues that indicate the presence of a pathological area where tissues have changed their physical properties before and after pressure has been applied. Simulations have shown that a pressure ulcer can theoretically be detected at a very early stage with ultrasound elastography [12]. Even when the ulcer region is presenting very low stiffening, the corresponding elastogram is able to underline the pathological area. An elastogram can be created by using ultrasound to induce a shear force through a specific tissue which causes the tissue to move laterally. This movement can be detected via ultrasound and the stiffness of the tissue can be inferred by measuring how fast the tissue moves to certain lateral positions [13]. In a study recently conducted by a company called ScandiDos, the authors were able to show how tissue that was stiffer due to pressure had different strain properties than healthy tissues which are shown in Figure 10 [11].

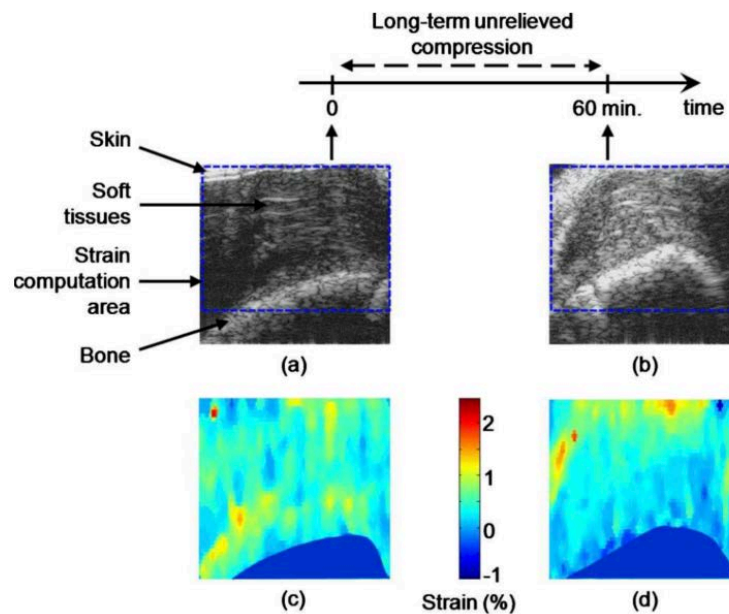


Figure 10: Difference in tissue strain amongst healthy and unhealthy tissue as shown in figures C and D [11]

In addition to measuring physical properties of tissue via ultrasound elastography, another method to detect pressure ulcers is with the use of optical sensors to detect blood flow. These sensors can use different methods of measurement that can either measure the physical speed of blood flowing throughout the body or the concentration of oxygen within the blood itself. Both of these methods can essentially show signs of tissue damage because if blood vessels are occluded due to excess pressure the speed of blood flow will decrease and the oxygen concentration of the tissue will also decrease as a result.

Laser Doppler flowmetry can be used to measure blood flow via the fact that the Doppler frequencies shift differently based on the light hitting blood cells and reflecting back towards the sensor (Moor Instruments). However, differences in blood flow are difficult to measure in areas prone to pressure ulcers such as the heel area, as there is a lack of blood flow [14].

Pulse oximetry relies on infrared and visible light and is based on the principle that the absorbance of red and infrared light varies upon proportion of oxygenated and deoxygenated hemoglobin present in the blood stream. Similarly, to Laser Doppler Flowmetry, this method is not suitable for areas susceptible to all areas at risk of pressure ulcers due to the fact that some areas lack of blood flow in these makes it hard to quantify the difference between oxygenated and deoxygenated hemoglobin and would lead to errors in the SpO<sub>2</sub> result [13].

### ***2.2.3 Bioimpedance***

In addition to the methods described above, bioimpedance is another method that can potentially be used for pressure ulcer detection. Bioimpedance is a measure of how well the body impedes electrical current flow when a potential difference is applied. The body usually has a high resistance to electric current when healthy due to the tough exterior of the stratum corneum. However, when cells die due to a lack of nutrients, their interior contents release into the interstitial fluid of tissue which lowers the impedance to electric current and that decrease can be detected using bioimpedance.

The impediment that the electric current faces when flowing through the skin consists of both resistive and reactive components. The presence of both resistive and reactive elements is referred to as impedance in electrical circuits. The main elements in the body that account for the resistance are both intracellular and extracellular fluids. The main element that accounts for the

reactance is the cellular membrane [15]. The physiological state of a cell, whether healthy or not, can be determined by observing the changes in the impedance. In addition to being able to detect pressure ulcer before presentable symptoms, a bioimpedance device can be made using simple components and can potentially be worn as a patch for patient convenience [14]

Figure 11 shows how the current flows in human tissue according to its frequency, which allows for penetration within the cells.

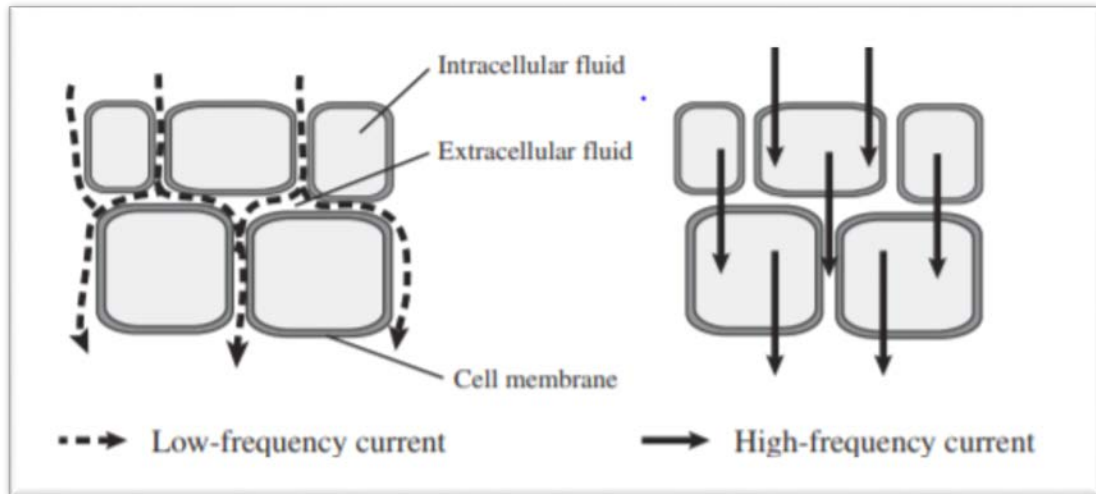


Figure 11: Current propagation through cells according to frequency [16]

The electrical impedance of the human skin has been modeled using electrical circuits. One of them is the simplified Hayden model which is shown in Figure 12 [21]. In this model, the impedance of the human skin is modeled with a resistor ( $R_{ext}$ ), which represents the extracellular fluid resistance, in series with another resistor ( $R_{in}$ ), which represents the intracellular fluid resistance, and a capacitor ( $C_m$ ) in parallel to  $R_{in}$ , which represents the capacitance of the cellular membrane.

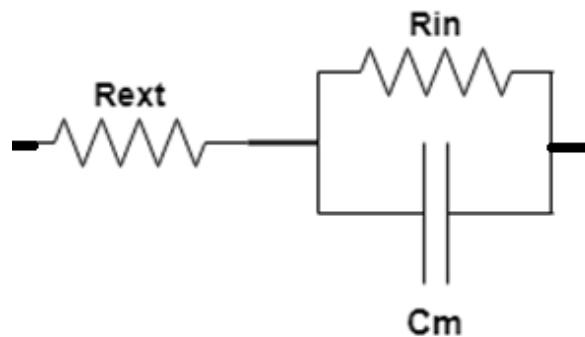


Figure 12: Simplified Hayden Model [21]

Bioimpedance has been used in the past for many applications including monitoring of respiration [22] and body fat composition [23]. Bioimpedance is most commonly measured using 2 or 4 electrodes in a bipolar or tetrapolar configuration respectively. The main difference between the two methods is that in the tetrapolar configuration 2 electrodes are responsible for injecting current and the other 2 electrodes are responsible for measuring voltage, which avoids the electrode polarization that is present in a bipolar configuration [16].

Bioimpedance has also been widely used to measure the physiological state of the cells in plants. More specifically, bioimpedance has been used to measure tissue damage in potatoes and the electric current has been shown to flow in a similar manner to human skin, as shown in Figure 11 [17].

## 3 Project Approach

The purpose of this chapter is to describe the strategy the team used to achieve all the objectives of the MQP. This section contains key information such as the initial and revised client statements, the design requirements, standards for the requirements, and the management style used to coordinate both group members.

### 3.1 *Initial Client Statement*

The initial client statement was to assist in the design of a wearable, low cost device for pressure ulcer detection. At the same time, a tissue phantom that can effectively be used as an *in vitro* model for the testing of the designed bioimpedance device should be developed.

### 3.2 *Technical Design Requirements*

Several design constraints and objectives were created from the initial design process and used to aid the design process. Regarding the development of the Bioimpedance Analyzer the design requirements were to be addressed by the research team at Professor Mendelson's laboratory. Both constraints and objectives are listed as follow for both aspects of the overall project.

#### **Bioimpedance Analyzer**

1. *Sensitivity*: The designed impedance analyzer needs to be able to detect small changes in fluid as changes in impedance.
2. *Accuracy*: The designed impedance analyzer should be able to measure complex impedance ( $Z$ ) with an error of less than 5 percent.
3. *Safety*: The impedance analyzer should be able to restrict the current injected to less than the FDA limit of  $200\mu\text{A}$  [18]
4. *Wearable*: The impedance analyzer should be small enough in dimensions that it can used as a wearable device.

### **Development of Tissue Phantom**

1. *Analogous Impedance*: The chosen tissue phantom should be able to show a similar impedance response to that of humans.
2. *Strength*: The tissue phantom should be able to have enough mechanical stability to hold electrodes in place when pressure is applied.

### **3.3 Revised Client Statement**

Assist in the design and development of a bioimpedance analyzer prototype and enhance its measurement range and accuracy. In addition, measure key parameters such as current depth, electrode type, and electrode separation distance. Finally, design a tissue phantom suitable for the *in vitro* modelling of human tissue in addition to being suitable as a platform for pressure ulcer simulation testing.

### **3.4 Management Process**

After understanding the project's intricate details, we broke the project into smaller tasks that would be easier to complete. The project was broken down into four main sections that are summarized in Figure 13.

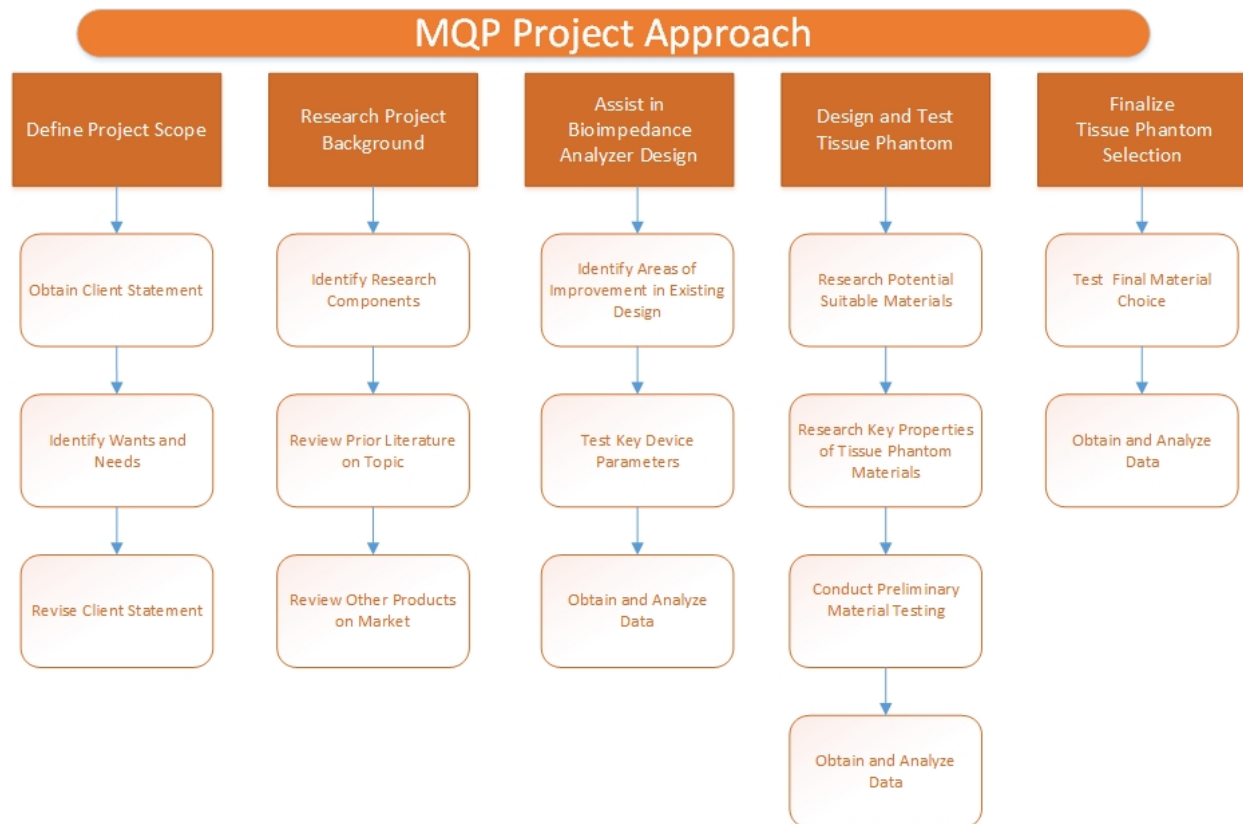


*Figure 13: Project Approach Diagram*

## 4 Existing Bioimpedance Analyzer

The purpose of this chapter is to describe the operation and limitations of the design of a bioimpedance device.

### 4.1 Operation of the Existing Bioimpedance Device

The electrical circuit of the bioimpedance device was designed the AD5933 Network Analyzer Chip by a graduate student in Professor Mendelson's lab. The electrical circuit shown in Figure 14 performs both real and imaginary impedance measurements by keeping a controlled voltage across the two electrodes.

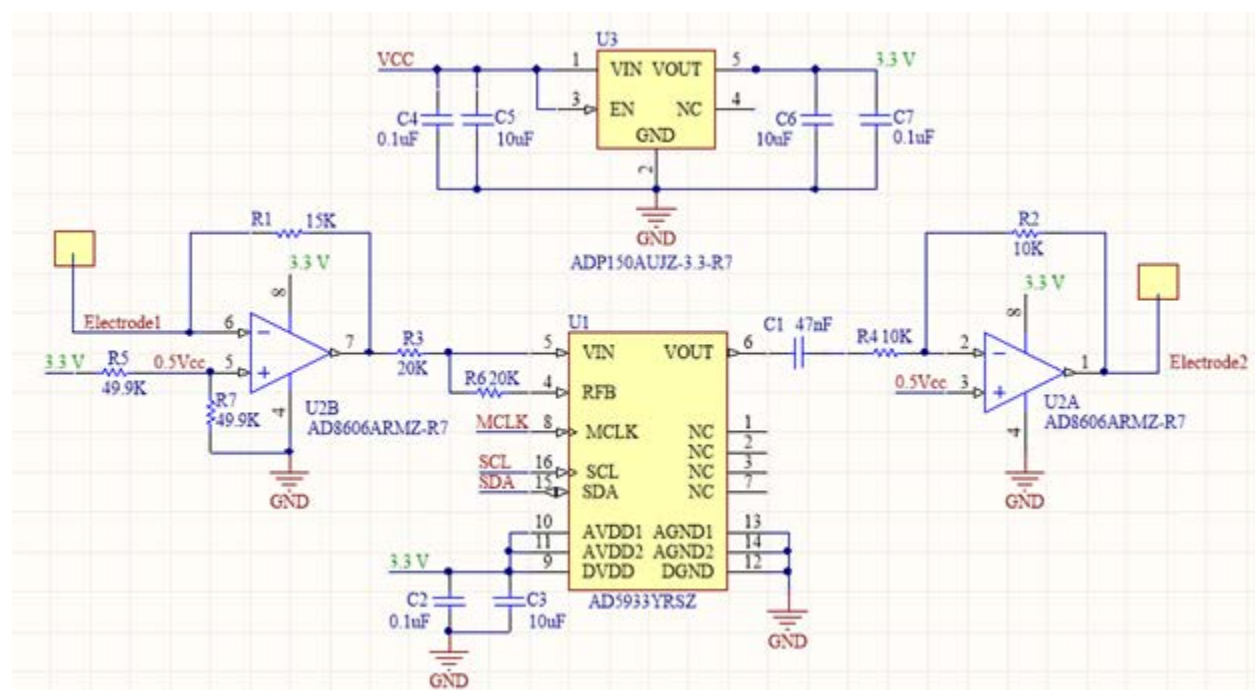


Figure 14: Electrical Circuit Diagram of the Existing Bioimpedance Device

The electrical circuit shown in Figure 14 consists of two parts. In the first part, at the VOUT of the AD5933 there are 4 programmable sinusoidal waveforms that can be generated (2V, 1V, 0.4V, and 0.2V peak to peak). Capacitor C1 was used to remove any unwanted DC voltage. An

inverting amplifier (U2A) with a DC Bias voltage of  $0.5V_{cc} = 1.65V$  was used to select the gain of the signal which appears as an output at electrode 2.

Electrode 1 was connected to the negative terminal of a transimpedance amplifier (U2B) with a gain of 15,000. The non-inverting terminal of the transimpedance amplifier was connected to  $0.5V_{cc} = 1.65V$  similarly to the inverting amplifier. As a result, no DC voltage is applied across the two electrodes but rather only the sinusoidal waveform generated by the AD5933. Due to the presence of a potential difference between the two electrodes a current is injected in the skin and passed through electrode 1 which is connected to the inverting terminal of the TIA. Since the current can only flow through R1 the TIA acts as a current to voltage converter with a gain of 15,000. A resistor, R3, in series with the output of the transimpedance amplifier was used to convert this voltage to current which was then passed to another (built in the AD5933) transimpedance amplifier with the resistor in the feedback loop, R6, being the same as the resistor that was connected in series with the output of the transimpedance amplifier. Inside the AD5933 the output voltage of the second transimpedance amplifier is gained, low pass filtered and passed to the ADC for impedance and phase angle measurements. Table 1 shows the impedance measurement capabilities of the AD5933 in the initial design of the Bioimpedance Analyzer.

The maximum and minimum impedances that the bioimpedance device can measure is limited by the ADC voltage. Table 1 was generated assuming that the ADC can take voltages from 0.05V to 2.9V without introducing too much error in the impedance measurement and using the following formulas. The lowest ADC voltage occurs with the highest impedance possible ( $Z_{max}$ ) and the lowest ADC voltage occurs with the lowest impedance possible ( $Z_{min}$ ).

$$I = \frac{V_{ADC}}{R1} \quad (1)$$

$$Z = \frac{V_{mode}}{I} \quad (2)$$

*and after substituting (1) into (2)*

$$Z = \frac{V_{mode}}{\frac{V_{ADC}}{R1}} \quad (3)$$

*where  $V_{ADC}$  is the ADC voltage,  $V_{mode}$  is the programmable peak to peak voltage, and  $R1$  is the feedback resistor of the TIA ( $15k\Omega$ ).*

Table 1: Impedance measurement range for the initial design.

Mode (V)	$Z_{MAX}$ (k $\Omega$ )	$Z_{MIN}$ (k $\Omega$ )
2	600	10.3
1	300	5.2
0.4	120	2.1
0.2	60	1.0

## 4.2 Safety of the Device

The main consideration for safety was the current that could be injected to the subject when applying a potential difference between the two electrodes. Since the skin impedance can drop as low as 100 $\Omega$  at high frequencies such as 100 kHz which was the highest frequency sinusoid that was generated by the AD5933, proper protection to avoid shocking had to be considered. To ensure that this device was safe to use the following three steps were taken:

- A 47nF capacitor (C1) was used to remove any unwanted DC bias voltage.
- The two amplifiers (TIA and inverting – U2B and U2A respectively) were offset by 0.5 V<sub>CC</sub> or 1.65V so that no DC voltage difference was applied to the electrodes which can potentially burn marks on the skin.
- The feedback resistor of the transimpedance amplifier (R1) was chosen to be 15k $\Omega$  so that in the worst-case scenario of a short circuit ( $Z= 0\Omega$ ) the current experienced by the subject is limited by the saturated transimpedance amplifier and is smaller than 200 $\mu$ A (3V/15k $\Omega$ ).

## 5 Design Modifications of the Existing Bioimpedance Analyzer and Validation

The purpose of this chapter is to describe the modifications and improvements that were made to the initial design of the bioimpedance by the graduate student in Prof. Mendelson's lab that led to the development of our final design and its validation.

### 5.1 Design Improvements

#### 5.1.1 Impedance Measurement Capabilities

Human skin impedances vary significantly over a frequency range of 5 kHz to 100 kHz. Human skin impedance is typically around 100k $\Omega$ -200k $\Omega$  for the lowest frequencies (5 kHz) and around 500 $\Omega$  for the highest frequencies (100kHz). Due to this fact in conjunction with the fact that the current flowing through  $Z_{\text{Unknown}}$  must be lower than 200 $\mu\text{A}$ , and the concern for the ADC voltage to not saturate it was necessary for some changes to be made in order to increase the impedance measurement capabilities of the device. In the topology of the initial design, and with limited electrical components available for changes due to their functionality, the most appropriate place for signal manipulation was chosen to be the resistor controlling the gain of the inverting amplifier, R2.

In order to measure larger skin impedances, the potential difference across the two electrodes was increased in order to increase the current that would be amplified by the transimpedance amplifier. When measuring larger impedances, the potential difference across the two electrodes in the original design would lead to smaller currents generated which would effectively lead to noise amplification by the transimpedance amplifier. A maximum output voltage of 3V at the inverting amplifier was used by amplifying the 2V peak to peak signal with a gain of 1.5 (R2=15k $\Omega$  and R4=10k $\Omega$ ) due to the instability that would occur if the V+ rail was approached at 3.3V.

On the other hand, in order to measure lower skin impedances, the potential difference across the two electrodes was decreased so that the current that would later be amplified by the transimpedance amplifier would be decreased. If the potential difference across the two electrodes was not stepped down it would lead to large currents being amplified which would saturate the ADC and lead to inaccurate impedance and phase angle measurements.

By altering the gain of the inverting amplifier to gains of greater than 1 for higher impedances and gains of smaller than 1 for smaller impedances, the voltage at electrode 2 was changed accordingly while the voltage at electrode 1 was kept constant due to the non-inverting input of the transimpedance amplifier which was biased at 0.5V<sub>cc</sub>. Therefore, the controlled change of the potential difference allowed for an expansion of the impedance measurement capabilities of the device by increasing the range.

The new maximum and minimum impedance measurement capabilities shown in Table 2 were calculated using the same formulas (Eq. 1, 2, 3) that are shown in section 4.2.

Table 2: Impedance measurement range for the final design.

Mode (V)	Z <sub>MAX</sub> (kΩ)	Z <sub>MIN</sub> (kΩ)
3	900	15.5
2	600	10.3
1	300	5.2
0.4	120	2.1
0.2	60	1.0
0.04	12	0.2

### 5.1.2 Noise Reduction

After the signal was stepped down to 40 mV peak to peak some high frequency noise was observed. The noise was measured at the output of the inverting amplifier (U2A to have a frequency of approximately 8 MHz and an amplitude 30 mV peak to peak voltage. 1.1 $\mu$ F bypass capacitors were used to remove the noise that was introduced to the AD5933 from the supply, which made the signal cleaner in all modes of operation. Figure 15 and Figure 16 show the noisy and cleaned up signal respectively.

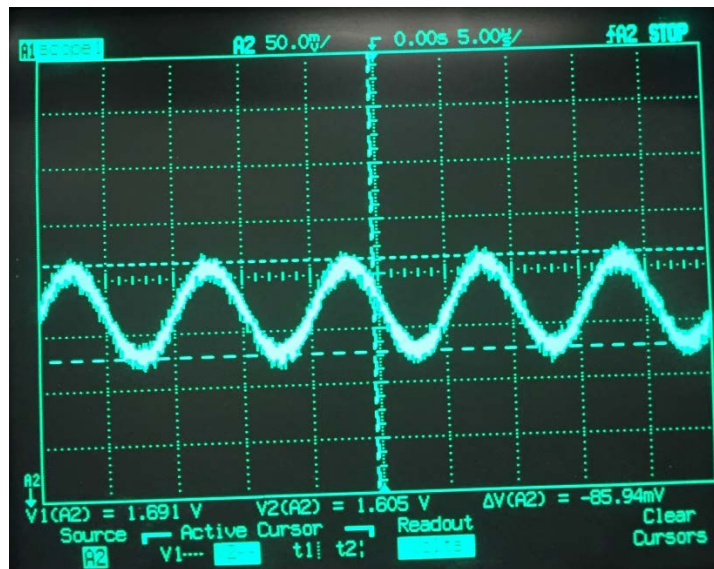


Figure 15: High frequency noise present in low amplitude sinusoidal signal



Figure 16: Signal without noise

### 5.1.3 Automatic Switching of Modes

The AD5933 was programmed in Arduino to change modes from 2V to 0.2V peak to peak output voltage according to the ADC voltages. During a frequency sweep, the varying  $Z_{\text{Unknown}}$  causes changes in the current flowing through it which consequently cause changes to the ADC voltages. By continuously checking the ADC voltages and monitoring the mode of operation, voltages at the extremities of the ADC range (higher than 2.9V and lower than 0.1V) were programmed to switch mode accordingly for a more accurate reading. Also, the gain of the inverting amplifier which controlled the 3V and 0.04V peak to peak signals was achieved using multiplexer switches whose logics were programmed in Arduino as well using analog outputs. The multiplexer switch that was used was the MAX4618 due to its very low on-resistance, 2V-5V operation, and its logic thresholds. Figure 17 shows the inverting amplifier with the switches to control the gain of the inverting amplifier. The Arduino code used for the operation of the AD5933 is included in Appendix E.

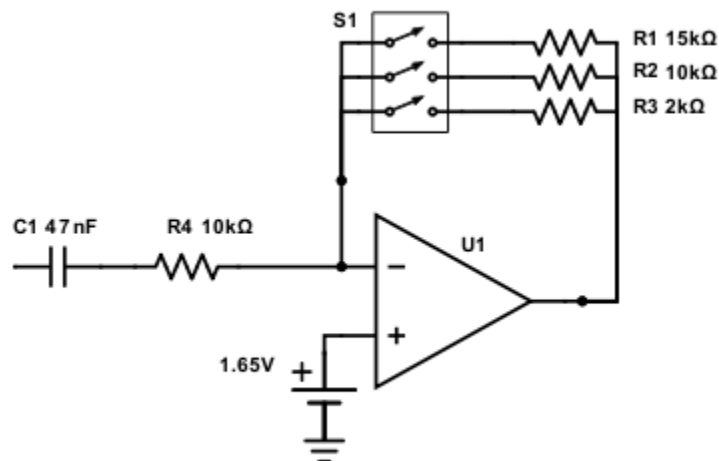


Figure 17: Inverting amplifier with switches to control gain

## 5.2 Final Design Validation

After finalizing the design modifications of the bioimpedance device, the accuracy of the device was investigated. The impedance measurement capabilities of the final design were examined using standard electrical components, such as resistors and capacitors, in various configurations.

### 5.2.1 Testing using Resistors

The impedance measurement capabilities of the final design of the bioimpedance device were investigated using resistors on each mode that the AD5933 operates. Theoretically, the impedance of resistors is the resistance value and the phase angle is 0, independent of the frequency.

The bioimpedance device was used to measure the impedance and phase angle of the resistors and the frequency sweeps were repeated 10 times to assess statistical significance.

### 5.2.2 Testing using Resistors and Capacitors

The impedance measurement capabilities were also investigated using a resistor in parallel with a capacitor on each mode that the AD5933 operates. Figure 18 shows the circuit that the typical circuit that was used in this section.

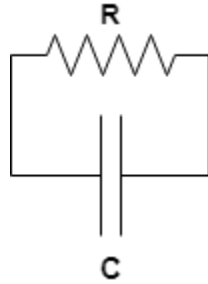


Figure 18: Resistor and Capacitor in parallel configuration

The theoretical impedance of the circuit was calculated using the formula below (Eq. 4).

$$\begin{aligned}\frac{1}{Z} &= \frac{1}{R} + j\omega C \\ \Rightarrow \frac{1}{Z} &= \frac{1}{R} + \frac{Rj\omega C}{R} \\ \Rightarrow Z &= \frac{R}{1 + Rj\omega C}\end{aligned}$$

$$\Rightarrow |Z| = \frac{1}{\sqrt{\frac{1}{R^2} + (\omega C)^2}}$$

and since  $\omega=2\pi f$

$$\Rightarrow \textit{Theoretical Impedance} = \frac{1}{\sqrt{\frac{1}{R^2} + (2\pi f * C)^2}} \quad (4)$$

The theoretical phase angle ( $\theta$ ) of the circuit was calculated using Eq. (5).

$$\begin{aligned} \theta &= \tan^{-1}\left(-\frac{\textit{Imaginary}}{\textit{Real}}\right) \\ &= \tan^{-1}\left(\frac{-\omega C}{\frac{1}{R}}\right) \\ \Rightarrow \theta &= \tan^{-1}\left(\frac{\frac{1}{R}}{\frac{1}{R}}\right) \\ &= \tan^{-1}(-\omega CR) \end{aligned}$$

and since  $\omega=2\pi f$

$$\Rightarrow \theta = \tan^{-1}(-2\pi fCR) \quad (5)$$

After the theoretical impedance and phase angle measurements were calculated, the percent error of all the measurements using the bioimpedance device was calculated using Eq. (6).

$$\% \textit{ error} = \frac{\textit{Measured} - \textit{Theoretical}}{\textit{Theoretical}} * 100 \quad (6)$$

### 5.2.3 Testing using the simplified Hayden Model

One of the most interesting configurations that was used to test the device was the simplified Hayden Model since it is representative of the human skin impedance [21]. In this

model, the opposition that the human body presents to a current when a voltage is applied is electrically modelled using two resistors and a capacitor, as shown in Figure 12.

To test for the accuracy of the device, we measured the average impedances and phase angles from 10 frequency sweeps. Also, the theoretical impedance the circuit was calculated using Eq. (7).

$$\text{Total Impedance} = R_{ext} + \text{Impedance of } R_{in} \text{ and } C_m \text{ in parallel} \quad (7)$$

After substituting (4) into (7), Eq. (7) becomes

$$\text{Theoretical Impedance} = R_{ext} + \frac{1}{\sqrt{\frac{1}{R_{in}^2} + (2\pi f * C_m)^2}} \quad (8)$$

The theoretical phase angle ( $\theta$ ) of the circuit was calculated using the Eq. (9).

$$\begin{aligned} \theta &= \tan^{-1} \left( -\frac{\text{Imaginary}}{\text{Real}} \right) \\ \Rightarrow \theta &= \tan^{-1} \left( \frac{-\frac{\omega C_m}{\left(\frac{1}{R_{in}}\right)^2 + (\omega C_m)^2}}{R_{ext} + \frac{1}{\left(\frac{1}{R_{in}}\right)^2 + (\omega C_m)^2}} \right) \\ \Rightarrow \theta &= \tan^{-1} \left( \frac{-\frac{\omega C_m}{\left(\frac{1}{R_{in}}\right)^2 + (\omega C_m)^2}}{R_{ext} * \left(\left(\frac{1}{R_{in}}\right)^2 + (\omega C_m)^2\right) + \frac{1}{R_{in}}} \right) \\ \Rightarrow \theta &= \tan^{-1} \left( -\frac{\omega C_m}{R_{ext} * \left(\left(\frac{1}{R_{in}}\right)^2 + (\omega C_m)^2\right) + \frac{1}{R_{in}}} \right) \end{aligned}$$

$$\Rightarrow \theta = \tan^{-1} \left( - \frac{2\pi f C m}{R_{ext} * \left( \left( \frac{1}{R_{in}} \right)^2 + (2\pi f C m)^2 \right) + \frac{1}{R_{in}}} \right) \quad (9)$$

After the theoretical impedances and phase angles were calculated, the percent error of all the measurements was calculated using Eq. (6). Lastly, the graphs were generated using MATLAB.

#### 5.2.4 Systematic Error Investigation

The AD5933 Network Analyzer Chip is capable of making impedance measurements without the need of additional circuitry. However, since the bioimpedance device is intended to be used in healthcare, the additional circuitry is important to ensure safety with controlled currents injected to the body and without DC voltages applied across the electrodes.

In the characterization of the device it was important to understand the errors that each component added to the impedance and phase angle measurements. The main potential sources of error were the two operational amplifiers. For this reason, the measuring capabilities of the circuit and the errors associated with each component were investigated by measuring the same resistor in 3 different cases. In the first case, the resistor was measured using the AD5933 alone. In the second case, the resistor was measured using the AD5933 and the inverting amplifier. In the third case, the resistor was measured using the AD5933, the inverting amplifier, and the transimpedance amplifier.

Since this investigation attempted to characterize the systematic error of the circuit the AD5933 was programmed to the 200mV peak-to-peak output voltage mode. The resistor that was used was a 1.8kΩ resistor to ensure that the ADC voltage was at the middle of its range.

#### 5.2.5 Testing Results using Resistors

The impedance measurement error was calculated for a 249.5kΩ resistor. Figure 19 and Figure 20 show the percent error of impedance and phase angle measurements respectively over the entire frequency range when the AD5933 was programmed to the 2V peak-to-peak voltage.

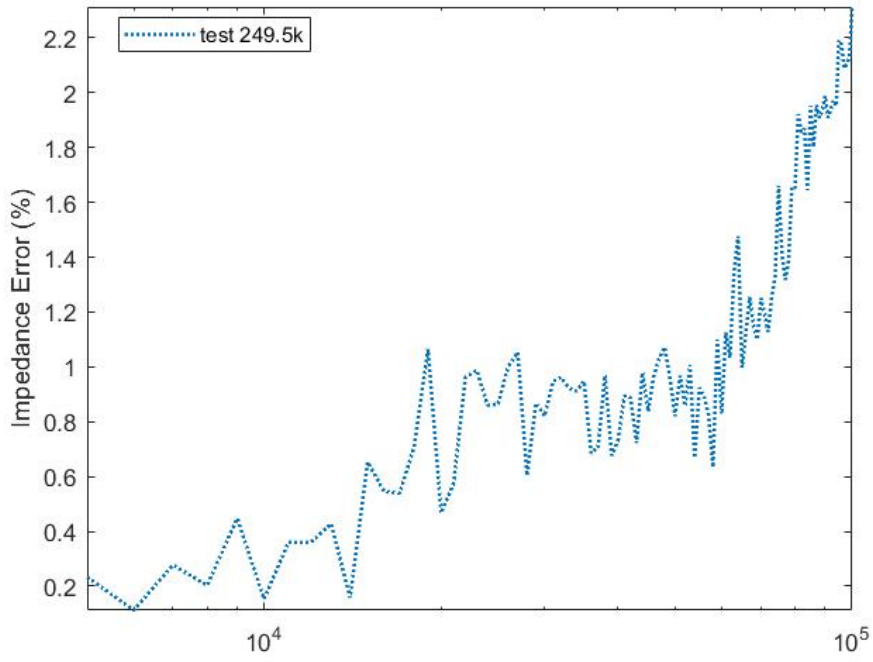


Figure 19: Impedance measurement error using a 249.5k $\Omega$  resistor

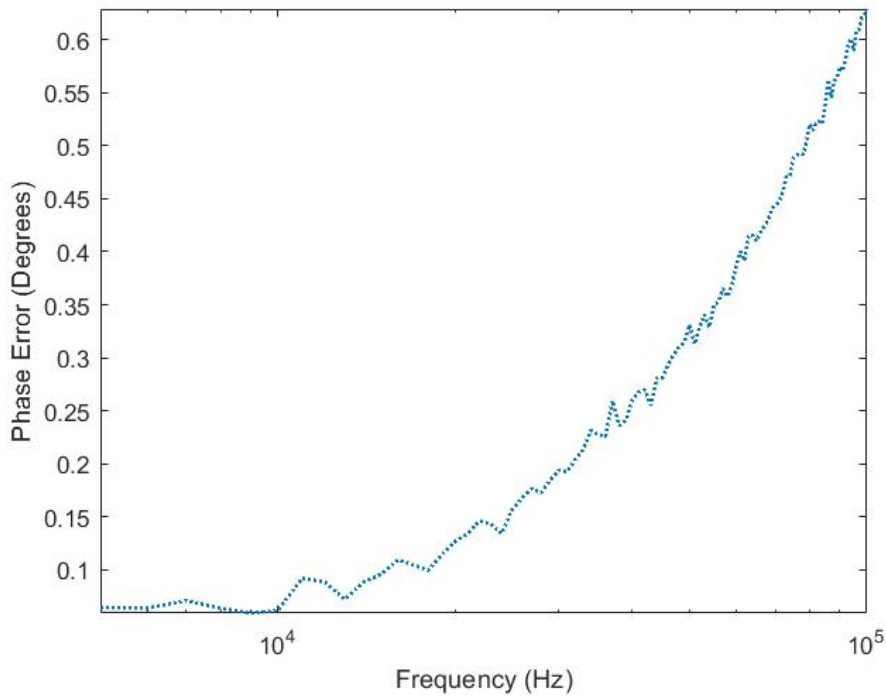


Figure 20: Phase angle measurement error using a 249.5k $\Omega$  resistor

### 5.2.6 Testing Results using Resistors and Capacitors

Figure 21 shows the measured and theoretical impedance and phase angle of a  $100\text{k}\Omega$  resistor and  $100\text{pF}$  capacitor in parallel. The dashed and solid curves depict the measured and theoretical impedance and phase angle, respectively.

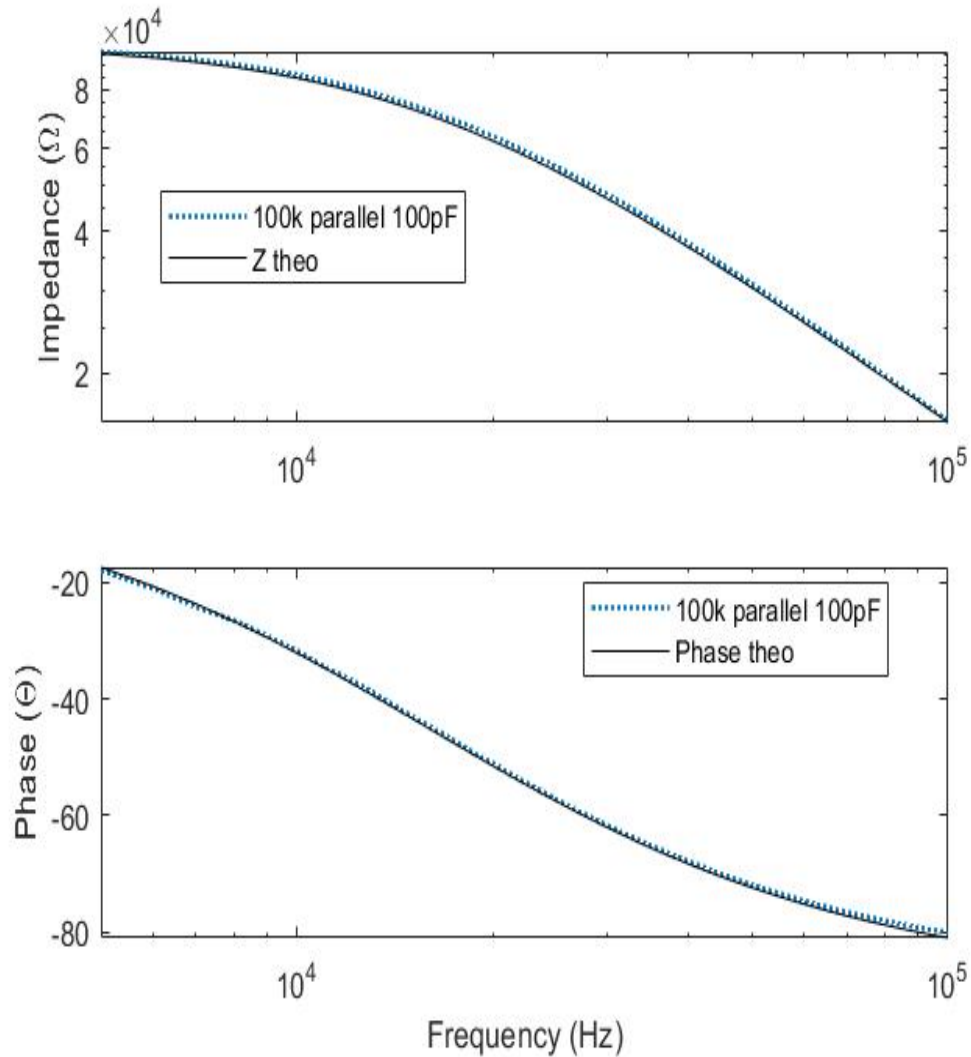


Figure 21: Impedance and phase angle of both theoretical calculations and bioimpedance device measurements using  $100\text{k}\Omega$  resistor and  $100\text{pF}$  capacitor in parallel

Figure 22 shows the impedance and phase angle measurement errors using the bioimpedance device.

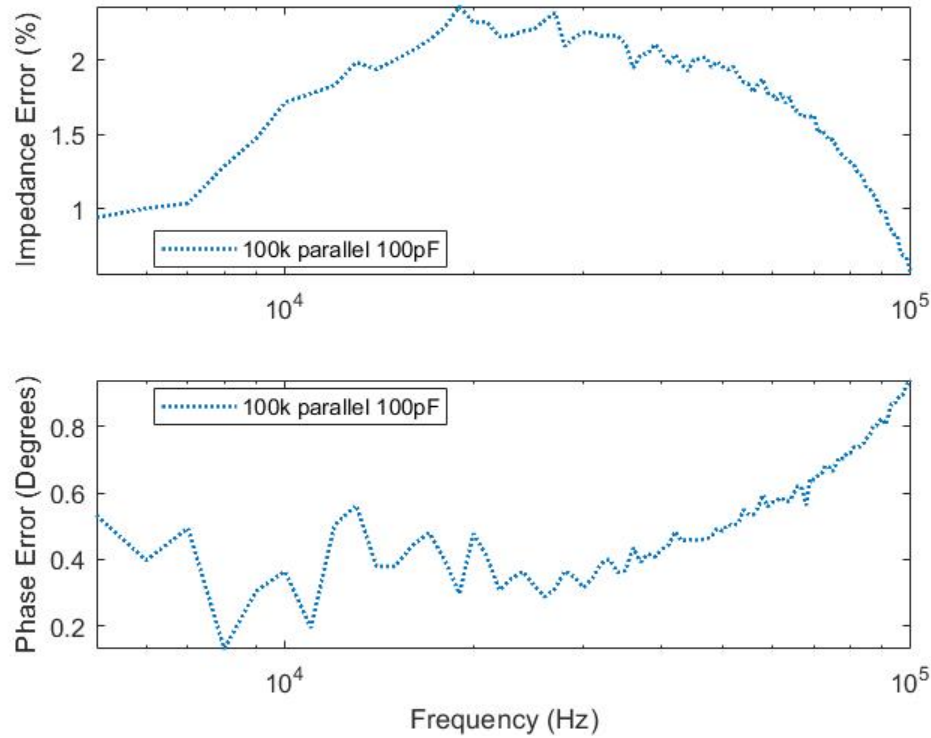


Figure 22: Impedance and phase angle measurement error using 100k $\Omega$  resistor and 100pF capacitor in parallel

### 5.2.7 Testing Results using the simplified Hayden Model

Figure 23 shows the measured and theoretical impedance and phase angle of the simplified Hayden Model with the dashed curve being the measured and the solid curve being the theoretical impedance and phase angle, respectively. It is observed that the bioimpedance device is fairly accurate at measuring the impedance of the electrical circuit of interest. Figure 24 and Figure 25 show the percent errors regarding the measurements of the bioimpedance device. As it is observed, the errors involved are very minimal suggesting that the final design is very accurate in its measuring capabilities.

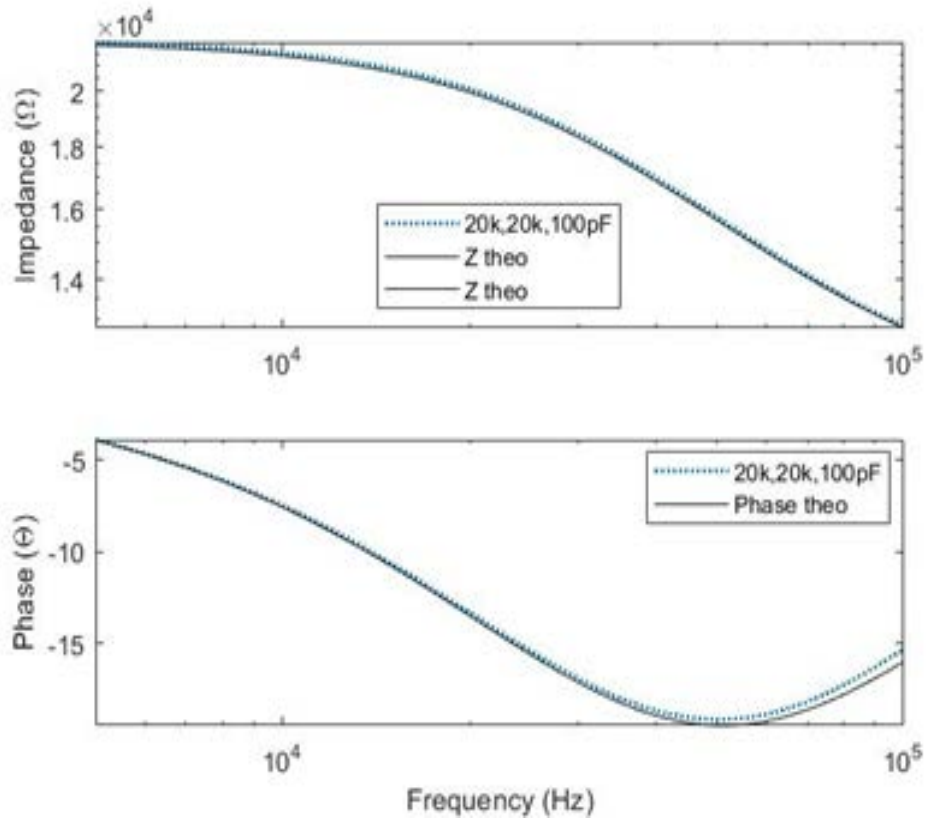


Figure 23: Impedance and phase angle of both theoretical calculations and bioimpedance device measurements

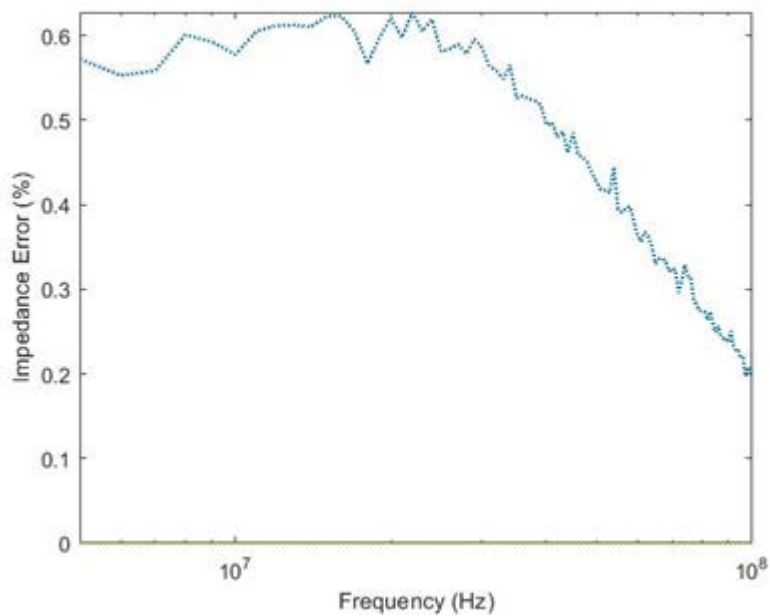


Figure 24: Percent Impedance Measurement Error

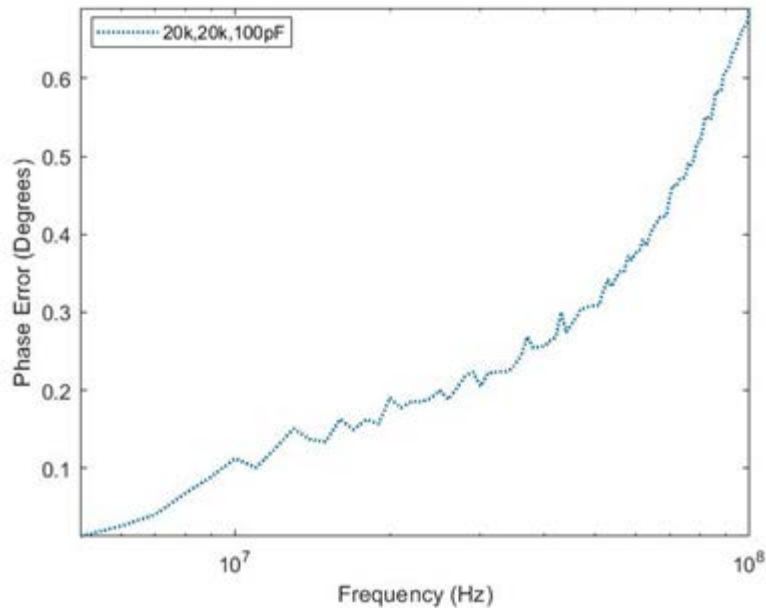


Figure 25: Phase angle measurement error

### 5.2.8 Results of Systematic Error Investigation

Figure 26 and Figure 27 show the impedance and phase angle measurement error when the AD5933 alone was used to measure a  $1.8\text{k}\Omega$  resistor. It is evident that the AD5933 alone is very accurate in its impedance measurement with a maximum error of 0.50%.

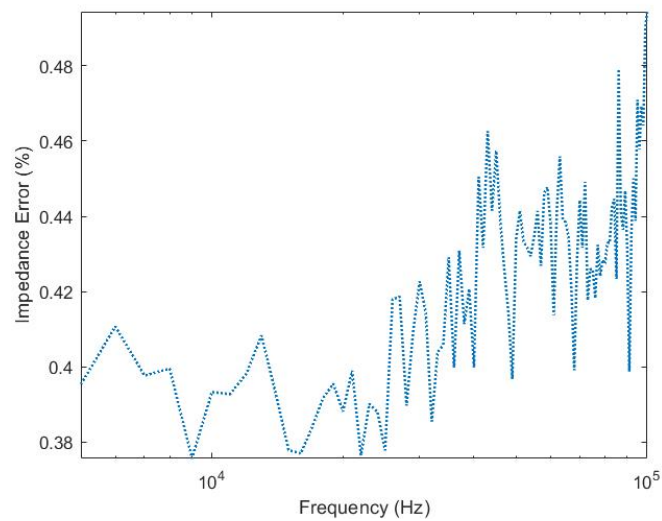


Figure 26: Impedance error using the AD5933 only to measure a  $1.8\text{k}\Omega$  resistor

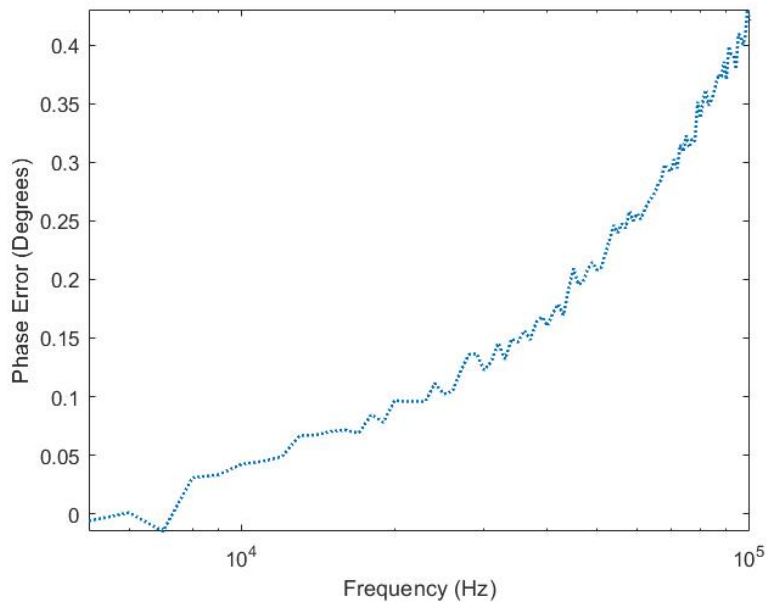


Figure 27: Phase angle error using the AD5933 only to measure a 1.8kΩ resistor

Figure 28 and Figure 29 show the impedance and phase angle measurement error using the AD5933 and the inverting amplifier.

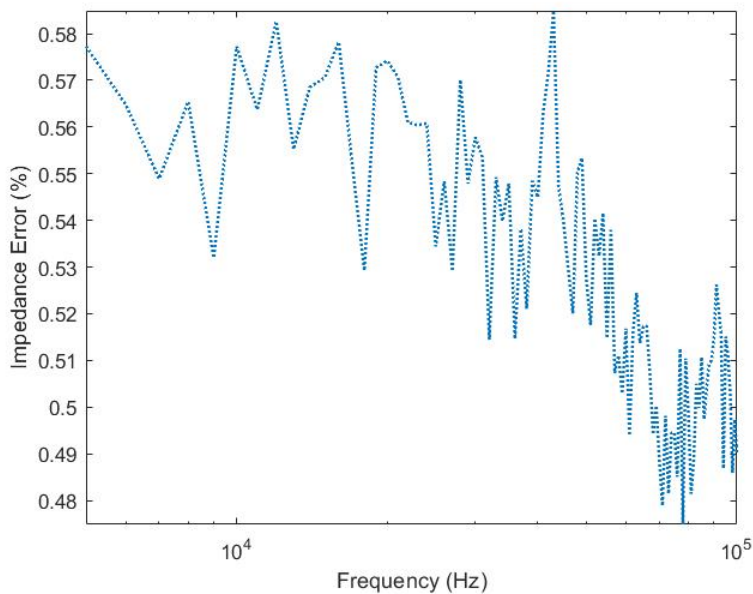


Figure 28: Impedance error using the AD5933 and the inverting amplifier to measure a 1.8kΩ resistor

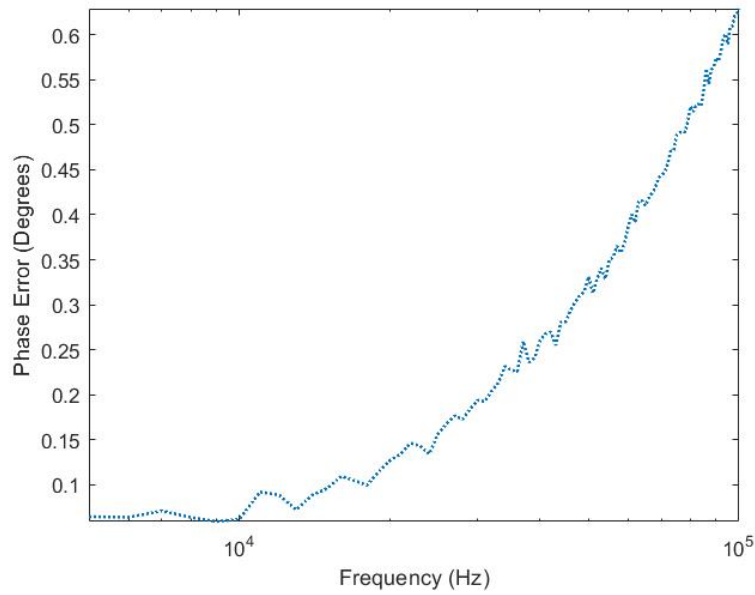


Figure 29: Phase angle error using the AD5933 and the inverting amplifier to measure a 1.8kΩ resistor

With a maximum impedance measurement error of 0.58% using the AD5933 and the inverting amplifier to measure the 1.8kΩ resistor the maximum error that the inverting amplifier added to the system was shown to be approximately 0.08%.

Figure 30 and Figure 31 show the impedance and phase angle measurement error using the AD5933, the inverting amplifier, and the transimpedance amplifier.

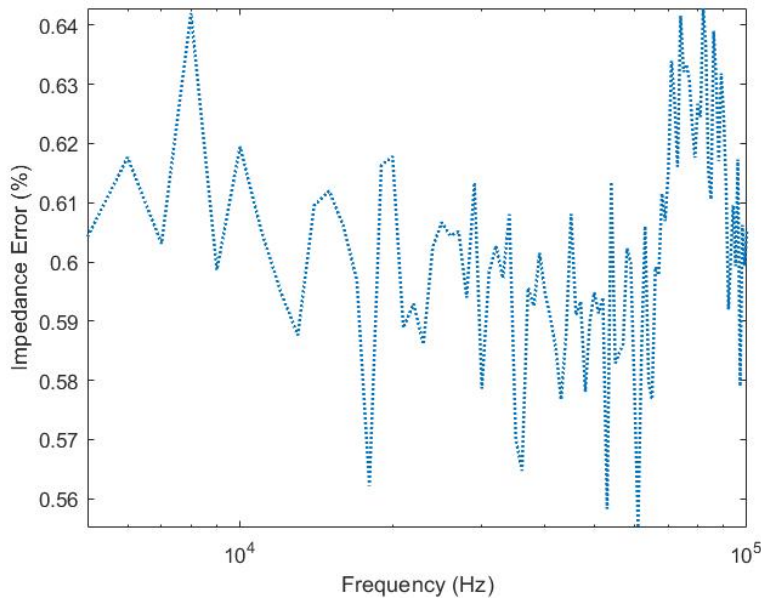


Figure 30: Impedance error using the AD5933, the inverting amplifier and the TIA to measure a 1.8kΩ resistor

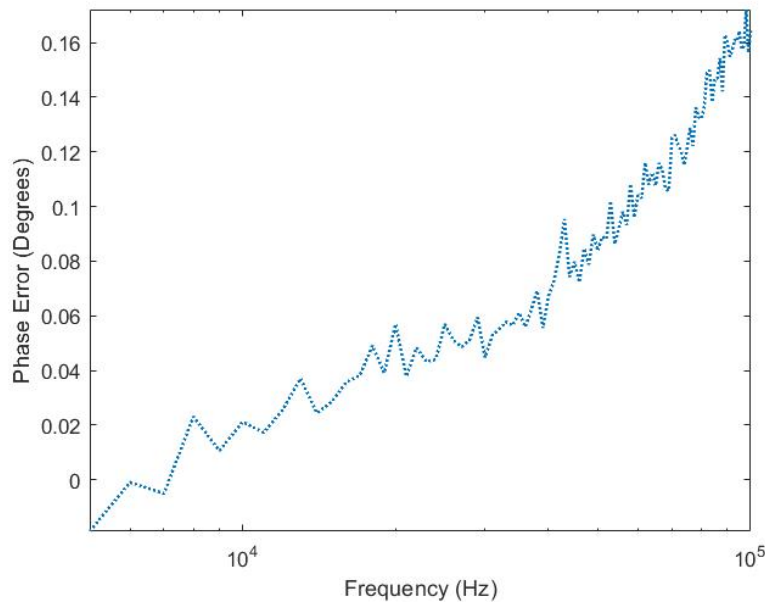


Figure 31: Phase angle error using the AD5933, the inverting amplifier and the TIA to measure a 1.8kΩ resistor

Lastly, with a maximum impedance measurement error of 0.64% using the AD5933, the inverting amplifier, and the transimpedance amplifier to measure the 1.8kΩ resistor, we found that the maximum error that both amplifiers added to the system was approximately 0.14%.

This investigation showed that the bioimpedance device is accurate and that the additional circuitry did not add significant errors to the impedance and phase angle measurements.

### 5.2.9 Statistical Significance Analysis

Each frequency sweep was repeated 10 times for each configuration. Certain important frequencies throughout the entire frequency range were selected and the mean and standard deviation of the measurements that were collected using the AD5933 were calculated. The frequencies that were selected were chosen in the lowest, middle and maximum of the frequency range of interest. These calculations are shown in Tables 3, 4 and 5.

Table 3: Mean and Coefficient of Variation (CV) of measurements using a 249.5k $\Omega$  resistor at selected frequencies.

Frequency (kHz)	Impedance		Phase Angle	
	Mean (k $\Omega$ )	CV (%)	Mean (degrees)	CV (%)
5	249.9	0.02	0.11	0.04
50	250.7	0.01	0.19	0.03
100	253.5	0.07	0.65	0.06

Table 4: Mean and Coefficient of Variation (CV) of measurements using 100k $\Omega$  resistor and 100pF capacitor in parallel at selected frequencies.

Frequency (kHz)	Impedance		Phase Angle	
	Mean (k $\Omega$ )	CV (%)	Mean (degrees)	CV (%)
5	104.3	0.10	-17.9	0.03
50	37.2	0.15	-72.0	0.09
100	15.7	0.05	-81.9	0.11

Table 5: Mean and Coefficient of Variation (CV) of measurements using the simplified Hayden model at selected frequencies.

Frequency (kHz)	Impedance		Phase Angle (Degrees)	
	Mean ( $\Omega$ )	CV (%)	Mean (degrees)	CV (%)
5	21969.7	0.01	-3.90	0.01
50	15768.4	0.02	-19.16	0.01
100	12810.0	0.01	-15.31	0.01

### 5.2.10 Summary of Testing Results

Table 6: Results for all the tests that were performed.

<b>Electrical Components Tested</b>	<b>Mode of Operation V (pk-to-pk)</b>	<b>Maximum Impedance Error (%)</b>
Resistor	3	4.13
	2	2.00
	1	3.11
	0.4	2.37
	0.2	1.10
	0.04	3.78
Resistor and Capacitor in Parallel	3	3.41
	2	2.51
	1	2.89
	0.4	1.08
	0.2	2.66
	0.04	3.78
Simplified Hayden Model	3	1.14
	2	0.62
	1	2.59
	0.4	0.88
	0.2	1.30
	0.04	3.54

### *5.2.11 Limitations of Testing using Electrical Components*

Some of the electrical configuration that were tested, such as the simplified Hayden model, were very close to what would be expected from the AD5933 to be able to measure in terms of both resistive and reactive components present in human skin impedances. The performance of the device was very satisfactory regarding the measurement errors in both impedance and phase angle measurements from the theoretical impedances. A simplified Hayden model is known to be a human skin electrical equivalent model which the device can follow closely implying correct operation in a real case scenario where the  $Z$  unknown is the skin impedance of subjects.

However, testing on strictly electrical components does not indicate the accuracy and sensitivity needed from the device to be able to detect small impedance changes due to inflammation during a pressure ulcer. For this reason, further investigation of an appropriate tissue phantom medium was performed.

## 6 Tissue Phantom Selection

The objective of this chapter is to outline the process by which potential tissue phantom materials were chosen, tested, and compared. This section begins with essential background information on potential material choices that would be a good fit as a potential tissue phantom and then goes into detail regarding materials that are being used currently as tissue phantoms to study or utilize the bioimpedance technique. In addition to background research, this chapter also outlines the process by which a final tissue phantom was selected as well as the different testing protocols used.

### 6.1 *Analysis of Wants and Needs*

Using the revised client statement, the group decided to create wants and needs for the proposed tissue phantom selection and the experimental design for the pressure ulcer simulation on the phantom. An analysis of the needs based on a revised client statement is important as the scope of the MQP project changed significantly from when it was proposed originally.

The main requirement for any potential tissue phantom material was whether the impedance of the material showed similar characteristics to the impedance of human skin. This was assessed both qualitatively and quantitatively by analyzing impedances vs frequency data of both the material being tested and human impedance data gathered from the forearm. This is an important property because in order to be used as an *in vitro* model of human tissue, for the purpose of optimizing and determining the sensitivity required by the bioimpedance device, the phantom needed to show similar impedance properties to human skin.

The other main requirement for the phantom material was the ability to be manipulated easily. Measuring different parameters of the bioimpedance analyzer may require reconfiguring the selected material and to improve testing efficiency it is important that the material be easily manipulated into different shapes and sizes. In addition, different areas of the human body have different impedances and thus the electrical properties of the material should be able to be modified to suit the area being simulated.

Due to the fact that there were few restrictions overall on the possible materials that could be chosen as possible tissue phantoms, the wants were identified as items that would make the workflow of testing the impedance analyzer as efficient as possible. After conducting background research on prior uses of bioimpedance and device testing a matrix was created which included all the desired characteristics of the chosen material.

The first characteristic that was desired revolved around the structural integrity of the possible material that could be a potential tissue phantom. The material needed to be structurally strong so that when pressure would be applied it would not break. During the literature review process, it was found that blood vessels sustained permanent damage at 33 mmHg, thus the proposed material should be able sustain such pressure without deforming. [5]

The next want was that the proposed material should have been used in prior bioimpedance studies. By using prior studied materials, the team would be able to gain a better understanding of their properties and also understand how they may respond to impedance testing. This allowed for easier comparisons between different types of materials. However, the possibility of creating a tissue phantom that had never been used before in prior bioimpedance studies was not rejected. Therefore, the importance of this want was less weighted compared to the structural integrity of the material.

The final desired characteristic that was examined was the affordability of the material. One of the goals of a tissue phantom is to reduce the cost of testing medical devices. At the same time, any device intended to be used in the healthcare must undergo many rounds of testing and thus the phantom material should be inexpensive. However, since the overall budget allowed for flexibility on the cost of the materials this want was less weighted as well compared to the structural integrity of the material which was very important for the experimental design.

Table 7 lists the wants that were described above and their weight in the overall selection of the materials tested.

Table 7: Tissue Phantom Weighted Wants

Design Elements	Structural Integrity	Use in Prior Bioimpedance Studies	Cost	Total
Weight	.50	.25	.25	1

## 6.2 *Methods for Preliminary Material Testing*

There are various tissue phantom options available that can be used in the study of bioimpedance. Unfortunately, there were not enough resources to test every single possibility and the team decided to focus on categories of materials that had the most realistic chance of having similar impedance characteristics to human skin. In order to select different categories of materials the team decided to conduct a literature review to learn which types of materials were used in previous studies for bioimpedance applications.

As one of the objectives of the tissue phantom design process was to be cost efficient, many of the materials chosen for this project were obtained from local stores.

One of the first possibilities that was examined as a potential tissue phantom was animal meat, and more specifically chicken skin. Even though the meat that would be used was obtained from dead animals, it was once a living organism. It was believed that both resistive and capacitive properties would be present similar to living human skin.

Sponges were also selected as a potential tissue phantom because of the pores that are present in a sponge. It was believed that when saline was injected into the sponge, the pores would create a capacitive like structure while also having saline as the conducting media to allow for electric current flow.

Lastly, vegetables were also proposed as a potential tissue phantom since the impedance of vegetables has been researched in depth in the past for applications such as physiological investigations of plant tissue damage [19]. Some of those vegetables have also been used for bioimpedance studies and many electrical models of the human skin have been shown to fit the electrical impedance properties noticed in vegetables. The team decided to explore certain

vegetables that have been widely used in studies related to bioimpedance, such as cucumbers to simulate human torso.

When tested, each material was modified so that each sample was relatively the same thickness in order to maintain consistency and ensure reproducible measurements from the impedance analyzer. In addition, each material was tested in multiple configurations such as with and without the outer skin layer of the material. This was done in order to see the effect of the skin on the overall impedance of the material.

Table 8 shows the materials that were tested, the categories that they were grouped, and the tests that were conducted as the project progressed.

Table 8: Summary of Materials and Tests Performed

<b>Material</b>	<b>Category</b>	<b>Tests Conducted</b>
Coarse Sponge	Sponges/Foams	Preliminary Impedance Test
Dense Sponge	Sponges/Foams	Preliminary Impedance Test
Styrofoam	Sponges/Foams	Preliminary Impedance Test
Bologna	Meat	Current Depth Test
Chicken Tissue	Meat	Preliminary Impedance Test
Apples	Vegetables	Preliminary Impedance Test, Human Comparison Test
Cucumbers	Vegetables	Preliminary Impedance Test, Human Comparison Test
Potatoes	Vegetables	Preliminary Impedance Test, Human Comparison Test, Saline Sensitivity Test, Drying Test, Pressure Ulcer Simulation Test

### ***6.2.1 Preliminary Impedance Testing of Phantom Materials***

Although the team assisted in the design of the bioimpedance analyzer, the impedance analyzer was not utilized for the preliminary tests. Instead, the Keysight E4990A Network Analyzer was used as the gold standard due to its established accuracy in impedance and phase angle measurements. This device had a measurement range of frequencies between 20 Hz and 10 MHz, although the upper frequency limit was set to 100 kHz to simulate the design of the impedance analyzer designed in this project.

Due to the fact that there were so many materials that needed to be tested and each had different sizes and shapes it was necessary to standardize all samples from each potential material. Thus, samples were modified so that each one had a thickness of 3 cm and a width of at least 5 cm. The width of 5 cm was chosen so that there was enough space for the electrodes to be placed 3cm apart. The 3 cm thickness was chosen for two reasons. Firstly, the data collected from the potential tissue phantoms had to be compared to human forearm impedance data. The forearm thickness can be approximated to 3 cm which allowed for the samples to be standardized with the human forearm impedance data. Also, 3cm thickness was shown to be enough to penetrate deep in the structure of each material, as indicated by the following results of the current depth experiments using bologna.

Once the sizes of the samples were standardized, the samples were placed in front of the impedance analyzer on a regular lab bench and connected via silver-plated electrodes and at 200  $\mu$ A in order to ensure that only the phantom was the variable in the different impedance values measured. The electrodes for this test were placed at a 3 cm distance and this remained the same for each sample to ensure that there were no other variables except the material itself. From the current penetration depth experiment using bologna, a 3 cm electrode separation was also shown to be sufficient for the current to penetrate through deeper layers in each structure.

In order to ensure that the contact between the electrode and the surface of the material remained consistent a set of weights totaling 60g was placed upon each electrode. Finally, the impedance measurement was taken 5 times for each sample in order to assess statistical significance. In order to maintain consistency amongst the different materials some common parameters were utilized during these preliminary tests. The setup configuration of the impedance

analyzer is shown in Table 6. Figure 32 shows a diagram of the setup procedure used in the preliminary impedance testing phase of the design. The data gathered from this preliminary testing can be found in Appendix A-2

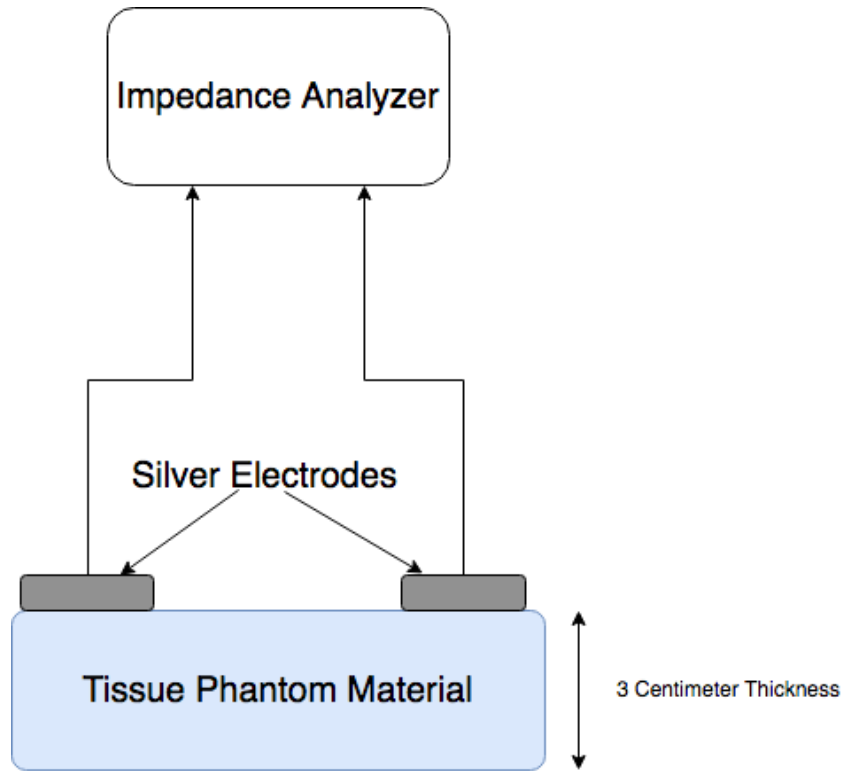


Figure 32: Setup for the Preliminary Impedance Measurement Test

Table 9: Parameters for the E4990A Impedance Analyzer

Parameter	Value
Current	200 $\mu$ A
Frequency	20 Hz to 100kHz
10x Point Averaging Enabled (Y/N)	Yes
Log Plot? (Y/N)	Yes

### ***6.2.2 Current Depth Testing***

In order to select the appropriate tissue phantom material, it was necessary to understand exactly how deep the current used by the impedance analyzer flows through a given material. At the same time, understand how deep the current flows according to the separation distance of the electrodes and the current that is being injected is of major importance for pressure ulcer detection since many times pressure ulcers occur as a result of injury deep within the tissue, close to the muscles.

As it is impossible to conduct this test accurately using live human skin, mixed meat bologna was used in order to simulate the heterogeneous nature of human tissue and the different layers of skin. The bologna was bought from a store and was cut to two-millimeter layers which were layered one at a time in order to understand how deep the current traveled. For example, the first iteration of this test used 1 layer of bologna placed upon an insulating surface such as the lab table and two silver electrodes were placed 3 centimeters apart. However, in each successive iteration another layer was added and the electrodes were placed on top of the stack of bologna layers. By analyzing the impedance measurements, we would be able to understand how deep the current flowed.

In addition to simulating the layers of the skin and its effect on the current flow, the bologna layers were also placed on both conducting and insulating surfaces in order to simulate the shunting effect of blood vessels as they contain the most conductive part of the body. Each layer was placed upon two different surfaces in order to compare the results and understand the effects of the conductive surface. Each iteration of this test also used different electrode spacing in order to gain valuable information on the relationship between electrode spacing and the resulting current penetration depth. This test also utilized the Keysight Impedance Analyzer and the settings shown in Table 6. A diagram of the setup which includes the bologna layers, the two different surfaces, and the electrode separation distance are shown in Figure 33.

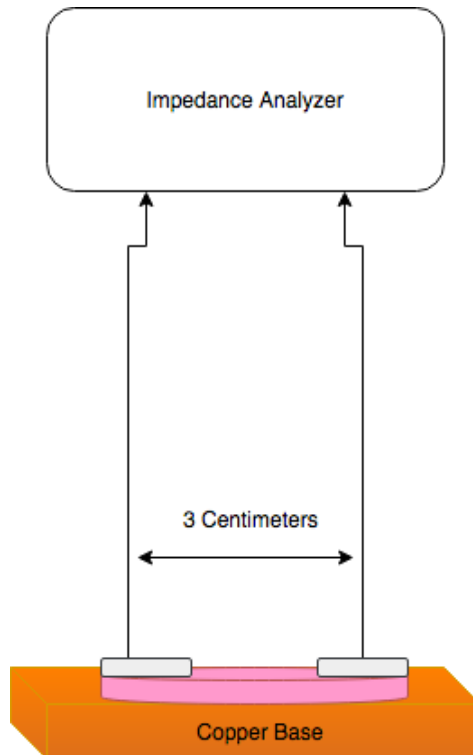


*Figure 33: Bologna Current Depth Test Diagram*

### ***6.2.3 Electrode Spacing and Type Test***

During our literature research on the principles of bioimpedance, it was noted that electrode separation distance may play a role in the impedance measurements gathered from phantom materials as well as humans. In order to test this theory, 7 different electrodes were placed upon a subject's forearm with a separation distance of 1.5 cm. In addition to providing a theory found in literature, this test is useful for the future design of the bioimpedance sensor as one of the constraints of a bioimpedance device patch if fully developed is the size. If there are negligible differences in impedance values at increasing separation distances then the electrodes can be placed relatively close together allowing for a more compact patch design and improved patient comfort. Figure 34 shows the setup that was used in this test.

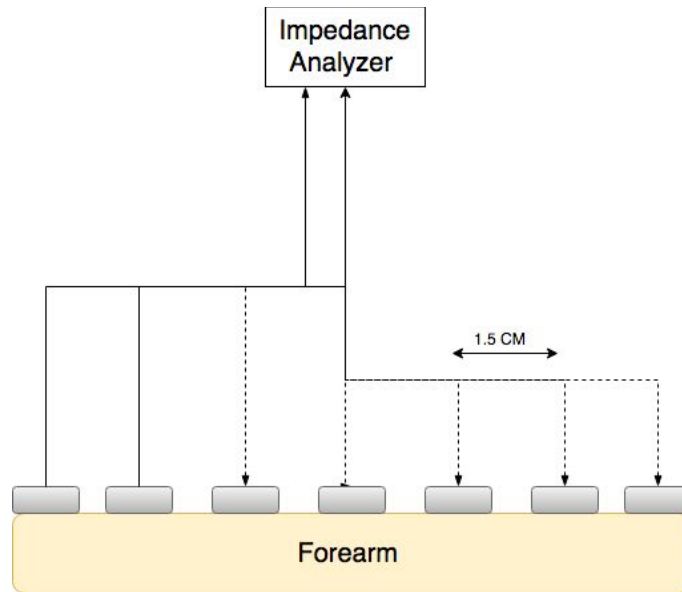
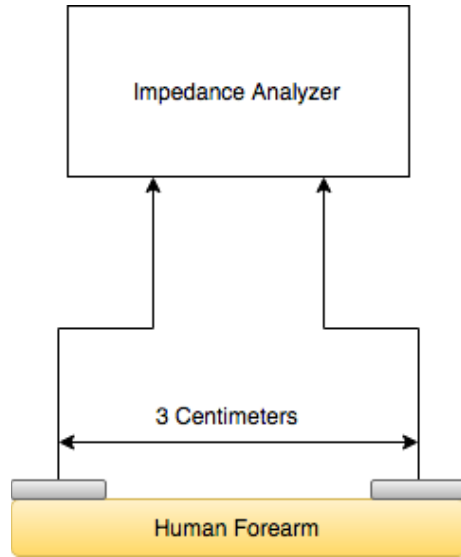


Figure 34: Diagram of electrode spacing testing

#### 6.2.4 Human Impedance Data Collection

In order to choose an appropriate tissue phantom, it was necessary to measure the impedance of human skin. By measuring human skin impedance, a decision could be derived based on how much error existed between the impedance frequency curve of a phantom and human skin. Figure 35 shows a representative image of the setup created in order to measure the impedance of the human skin on the forearm. The forearm was chosen as it was a convenient part of the body that was a suitable surface for attaching the silver electrodes. Prior to the attachment of the electrodes to the skin, isopropyl alcohol was used to remove any oily residues. The electrodes were only placed after the alcohol was dried as to prevent changes in measured impedance values. Electrical tape was utilized to secure the electrodes as it is electrically neutral. The experiment was run multiple times in order to gain information on statistics and to remove any possibilities of user bias.



*Figure 35: Setup Used for Gathering Human Impedance Data*

## **6.3 Preliminary Results of Impedance Testing**

### **6.3.1 Qualitative Analysis of Preliminary Impedance Testing Results**

The phantom impedance testing was conducted in order to discover a material that would have an impedance response that was similar to human skin.

The results of the preliminary impedance test were either “pass” or “fail” with “pass” assigned to materials that showed similar impedance characteristics to human skin after a qualitative observation was made. This included an observation of the slope or the rate of decrease of the impedance as the frequency increased. Materials that failed the preliminary impedance test mostly showed resistive behavior which was qualitatively observed to remain constant over the entire frequency range. The results for these materials are shown in Table 7. The materials that passed the preliminary impedance test were quantitatively analyzed using MATLAB.

Table 10: Results of Preliminary Impedance Test

<b>Material Name</b>	<b>Category</b>	<b>Result of Preliminary Impedance Test</b>
Coarse Sponge	Sponges/Foams	Fail
Dense Sponge	Sponges/Foams	Fail
Styrofoam	Sponges/Foams	Fail
Chicken Tissue	Meat	Fail
Apples	Vegetables	Pass
Cucumbers	Vegetables	Pass
Potatoes	Vegetables	Pass

### ***6.3.2 Quantitative Analysis of Preliminary Impedance Testing Results***

#### ***Frequency vs. Impedance and Phase Angle Response of Cucumbers***

The cucumber was one of three vegetables that passed the preliminary impedance test. The impedance testing for cucumbers was conducted with 3 separate cucumbers and repeated 5 times in order to assess repeatability. Figure 36 shows the impedance of cucumbers in the frequency range of 5 kHz to 100 kHz.

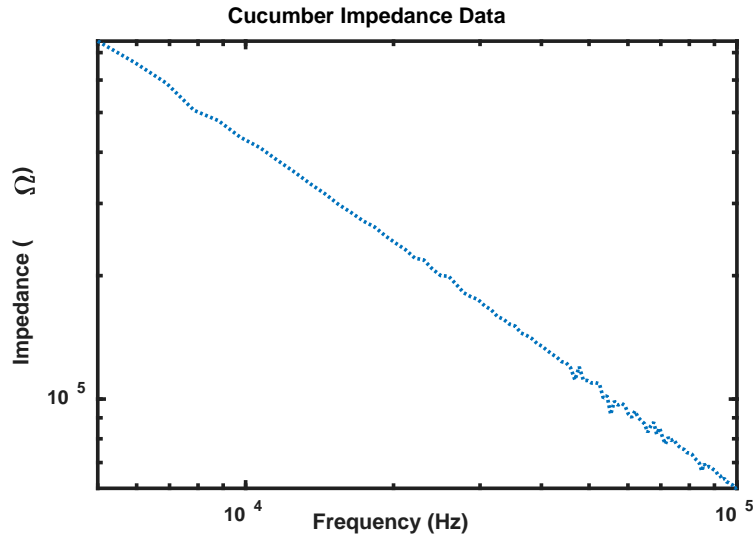


Figure 36: Impedance of cucumber

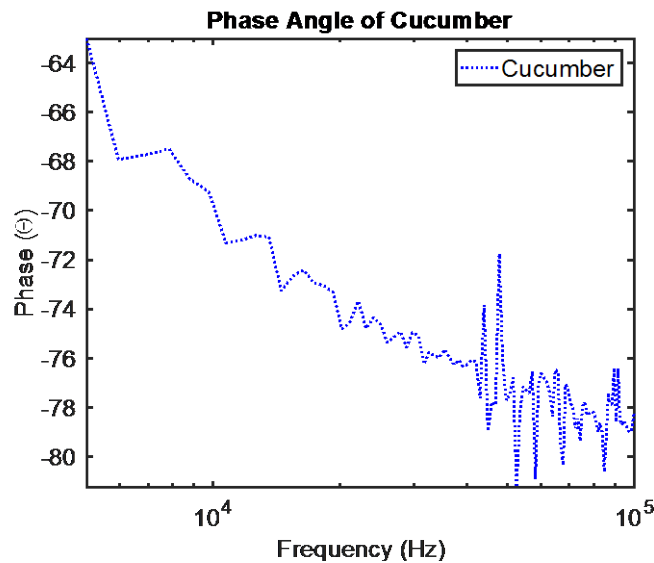


Figure 37: Phase Angle of Cucumber

The negative phase angle of the cucumbers shown in Figure 37 indicates that the cucumber has a capacitive effect similar to humans since both plant and human cells contain a phospholipid bi-layer which acts as a capacitor in regard to the flow of electricity.

In order for the experiments to be valid and statistically significant the mean and the coefficient of variance were calculated at 3 key frequencies as shown in Table 9. The coefficient of variance is calculated by first determining the standard deviation of impedance at the key frequencies and then dividing that by the mean.

Table 11: Statistical Analysis of Cucumber Samples

Frequency (kHz)	Average Impedance (k $\Omega$ )	Covariance (%)
5	494	7
50	109	13
100	45	5

***Frequency vs. Impedance and Phase Angle Results of Apples***

Apples also passed the qualitative preliminary impedance test. This test was conducted on 2 separate apples with 5 repetitions per sample. Figure 38 shows the impedance of apples over the desired frequency range.

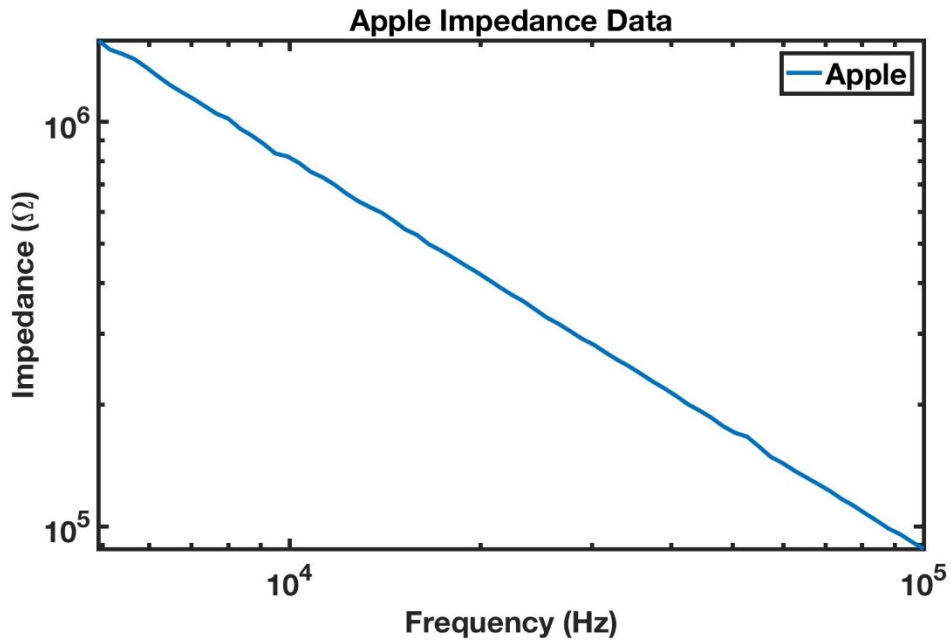


Figure 38: Impedance of apple

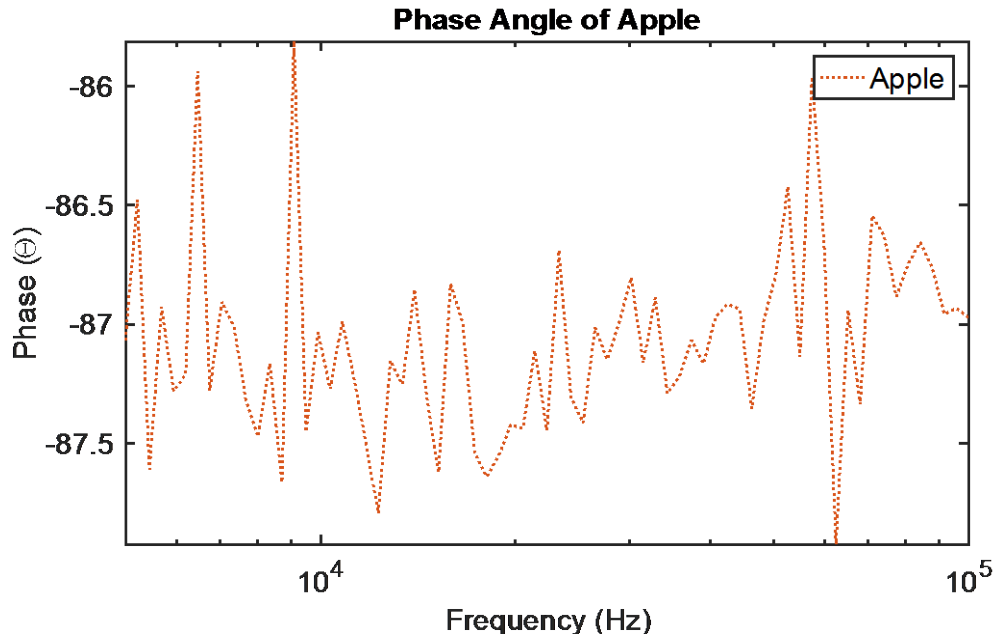


Figure 39: Phase Angle of Apples

Figure 39 describes the phase angle measurements that were measured using apples as potential tissue phantoms. Here it is important to note that the phase angle is negative which demonstrates the capacitive effects of the phospholipid bi-layer membrane of apple skin cells which is analogous to the same bi-layer found in human and animal cells.

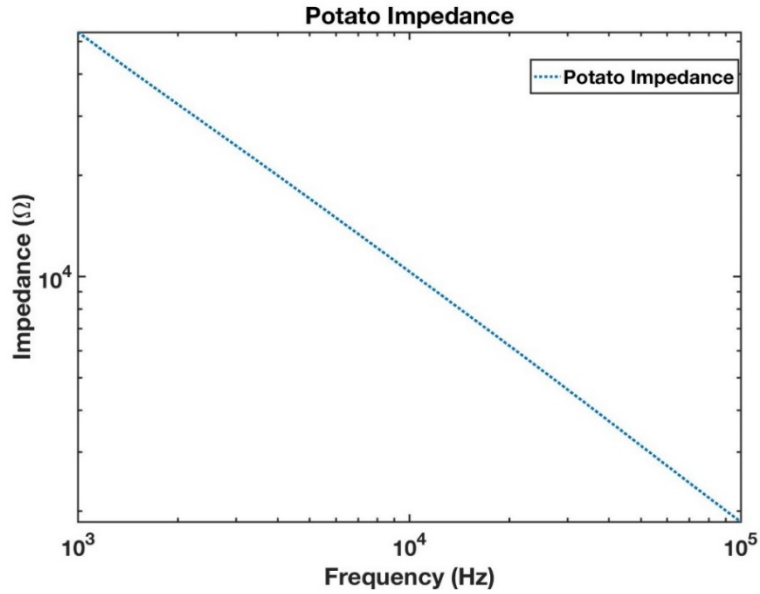
With regards to the statistical significance measurements of the apple impedance the average of the impedance measurements for apples and the coefficient of variation were calculated and shown in Table 10 for the 5 kHz, 50 kHz, and 100 kHz impedance measurements.

Table 12: Statistical Analysis of Apple Impedance Measurements

Frequency (kHz)	Average Impedance (Ohms)	Covariance (%)
5	146,000	12
50	15,900	4
100	8,180	9

### *Frequency vs. Impedance Results of Potatoes*

After conducting the preliminary impedance tests, the group found that potatoes were the best material to choose for the tissue phantom due to their smallest RMS error. For these tests 3 different potato samples were chosen and prepared following the preliminary impedance testing protocol. Each measurement was repeated 5 times for each sample. Figure 40 shows the results of the potato impedance measurements.



*Figure 40: Impedance measurement of potato*

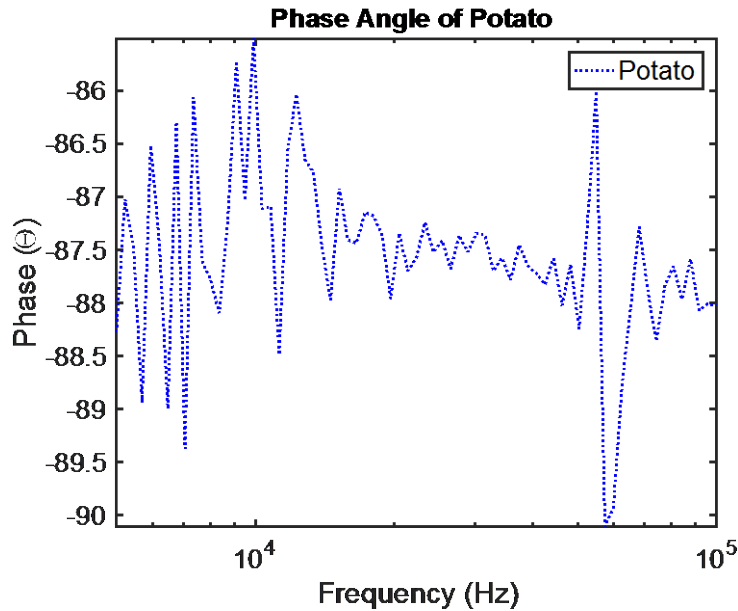


*Figure 41: Phase Angle of Potato*

Figure 41 describes the phase angle measurements that were measured using potatoes as potential tissue phantoms. Here it is important to note that the phase angle is negative which demonstrates the capacitive effects of the phospholipid bi-layer membrane of potato skin cells which is analogous to the same bi-layer found in human and animal cells. In addition, when compared to the phase angle of the cucumber, the potato shows a smaller range of variation.

Table 13: Statistical Analysis of Potato Impedance Measurements

Frequency (kHz)	Average Impedance (Ohms)	Covariance (%)
5	245,000	4
50	25,000	2
100	12,900	2

After the materials that qualitatively showed similar impedance characteristics to human skin impedances collected from the forearm were selected, it was important to analyze the data quantitatively to determine which material followed human skin impedances more closely.

The results from the preliminary impedance test showed that the impedances of vegetables had similar impedance characteristics to human skin impedances. Therefore, the data collected during the preliminary impedance test for vegetables were compared to human forearm skin impedance. This was done using a linear regression or linear transformation technique in MATLAB.

After the data for the vegetables were modified the Root Mean Squared Error (RMS) of impedance data of vegetables and human forearm skin were calculated. The material that had the smallest RMS error was chosen to be the appropriate skin phantom on which the next tests were performed. This analysis was performed using MATLAB.

$$RMS\ error = \sqrt{\frac{\sum_1^{96}(Z1 - Z2)^2}{96}} \quad (8)$$

where  $Z1$  is the impedance of the phantom and  $Z2$  is the impedance of the human skin at the same frequency

Figure 42 shows the potato impedance data that were linearly transformed to human impedance data. This was done by taking the first data point and the last data point in the human impedance curve. Two points are sufficient to define a line using the standard equation  $y = a*x+b$ , where  $a$  is the slope and  $b$  is the  $y$ -intercept. The parameters “ $a$ ” and “ $b$ ” that were found in the human impedance data were used to calculate the new potato impedance data which resulted in a linear transformation. This allowed for the calculation of the root mean squared errors between datasets which is shown in Table 14.

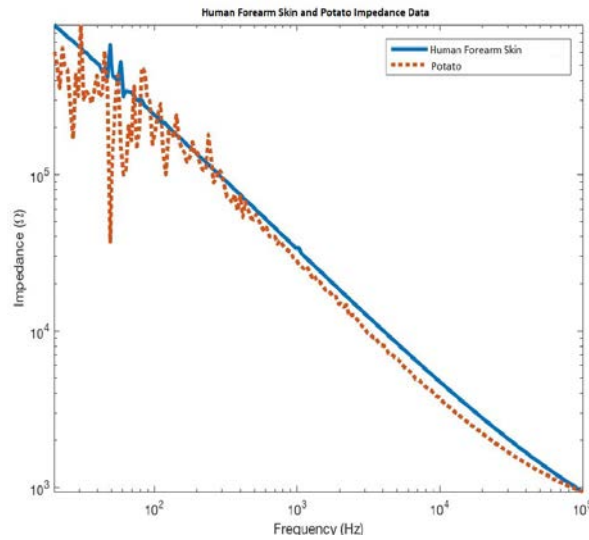


Figure 42: Human forearm skin and modified potato impedances for RMS calculation

Table 14: Root Mean Squared Error of tissue phantom and human impedances.

Material Name	Category	RMS Error
Apples	Vegetables	10.68
Cucumbers	Vegetables	18.21
Potatoes	Vegetables	6.83

### 6.3.3 Results of Electrode Spacing Testing

The goal of this experiment was to investigate if electrode distance is correlated to the depth of current flow when conducting bio-impedance measurements. The back of the human forearm was used for this experiment and 7 electrodes were placed approximately 1.5 cm apart in order to measure electrode separation distances ranging from 2 cm to 10 cm. Figure 43 shows the measured impedance values at each pair of electrodes. It demonstrates that as separation distance is increased, the impedance decreases.

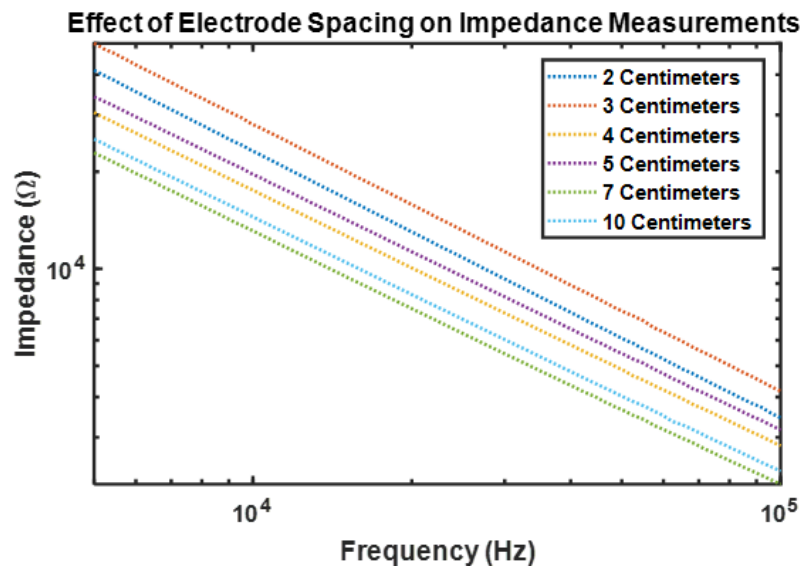


Figure 43: Impedance measurements for different electrode separation distances (2cm to 10cm)

## 7 Experimental Design – Post Material Selection

### 7.1 *Pressure Ulcer Simulation*

The main objective of the pressure ulcer simulations was to determine if the impedance analyzer and potato phantom could replicate the impedance changes that are suggested to occur from literature when pressure ulcer conditions are apparent. Fundamentally, as cells die they excise their electrolyte rich cytoplasm into the interstitial fluid in the surrounding area which reduces the overall electrical impedance of the area. The pressure ulcer simulation test attempted to match these conditions by first creating a vacuole or space for saline. The vacuole or space would simulate the approximate amount of tissue damage that is estimated to occur at each stage of a pressure ulcer. In addition, the vacuole would allow for saline to be added, to simulate the interstitial fluid being released by the cells when they are dying due to a lack of oxygen and nutrients.

The samples used for this test were modified so that a small punch was used to create a 1.5 cm hole in the center of the sample and saline was filled in 0.1 ml increments up to a total of 0.5 ml in total volume. After conducting an extensive review of literature to determine an accurate volume of fluid that may be present in a pressure ulcer, the team was not able to find any reported values. Thus, there was a need to make an educated estimate of how much saline would be enough to simulate the impedance change found at each stage of a pressure ulcer. This estimate was made based upon the fact that the fluid that is accumulated during inflammation of the forearm for example, would be approximately 5% of the total volume of the area. In this case, the amount of saline added to the hole created by the punch was approximately 5% of the volume of the potato sample. Figure 44 demonstrates the punches used and the overall setup of the pressure ulcer simulation experiment.

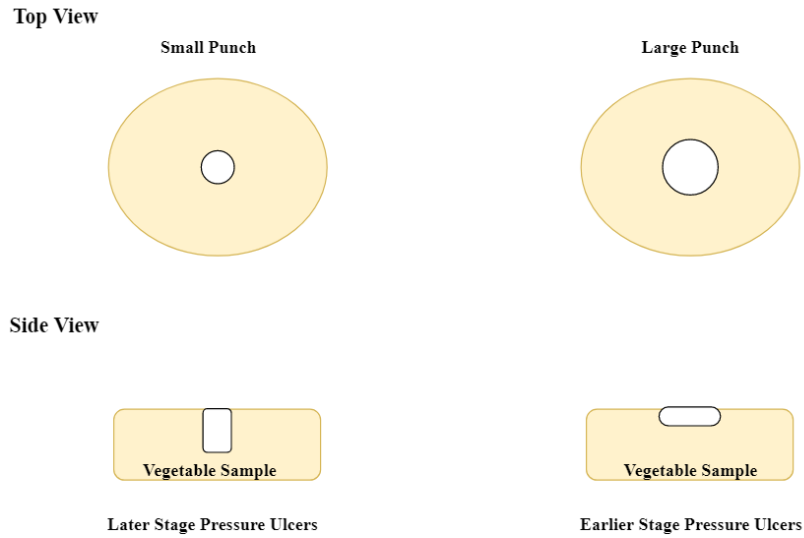


*Figure 44: Setup for the pressure ulcer simulation experiment*

### **7.1.1 Saline Sensitivity Test**

The saline sensitivity test was utilized in order to determine the maximum sensitivity of the impedance analyzer. This test was conducted in a similar manner to the pressure ulcer simulation tests. However, the punch was set at a certain level and the saline was added in increasingly smaller increments in order to determine sensitivity of the bioimpedance analyzer.

### **7.1.2 Potato Tissue Moisture Drying Test**

The drying test was conducted in order to examine the impedance of the potato tissue phantom under different states of moisture content. From prior research, it is well known that the addition of a liquid such as saline can reduce the impedance of the potato tissue. The purpose of this test was to determine whether different heat levels affect the overall impedance of potatoes mainly due to the breakdown of cellular membranes.

The rationale behind this test was obtained by studying the article by Yasumasa Ando where they studied various potatoes and measured their impedance while the potato samples were being dried and immersed in water [20]. The protocol for this experiment required a thermostatic chamber and precise temperature management which was not possible with the resources available to the team and thus needed to be modified. In order to measure the amount of water that had evaporated from the potato naturally, the potato sample was weighed in 10-minute intervals their impedance was measured. In addition to the natural drying process, the potatoes were also placed

on a heating plate in order to understand the effects of temperature and heat on the impedance of potatoes and consequently its moisture content.

## 7.2 Results of Pressure Ulcer Simulation Testing

The main purpose of the pressure ulcer simulation was to determine whether the potato could model the impedance changes associated with the formation of a pressure ulcer in the human body. The main focus in this simulation was to detect the initial impedance difference between the control which represents uninjured tissue and the stage 1 dataset which represents the tissue with fluid uptake as a result of inflammation.

It is evident that the bioimpedance device was capable of detecting impedance changes resulting from water accumulation. Additionally, as the water content increases (in later stages) the impedance decreases. Figure 45 shows the impedance in a simulated pressure ulcer potato.

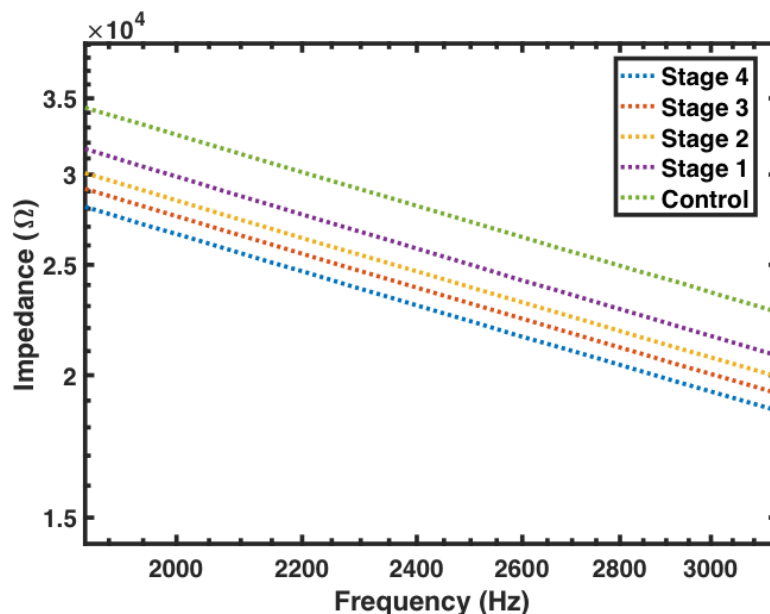


Figure 45: Impedances in a simulated pressure ulcer potato

### 7.2.1 Results of Saline Sensitivity Testing

During the course of this project the team conducted two saline sensitivity tests. One test was run by the MQP team and the other was run by, Joshua Harvey a PhD student in the Professor Mendelson's lab. It is important to note that the same conclusions were drawn from both sets of experiments. Both sets of results demonstrated that the impedance analyzer is sensitive to changes in fluid as small as 0.1mL. Results were evaluated based on the qualitative differences between

the frequency and impedance curves measured at each incremental volume increase of saline in the potato system. In Figure 46, it is evident that when electrodes are positioned 3 cm apart, the difference between the impedance curves at each level of saline are the greatest.

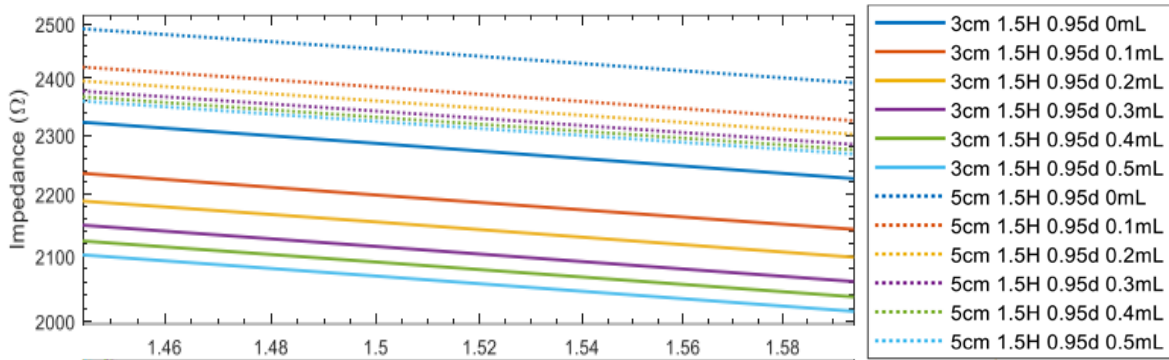


Figure 46: Impedance measurements of potato at 3cm and 5 cm (solid lines and dashed lines respectively)

When the MQP team repeated the experiment with smaller 0.05mL increments of saline, the impedance analyzer was able to see the initial increment of saline at 0.05mL. However, further addition of saline caused the impedance analyzer to lose resolution and it was not able to fully distinguish the impedance changes after the addition of more than 0.05mL of saline. Figure 47 shows the impedance measurements of the potato using 0.05mL saline increments

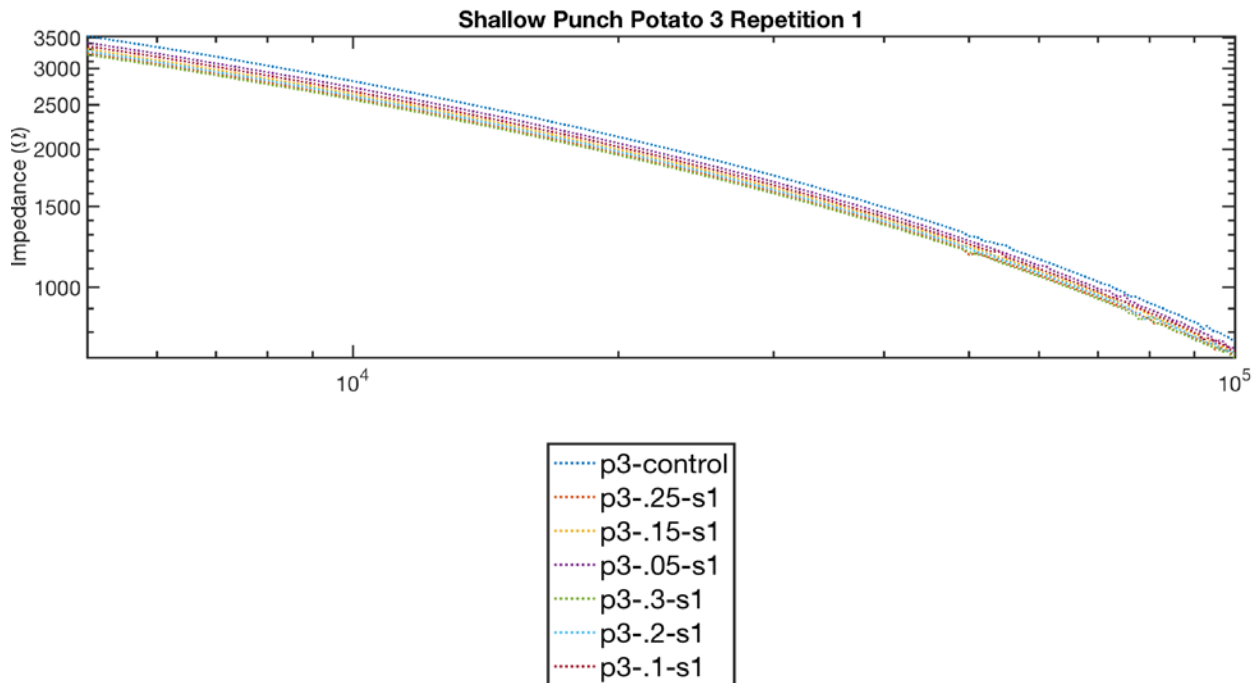


Figure 47: Impedance measurements of potato at saline increments of 0.05mL

### 7.2.2 Results of Potato Tissue Drying Experiment

The goal of the potato tissue drying experiment was to confirm the notion that the moisture in tissue is the primary source of changes in impedance. By heating the potatoes at different levels and decreasing moisture content, it was possible to compare the relationship between moisture within the sample and the overall impedance measured. It was discovered that when potatoes were heated to extreme levels, potato cells began to deform in a similar manner to human cells and lysed which released their contents into the rest of the potato. This caused the impedance values to significantly decrease. Figure 48 shows that the first two levels of heat produced a typical pattern of impedance values where the electrical impedance generally increases as the potato dries over time. However, impedance values of potatoes that were placed on the heat plate at its highest heat setting decreased due to the breakdown of the cell membrane and the resulting electrolyte filled fluid exiting the cell as shown in Figure 49.

In addition to measuring the impedance, potato samples were weighed every 10 minutes for 1-hour. Water loss of the potato in control conditions was very small, but significantly increased when heated to the highest level of heat.

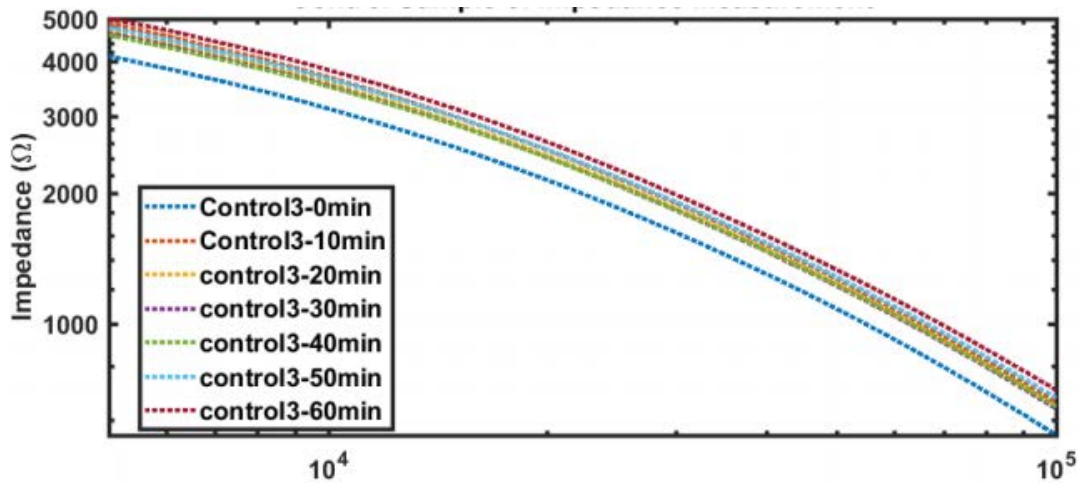


Figure 48: Impedance measurements of potato at different times of drying naturally

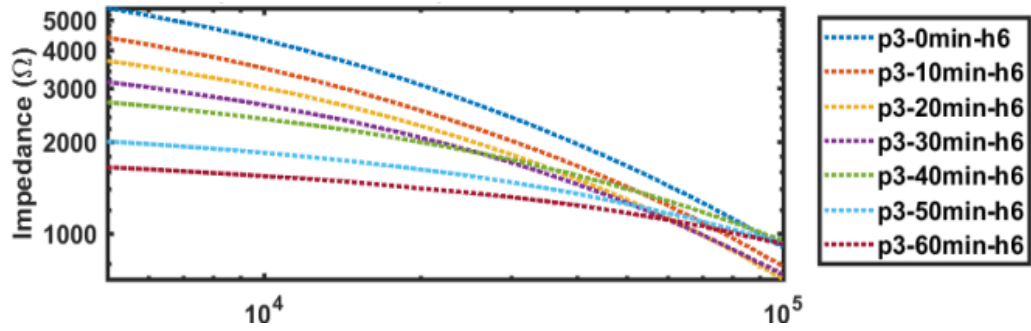


Figure 49: Impedance measurements of potato at different times of drying under hottest level

Table 15: Average and Coefficient of Variance (CV) for Control Group.

Frequency (kHz)	Time (min)	0	10	20	30	40	50	60
5	Average (kΩ)	4.27	4.53	4.60	6.60	4.69	4.25	4.33
	CV (%)	2	5	13	7	9	11	5
50	Average (Ω)	1243.9	1262.52	1277.08	1988.30	1374.23	1238.8	1248.77
	CV (%)	9	5	13	4	8	4	7
100	Average (Ω)	655.19	659.59	659.59	1258.05	733.14	653.92	656.74
	CV (%)	14	3	5	10	9	3	6

Table 16: Average and Coefficient of Variance (CV) for Highest Heat Level Group.

Frequency (kHz)	Time (Min)	0	10	20	30	40	50	60
5	Average ( $\Omega$ )	5096.94	3743.49	3723.46	3247.55	2961.20	2556.44	3322.49
	CV (%)	7	17	10	3	7	15	4
50	Average ( $\Omega$ )	1575.86	1451.82	1250.49	1175.09	1253.42	1310.63	1841.10
	CV (%)	4	4	2	5	8	3	5
100	Average ( $\Omega$ )	851.58	794.69	665.78	643.42	747.13	855.20	1237.84
	CV (%)	5	3	5	10	20	6	15

Table 17: The Weight Loss of Each Potato and the Average in the Control Group

<b>Control</b>		
<b>Potato #</b>	<b>Time (min)</b>	<b>Weight (g)</b>
Potato 1	0	77.39
	10	77.26
	20	77.14
	30	77.02
	40	76.9
	50	76.86
	60	76.77
<b>Total Loss</b>	<b>-0.62</b>	
<b>Total % Loss</b>	<b>1%</b>	
Potato 2	0	109.2
	10	108.83
	20	107.99
	30	107.01
	40	105.79
	50	104.27
	60	103.17
<b>Total Loss</b>	<b>-6.03</b>	
<b>Total % Loss</b>	<b>6%</b>	
Potato 3	0	123.27
	10	122.94
	20	122.19
	30	121.35
	40	120.23
	50	118.9
	60	117.96
<b>Total Loss</b>	<b>5.3184</b>	
<b>Total % Loss</b>	<b>4%</b>	
Average Mass (g)	0	103.29
	10	103.01
	20	102.44
	30	101.8
	40	100.98
	50	100.012
	60	99.3
<b>Average Total Loss</b>	<b>3.99</b>	
<b>Average Total % Loss</b>	<b>4</b>	

Table 18: The Weight Loss of Each Potato Sample and the Average in the Highest Heat Group

<b>Level 6 Heat Group</b>	<b>Time (min)</b>	<b>Weight (g)</b>
P1	0	65.19
	10	64.36
	20	60.52
	30	45.26
	40	53.05
	50	50.47
	60	47.85
	<b>Total Loss</b>	
<b>Total % Loss</b>		<b>27%</b>
P2	0	59.81
	10	58.48
	20	55.49
	30	51.71
	40	49.00
	50	46.64
	60	44.52
	<b>Total Loss</b>	
<b>Total % Loss</b>		<b>26%</b>
P3	0	61.21
	10	59.99
	20	56.16
	30	52.30
	40	49.15
	50	46.50
	60	44.16
	<b>Total Loss</b>	
<b>Total % Loss</b>		<b>28%</b>
<b>Average Mass (g)</b>	0	62.07
	10	60.94
	20	57.39
	30	49.75
	40	50.40
	50	47.87
	60	45.51
	<b>Average Total Loss</b>	
<b>Average Total % Loss</b>		<b>27.00</b>

### ***7.3 Ethical Concerns, Health and Safety Issues***

Since electric currents will be injected in the human body, the current design of the device meets the FDA criterion to limit the injected current below  $200\mu\text{A}$  which is considered to be safe. In addition, the Bioimpedance Analyzer, should never apply a DC voltage which can lead to skin burn marks [17].

However, since the device is still at its very initial stages of development the patch in which it will be contained needs to be very carefully designed. The intent of the patch is to detect pressure ulcers and since it is going to be used in areas of high risk for pressure ulcer formations where predominantly great pressures are applied on the skin, the chance that the device itself contributes to the formation of bedsores needs to be minimized.

### ***7.4 Manufacturability, Sustainability, and Environmental Impact***

A prototype that can be manufactured as of now has not been developed. However, it can be estimated that the costs to manufacture the device especially for a high demand system like this will be very low. Large scale manufacturing will also drive the cost of each device down allowing the device to be sold at a lower affordable cost which was one of the main objectives of this project. Future research should be done regarding the power of the device since currently it uses an Arduino board for power. Rechargeable batteries could be used to make the device more sustainable since it is intended to be disposable. Moreover, research on developing materials for the adhesive encasing that are both biocompatible and biodegradable should be done. Such materials would minimize wastes and the impact of the disposable device to the environment [18].

### ***7.5 Societal and Political Impacts***

An effective device for pressure ulcer prevention has great societal and political impacts. It increases the health and well-being of patients from reducing the risk of patients resulting in a painful condition. At the same time, it can save the healthcare industry millions of dollars annually from avoiding treatments of a condition that can be prevented. Lastly, an effective device can raise political awareness on the implications that pressure ulcers present in the modern society and thus result in the allocation of more funds in research for pressure ulcer prevention.

## 8 Conclusions and Recommendations

The bioimpedance device tested in this project was shown to be able to accurately measure impedances of both electrical components and human skin. The need for simulating a pressure ulcer in terms of the changes in the electrical impedances that are associated with it resulted in the research of a human tissue phantom. Potatoes were shown to have similar electrical impedance characteristics to the impedance of human skin and were therefore modified to simulate a pressure ulcer in terms of the water that is accumulated in underlying tissues as a result of inflammation during pressure injuries.

However, the volume of moisture that is present in underlying tissues during early pressure ulcer formations is still unknown. It is imperative that the volume is determined since it is critical in determining the sensitivity of the device that is needed to detect a pressure ulcer. In this project, this issue was tackled by characterizing the accuracy of the device and simulating the water uptake during a pressure ulcer to be less than 5% of the volume of the underlying tissue. The bioimpedance device was shown to be able to detect small impedance changes as a result of changes in the water content of potatoes.

Studies on live animals during pressure ulcer development are being conducted at UMass. The identification of one frequency where the impedance changes are maximized due to inflammation would be beneficial since it would make the device much smaller and cheaper and the overall operation of the device much simpler.

## References

- [1] M. Harold Brem, Jason Maggi, MD, David Nierman, MD, Linda Rolnitzky, MD, David Bell, BS, Robert Rennert, BA, Michael Golinko, MD, Alan Yan, Courtney Lyder, ND, Bruce Vladeck, PhD, "High Cost of Stage IV Pressure Ulcers " *PMC*, 2010.
- [2] M. T. L. Tatiana V. Boyko, George P. Yang, "Review of Current Management of Pressure Ulcers," *Advances in Wound Care* 2018.
- [3] R. Medzhitov, "Origin and physiological roles of inflammation," July 23, 2008.
- [4] S. Elmore, "Apoptosis: A Review of Programmed Cell Death " *Toxicol Pathol* 2007.
- [5] N. C. Karoon Agrawal, "Pressure Ulcers: Back to the basics," *Indian Journal of Plastic Surgery*, Journal Article vol. 45, pp. 244-254, May 2012 2012.
- [6] N. P. U. A. Panel. (2017). *NPUAP Pressure Injury Stages*. Available: <http://www.npuap.org/resources/educational-and-clinical-resources/npuap-pressure-injury-stages/>
- [7] W. Technologies. (2011, 10/16/2017). *Wellsense Unveils First-Ever Bedside Patient Pressure Mapping System Designed to Assist Caregivers in Effectively Repositioning Patients* [
- [8] WellSense. *V $\bar{U}$  is the first and only Advanced Pressure Visualization System™ (APVS). This transformational technology represents a significant paradigm-shift in Pressure Injury prevention.*
- [9] bruinBiometrics, "Subepidermal Moisture: Why do Pressure Ulcers Occur?," White Paper 2013.
- [10] . *LeafHealthcare*
- [11] B. E. Deprez JF1, Fromageau J, Cloutier G, Basset O., "On the potential of ultrasound elastography for pressure ulcer early detection.," *MedLine*, 2011.
- [12] P. M. Nightingale KR, Nightingale RW, Trahey GE, "On the feasibility of remote palpation using acoustic radiation force. ," 2001.
- [13] B. N. Raposio E, Moretti R, Grignaffini E, Grieco MP, "Laser Doppler Flowmetry and Transcutaneous Oximetry in Chronic Skin Ulcers: A Comparative Evaluation.," *Wounds*, 2017.
- [14] M. C. L. Sarah L. Swisher, Amy Liao, Elisabeth J. Leeflang, Yasser Khan, Felipe J. Pavinatto, Kaylee Mann, Agne Naujokas, David Young, Shuvo Roy, Michael R. Harrison, Ana Claudia

Arias, Vivek Subramanian & Michel M. Maharbiz, "Impedance sensing device enables early detection of pressure ulcers in vivo," *Nature Communications*, vol. 6, 2015.

- [15] A. L. F. T. S. Carvalho\*, A. B. B. Coutinho\*, B. Jotta\*, A.V. Pino, e M. N. Souza\*, "COMPARISON OF BIPOLAR AND TETRAPOLAR TECHNIQUES IN BIOIMPEDANCE MEASUREMENT," *Congresso Brasileiro de Engenharia Biomédica*, vol. 24, 2014.
- [16] C. A. M. R.I Hayden, FW Calder, DP Crawford, DS Fensom "Electrical Impedance Studies on Potato and Alfalfa Tissue," 1968.
- [17] R. M. B. Leonard Eisner, Dan Modi. (2004, 04/27/18). *Leakage Current Standards Simplified*.
- [18] B. M. M. Benjamin James John Parent, Rachel Misao Ooyama-Searls, , "A Pressure Ulcer Patch Material Study for a Wearable Sensor," WPI2017.
- [19] J. N. T.K Bera, "Studying the variations of complex electrical bio-impedance of vegetables and fruits under the different health status," 2013.
- [20] K. M. Yasumasa Ando, Naoto Wakatsuki "Electrical impedance analysis of potato tissues during drying. ," *Journal of Food Engineering* vol. 24, 2013.
- [21] Z. Moore, Patton D, O'Connor T, "Subepidermal moisture (SEM) and bioimpedance: a literature review of a novel method for early detection of pressure-induced tissue damage (pressure ulcers)," 2017.
- [22] O. Martinsen, Norbotten B, Grimnes S, "Bioimpedance-based respiration monitoring with a defibrillator," 2014.
- [23] M, Nayeli, et al. "Body fat measurement by bioelectrical impedance and air displacement plethysmography: a cross-validation study to design bioelectrical impedance equations in Mexican adults," 2007.

# Appendices

## Appendix A: Preliminary Impedance Testing Data

Apple

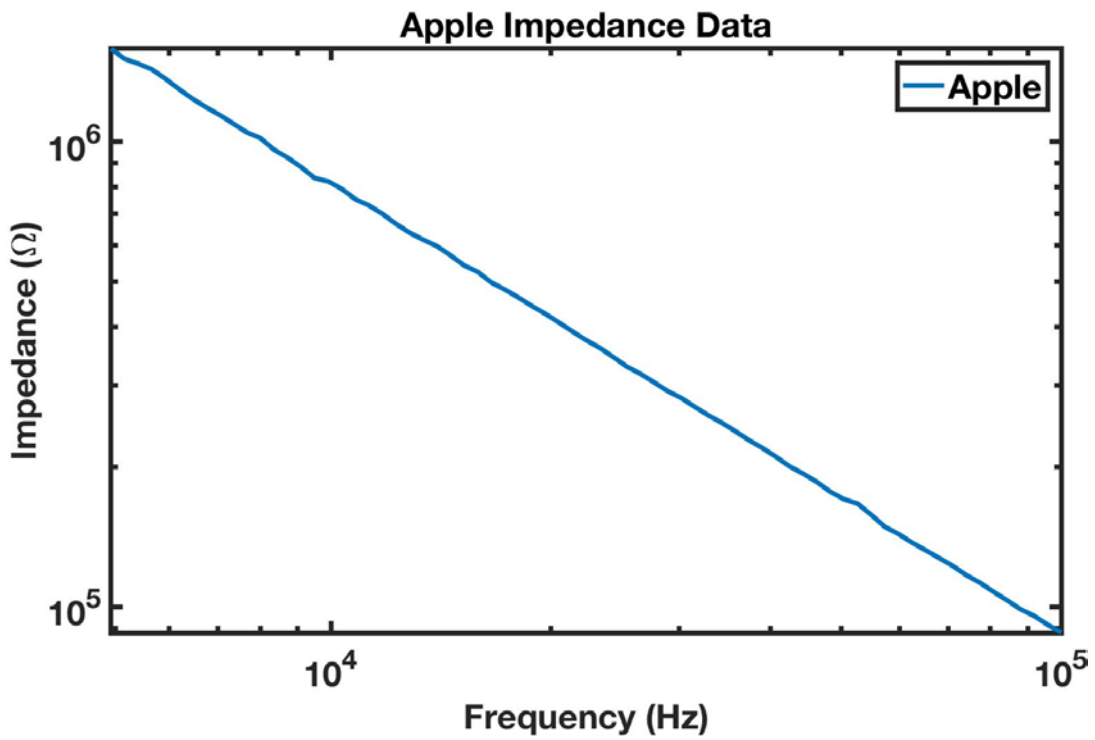
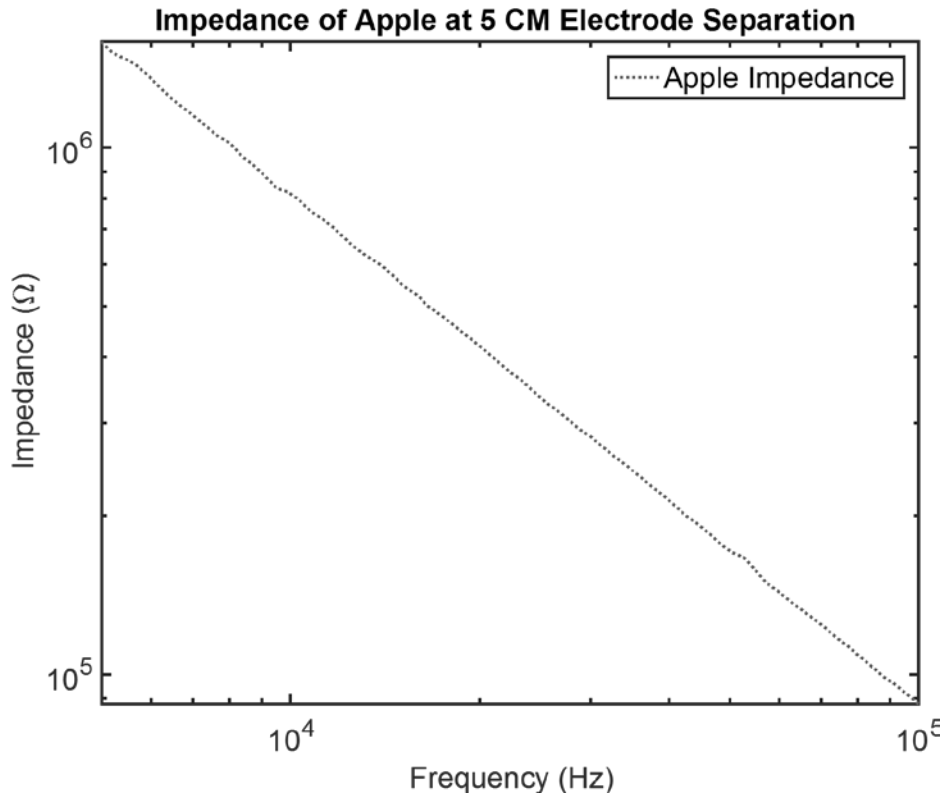


Figure A-1: Apple Impedance Graph from 5 kHz to 100 kHz, at 3CM Separation Distance



*Figure A-2: Apple Impedance Graph from 5 kHz to 100 kHz at 5CM Separation Distance*

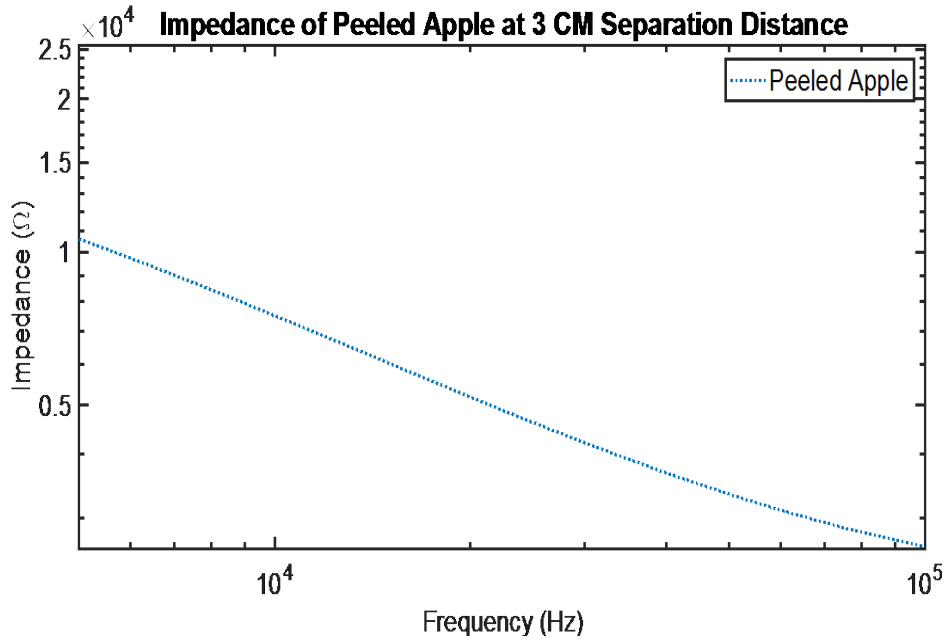


Figure A-3: Impedance of Peeled Apple at 3CM Electrode Separation

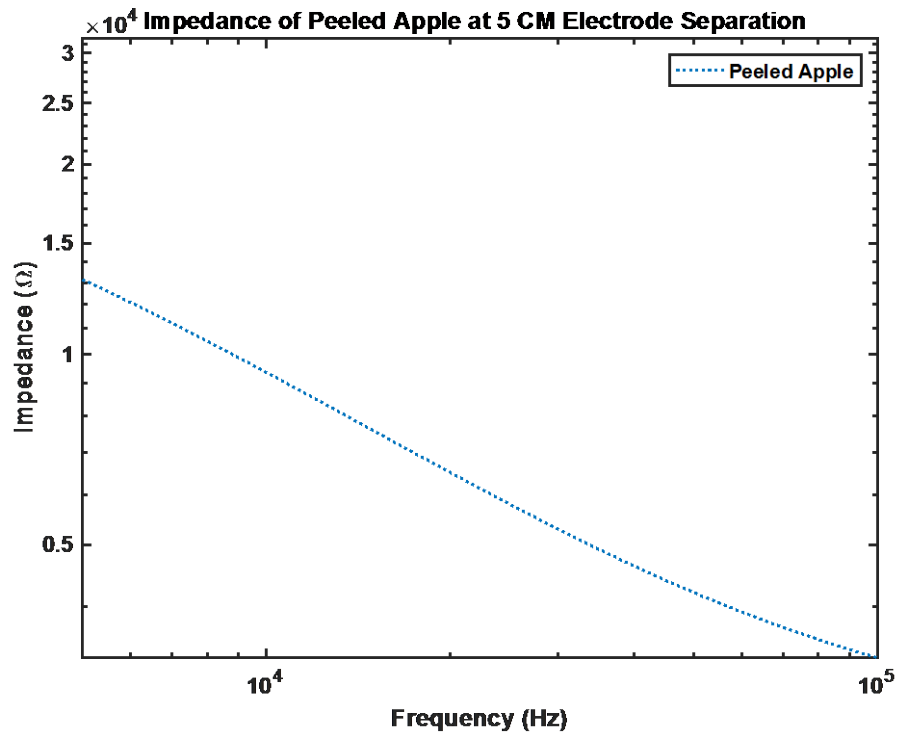
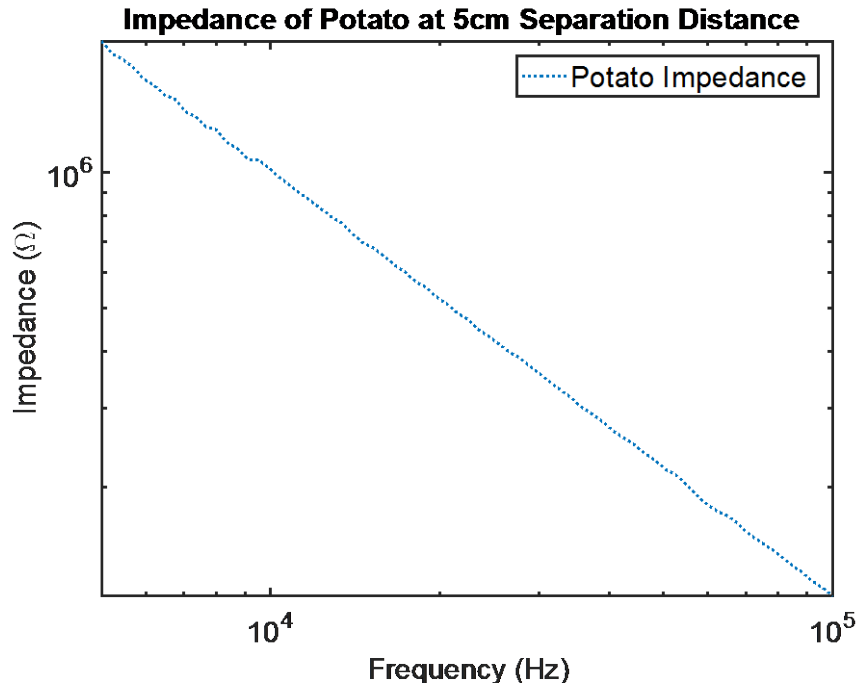
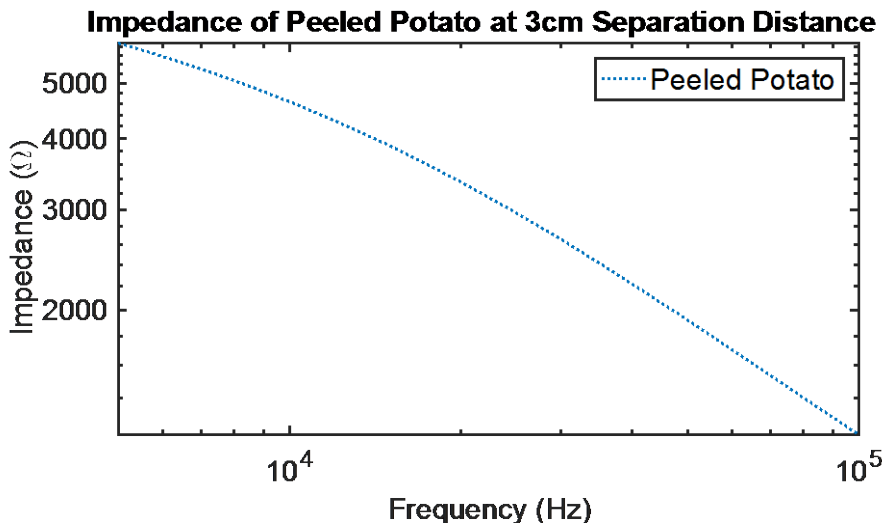


Figure A-4: Impedance of Peeled Apple at 5CM Electrode Separation

*Potato Impedance Data*



*Figure A-5: Impedance of Potato at 5cm Separation Distance*



*Figure A-6: Impedance of Peeled Potato at 3cm Separation Distance*

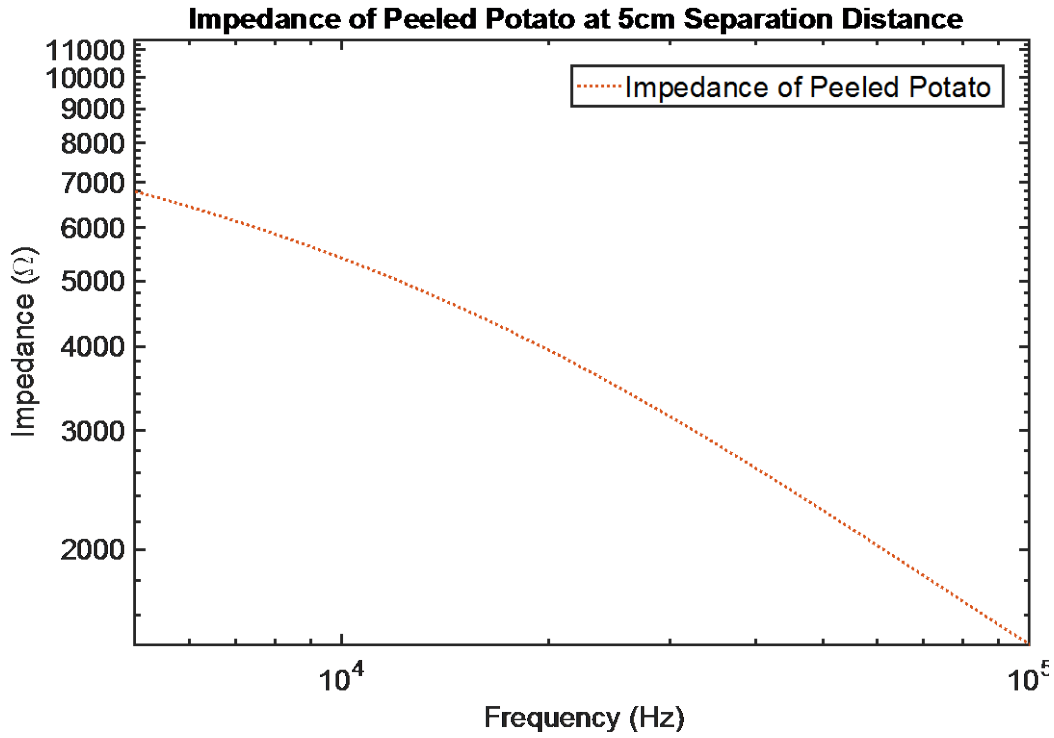


Figure A-7: Impedance of Peeled Potato at 5cm Separation Distance

*Cucumber Data*

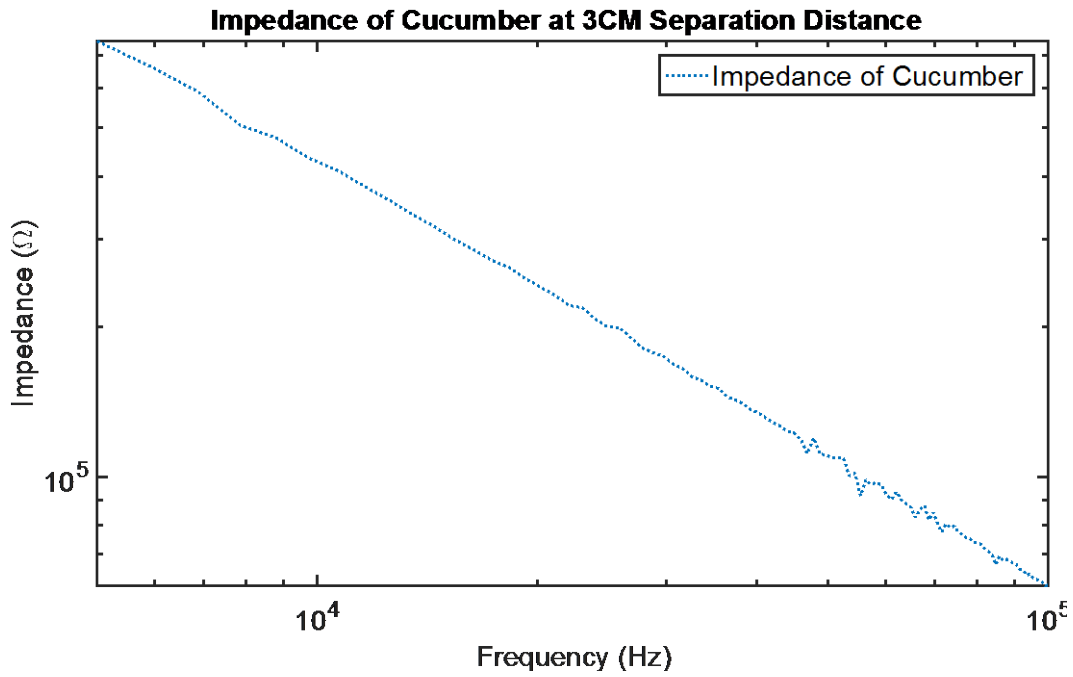
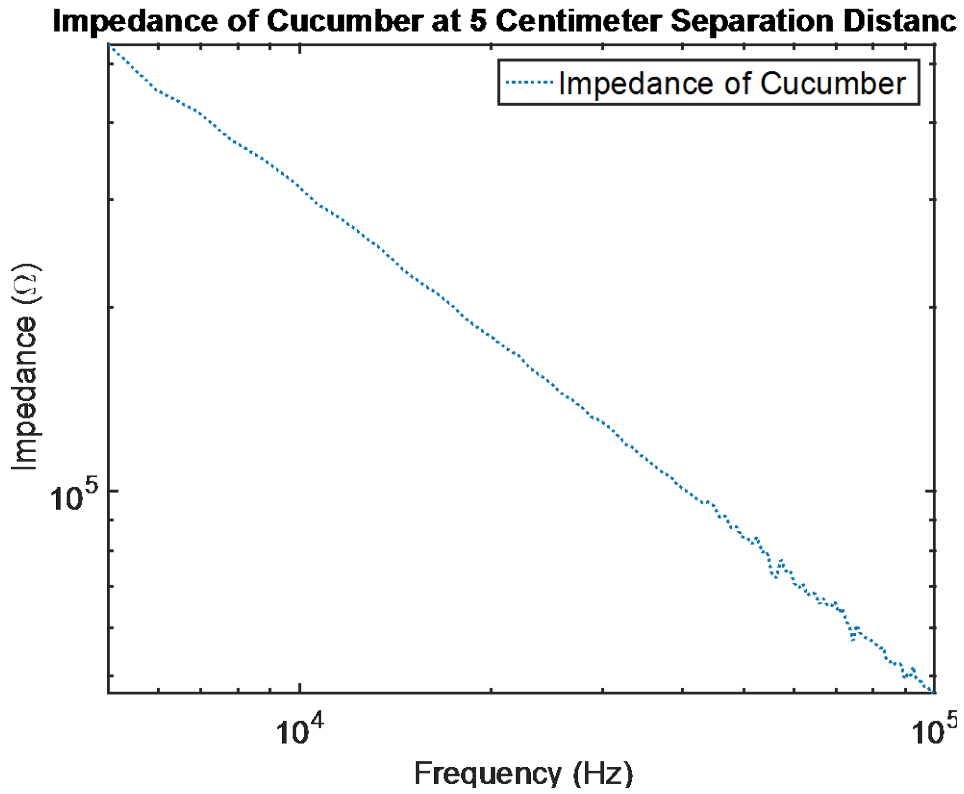
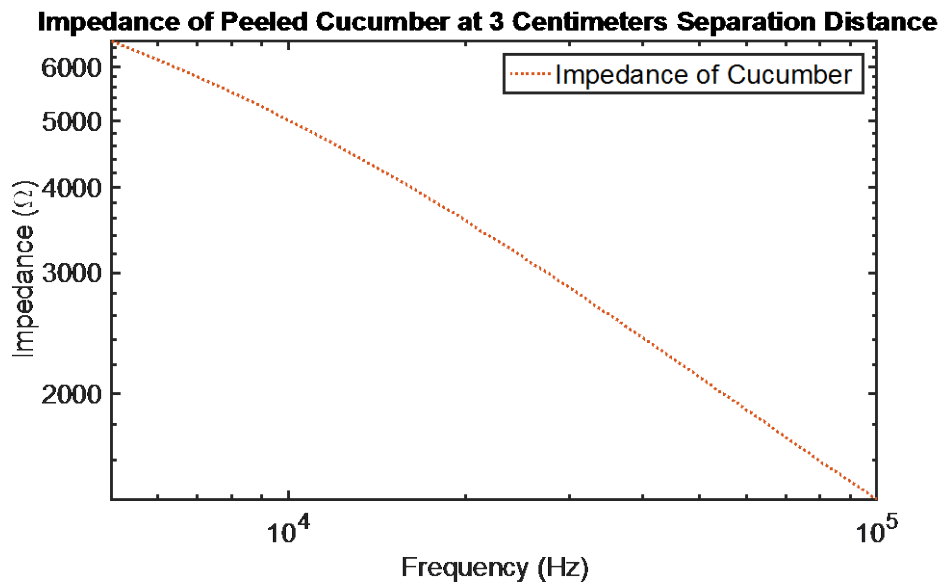


Figure A-8: Impedance of Cucumber at 3cm Separation Distance



*Figure A-9: Impedance of Cucumber at 5cm Separation Distance*



*Figure A-10: Impedance of Peeled Cucumber at 3cm Separation Distance*

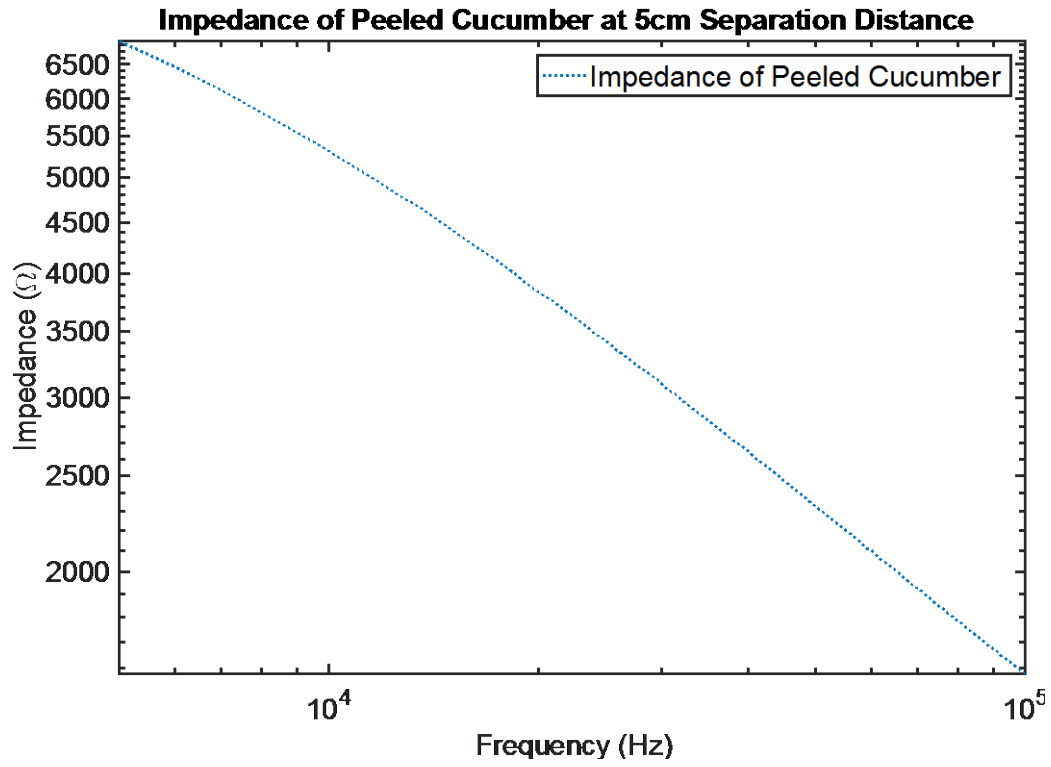


*Figure A-11: Impedance of Peeled Cucumber at 5cm Separation Distance*

*Appendix B: Post-Material Selection Experiments*

*Pressure Ulcer Simulation Experiment*

Potato I

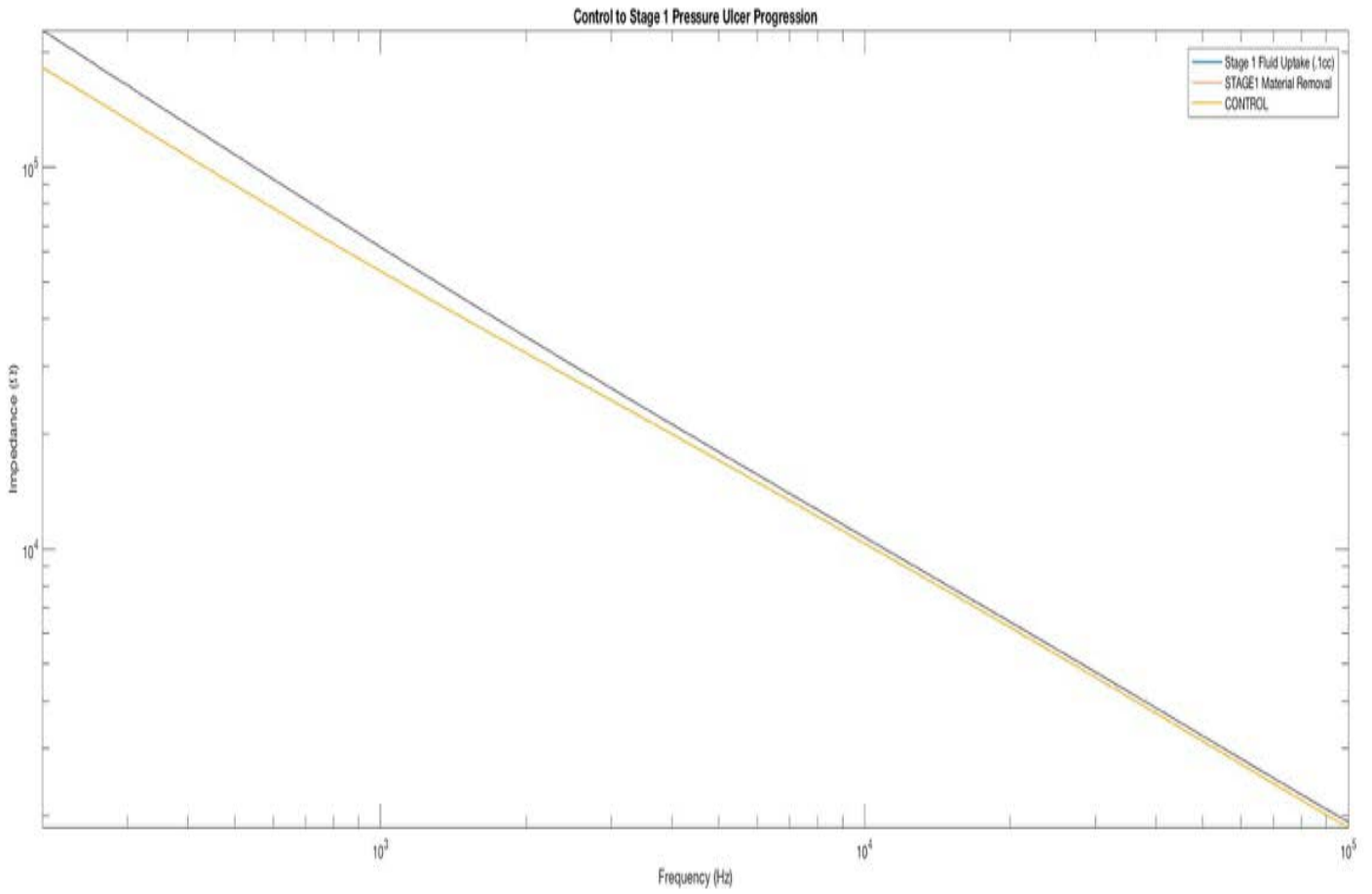


*Figure B-1: Progression from Control to Stage I Pressure Ulcer Simulation in Potato I*

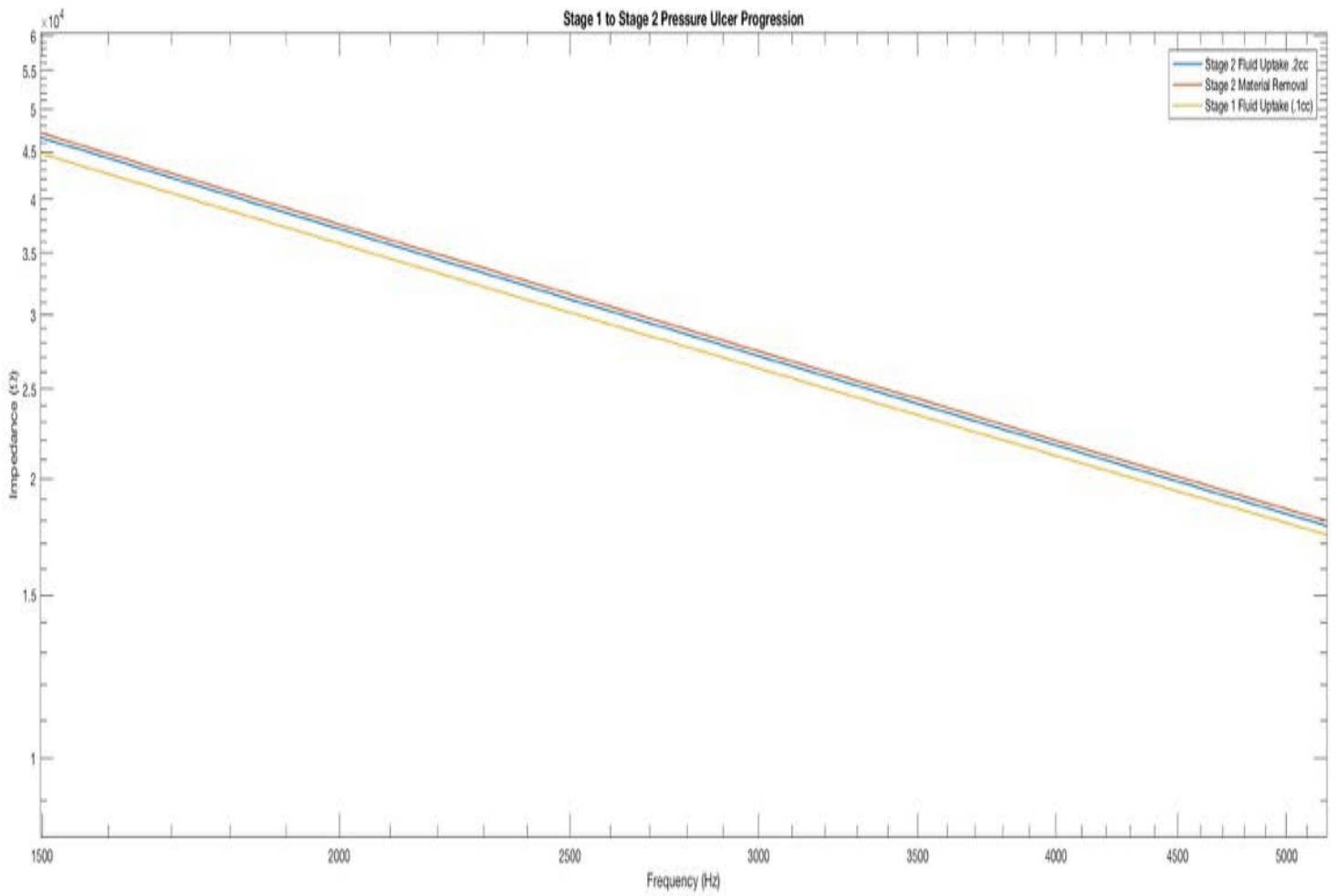


*Figure B-2: Progression from Stage I to Stage II Pressure Ulcer Simulation in Potato I*

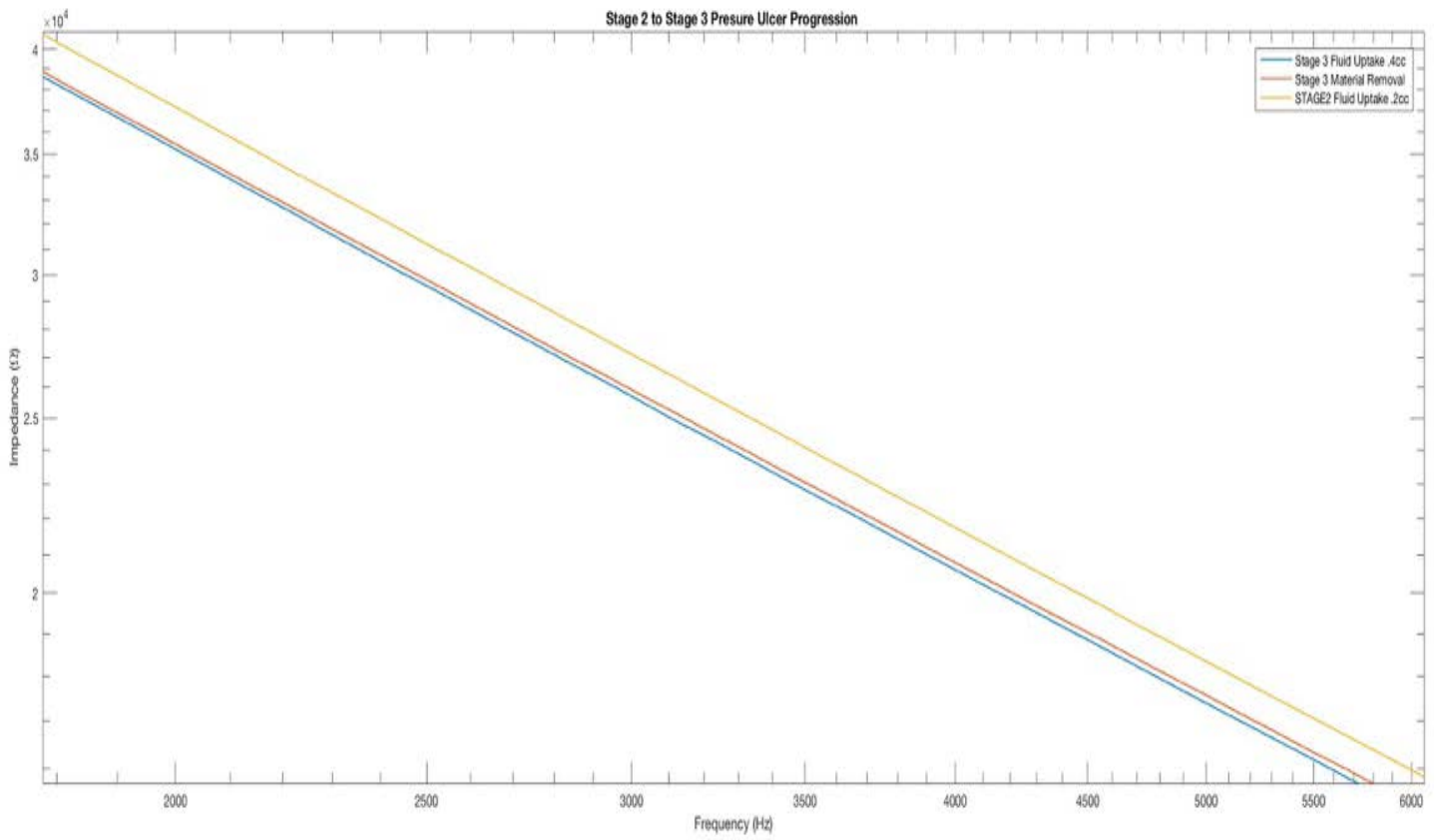


Figure B-3: Progression from Stage III to Stage III Pressure Ulcer Simulation in Potato I

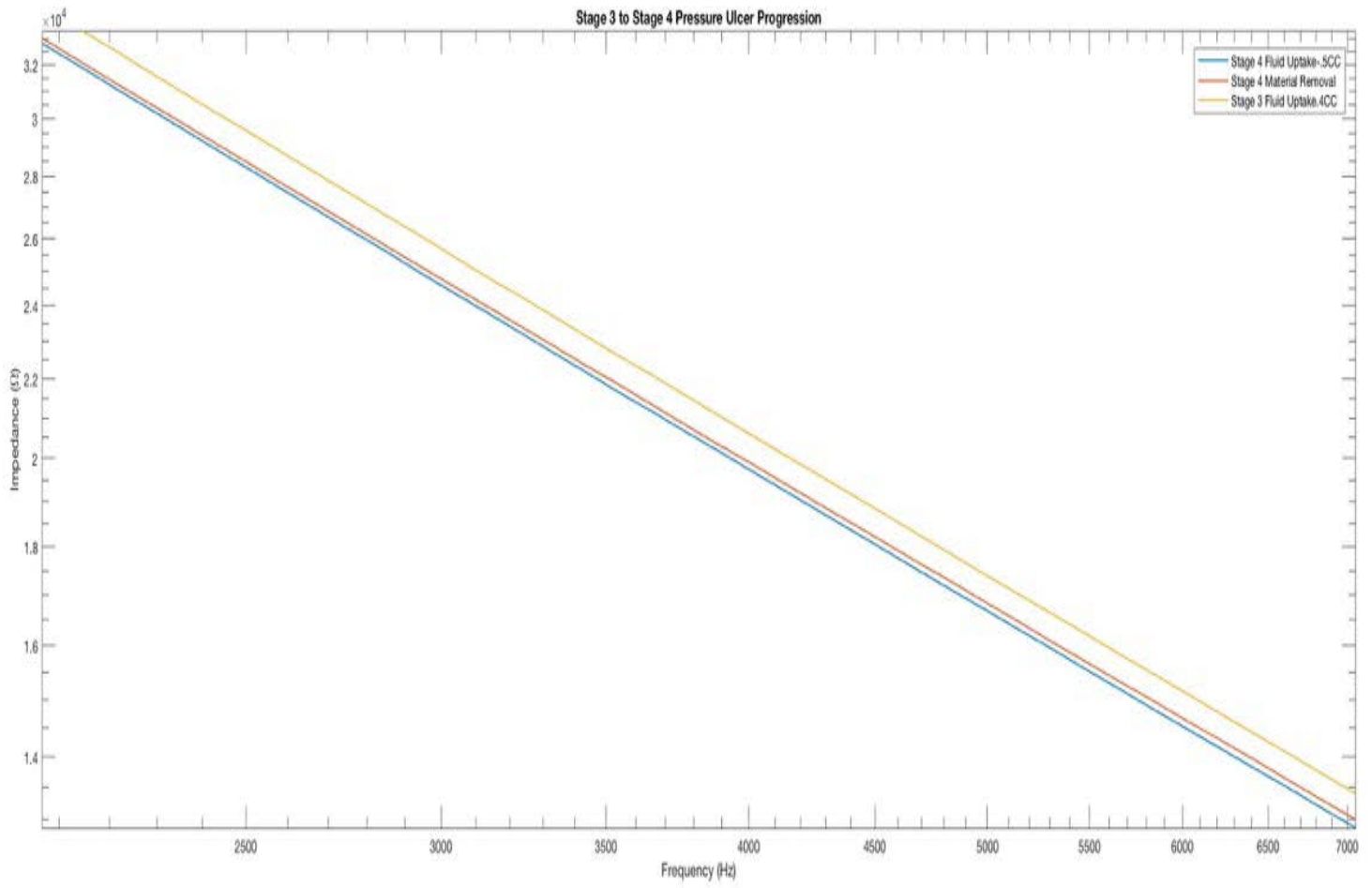


Figure B-4: Progression from Stage III to Stage IV Pressure Ulcer Simulation in Potato I

Potato II

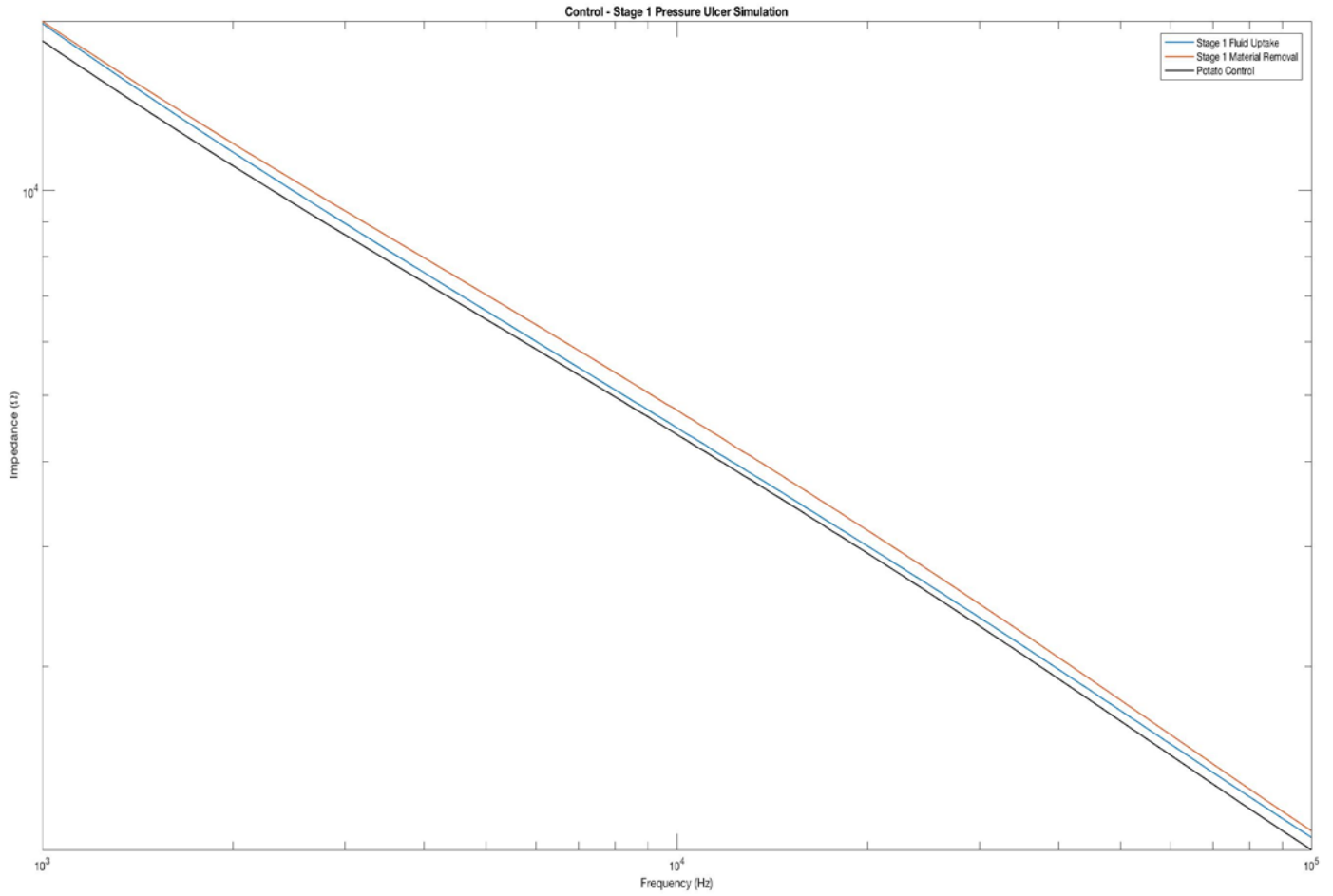


Figure B-5: Progression from Control to Stage I Pressure Ulcer Simulation in Potato Sample II

Stage 1 - Stage 2 Pressure Ulcer Simulation

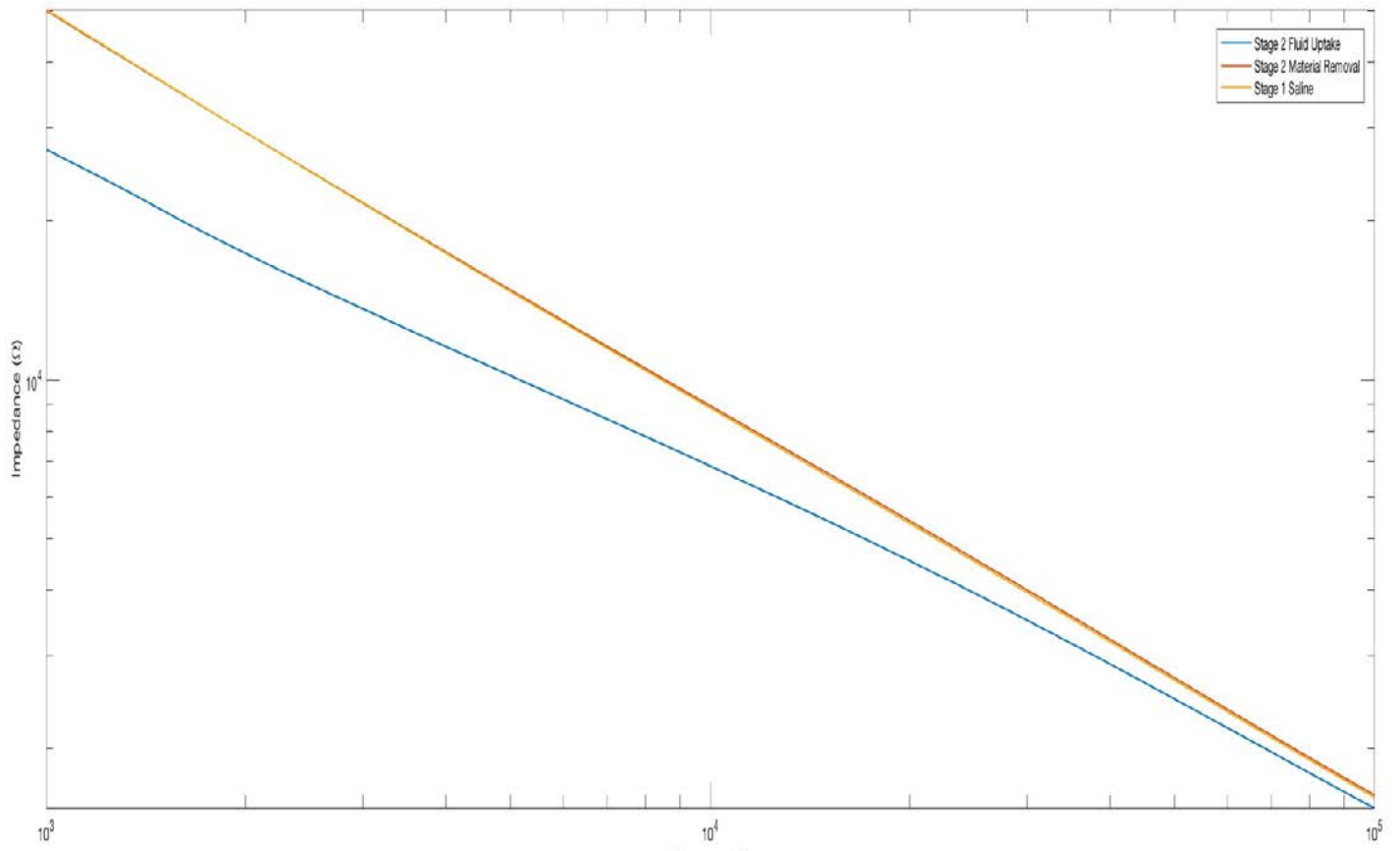


Figure B-6: Progression from Stage I to Stage II Pressure Ulcer Simulation in Potato Sample II

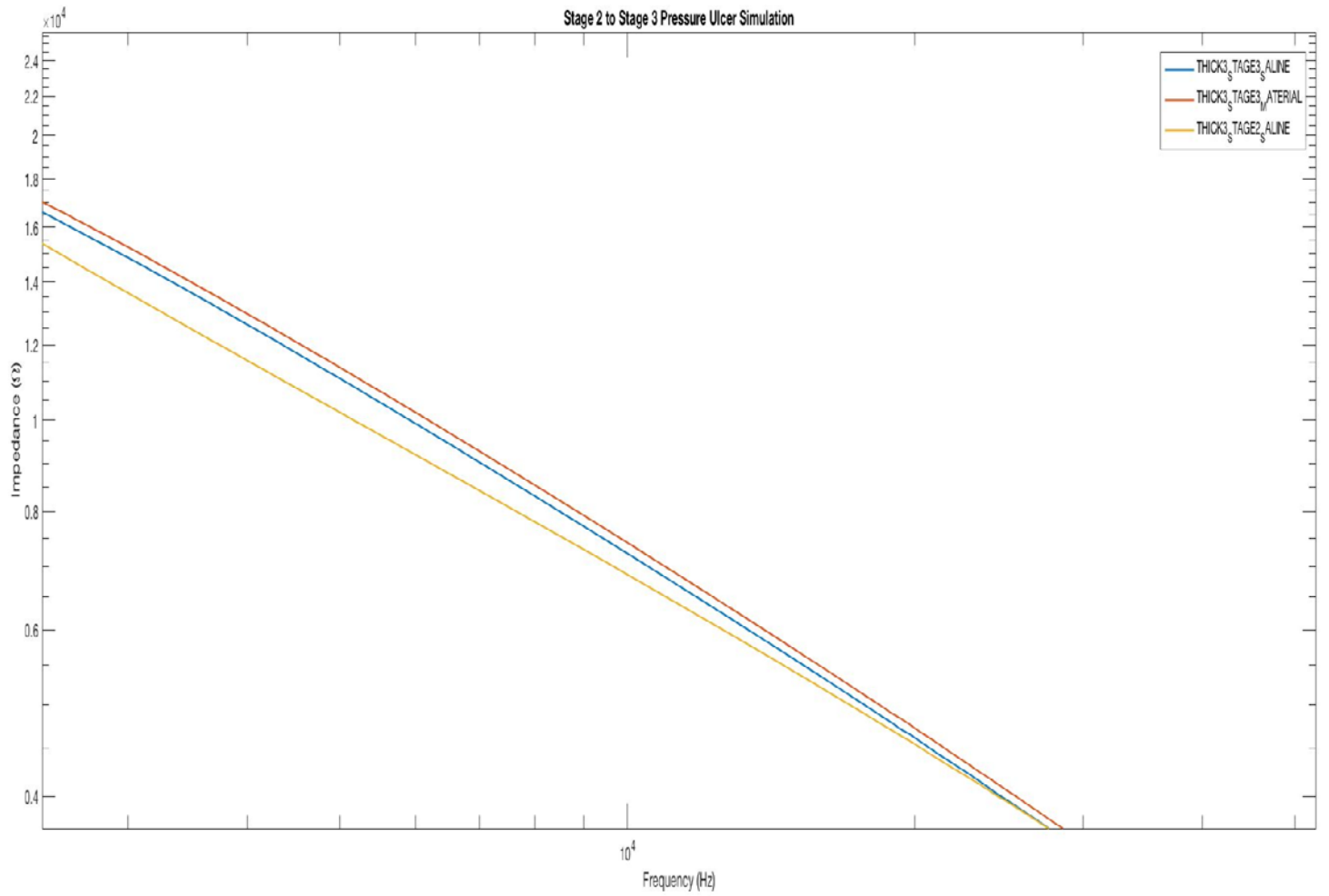


Figure B-7: Progression from Stage II to Stage III Pressure Ulcer Simulation in Potato Sample II

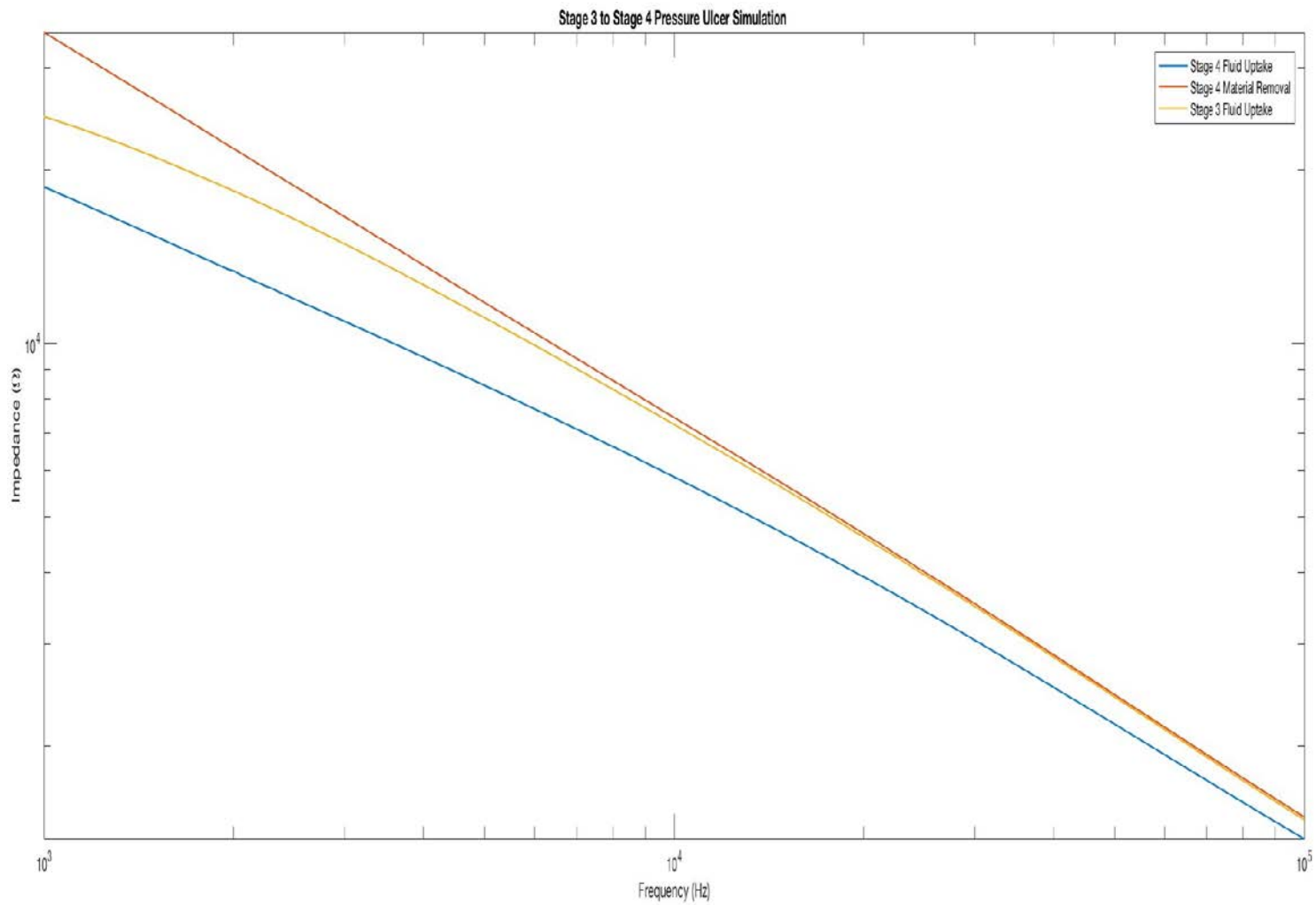
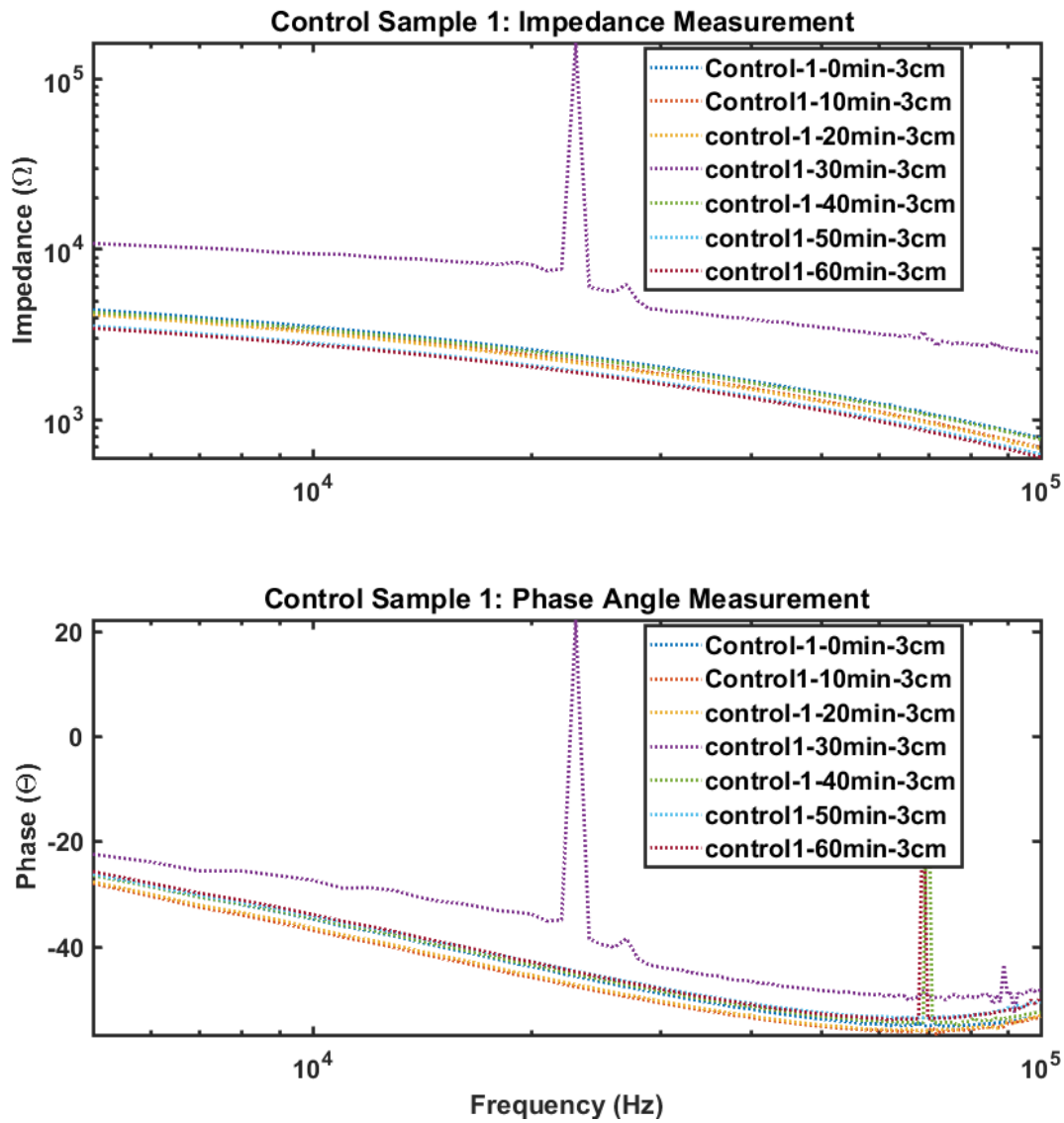


Figure B-8: Progression from Stage III to Stage IV Pressure Ulcer Simulation in Potato Sample II

*Appendix C: Potato Drying Experiment*

*Potato Sample I*

*Control*



*Figure C-1: Control Measurement of Potato Drying Sample I*

Level 2 Heat Setting (Low)

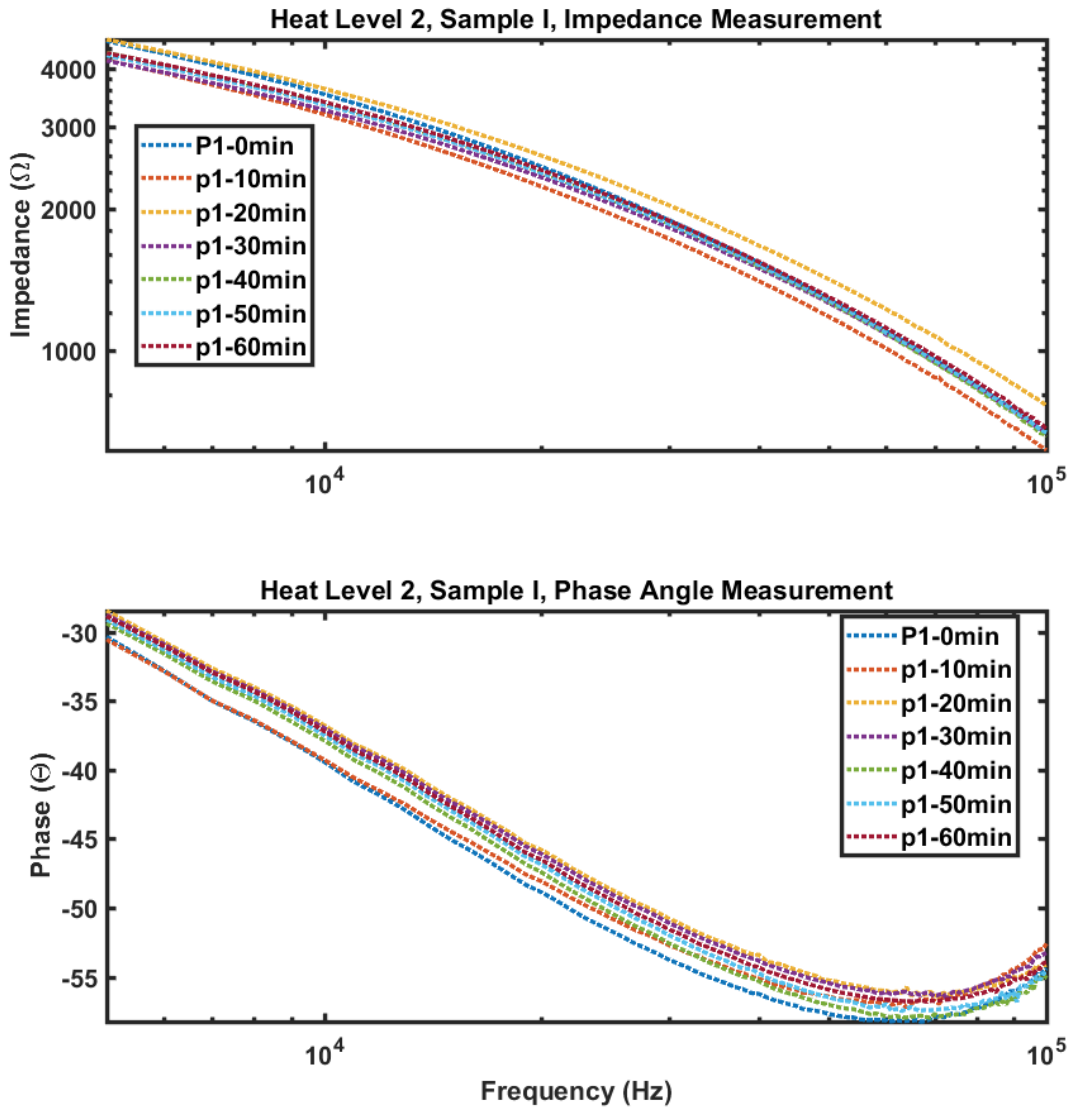


Figure C-2: Lowest Heat Setting for Potato I

Level 4 Heat Setting (Medium)

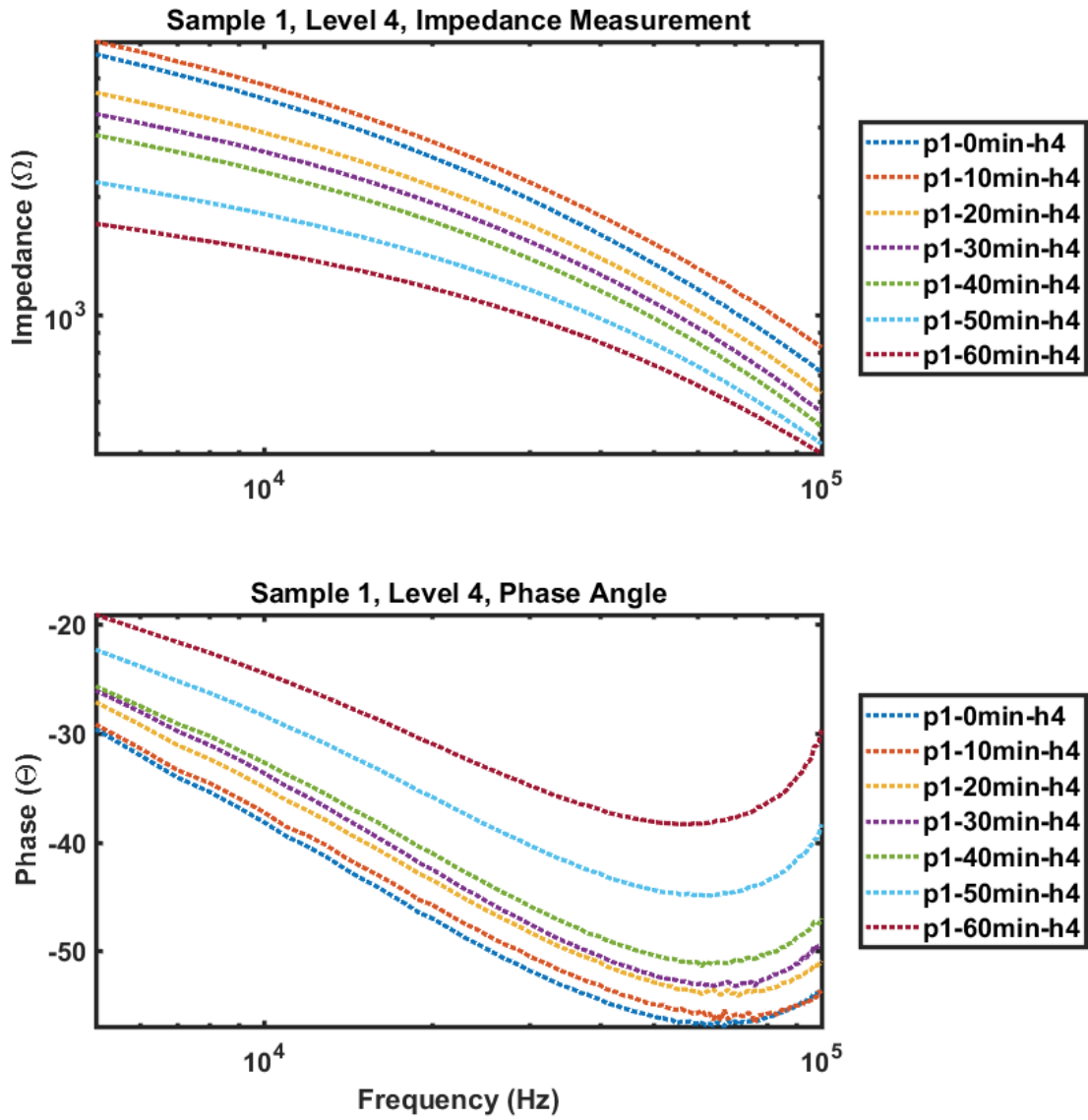


Figure C-3: Medium Heat Setting for Potato I

Level 6 Heat Setting (High)

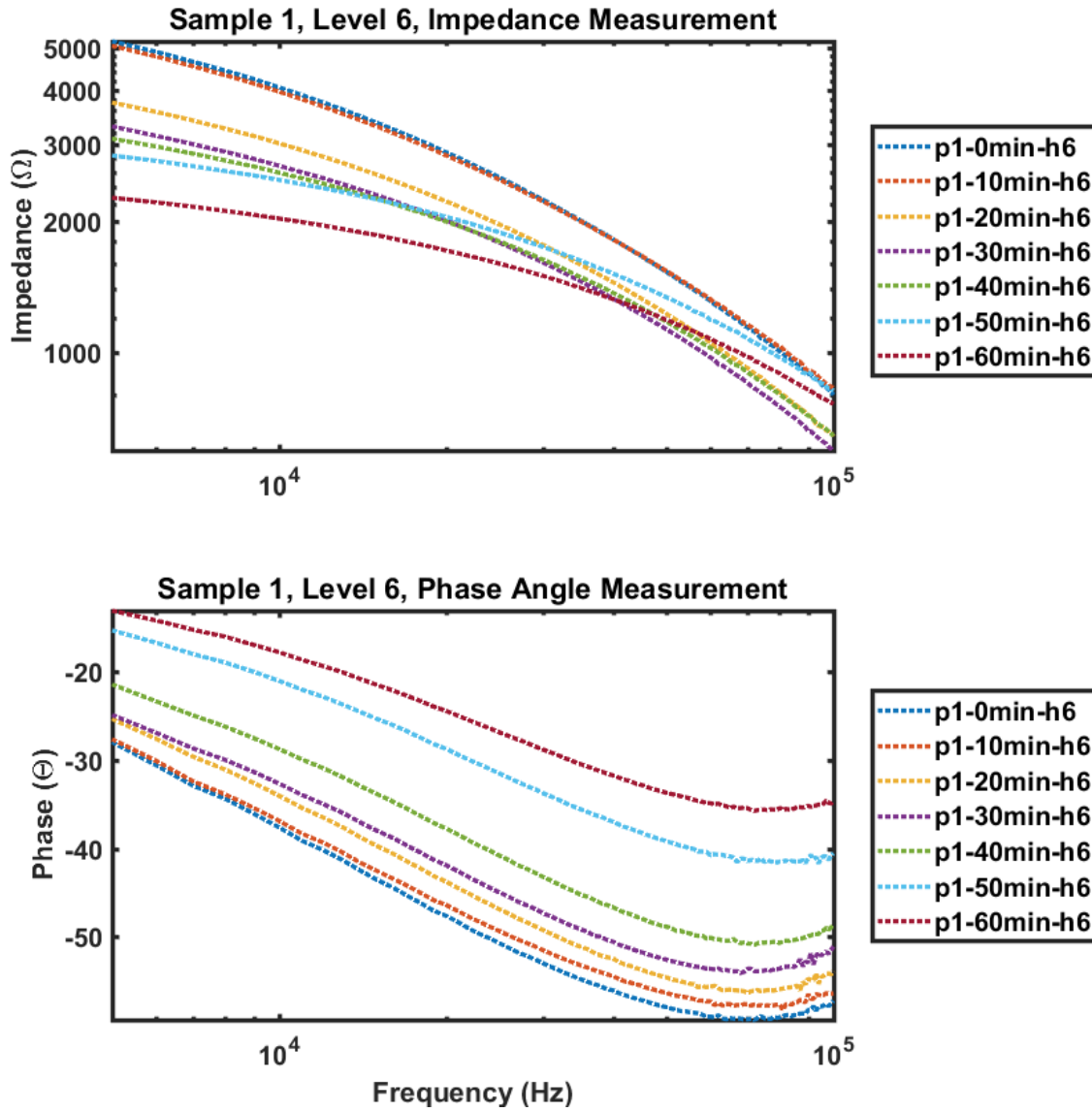


Figure C-4: High Heat Setting for Potato I

Potato Sample II

Control

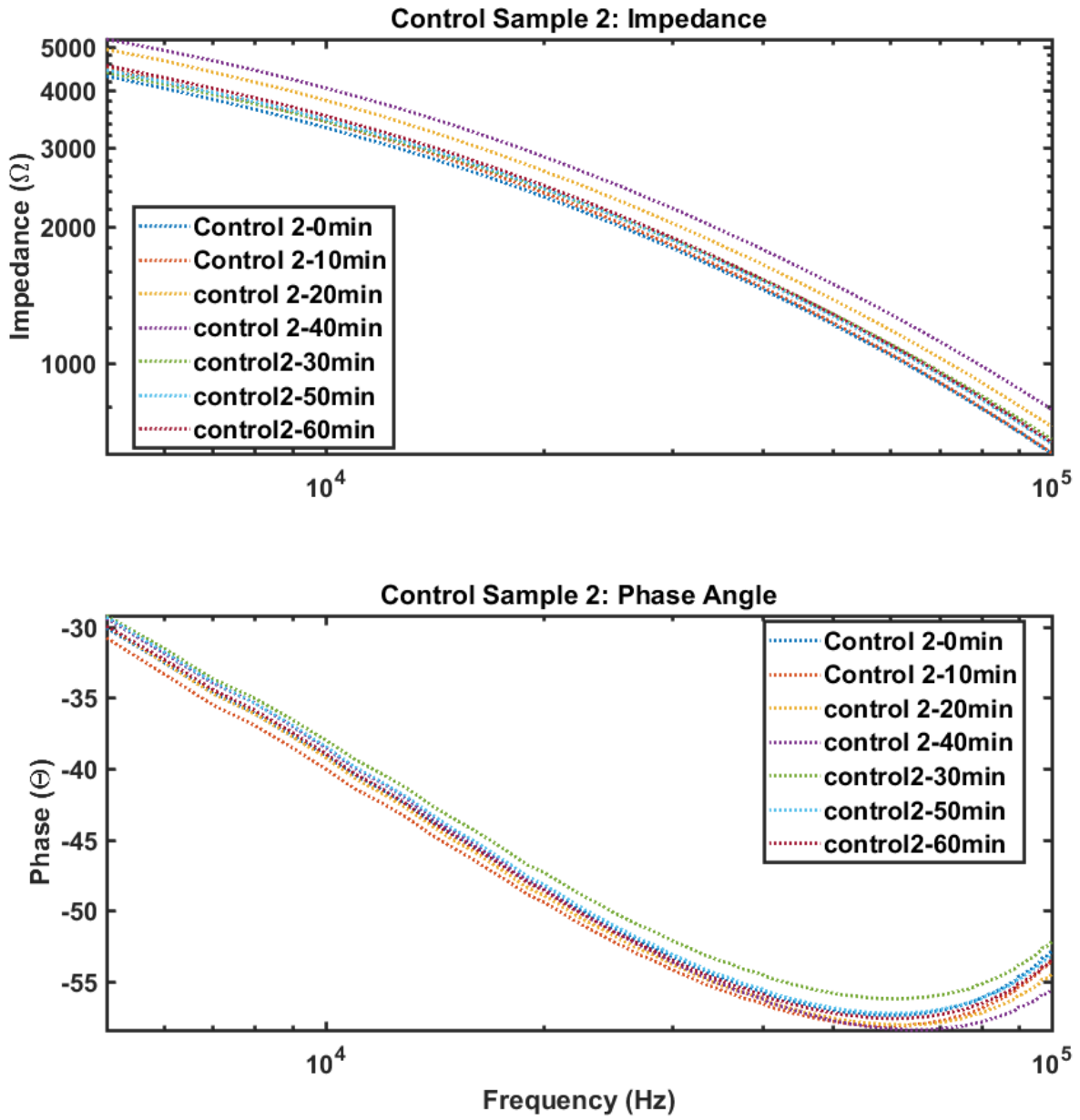


Figure C-5: Control Measurement of Potato Drying Sample II

Level 2 Heat Setting Low

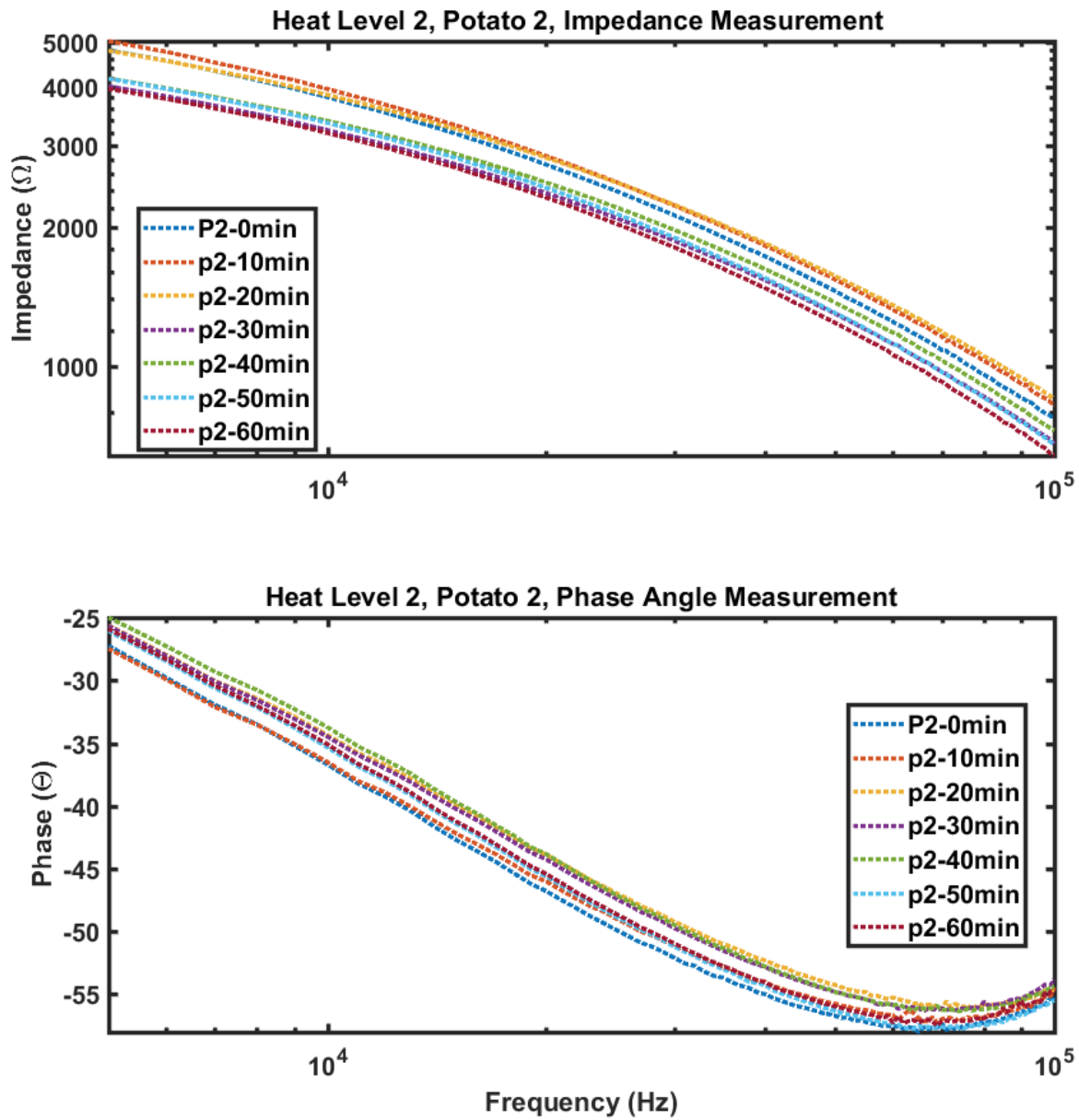


Figure C-6: Low Heat Setting for Potato II

Level 4 Heat Setting (Medium)

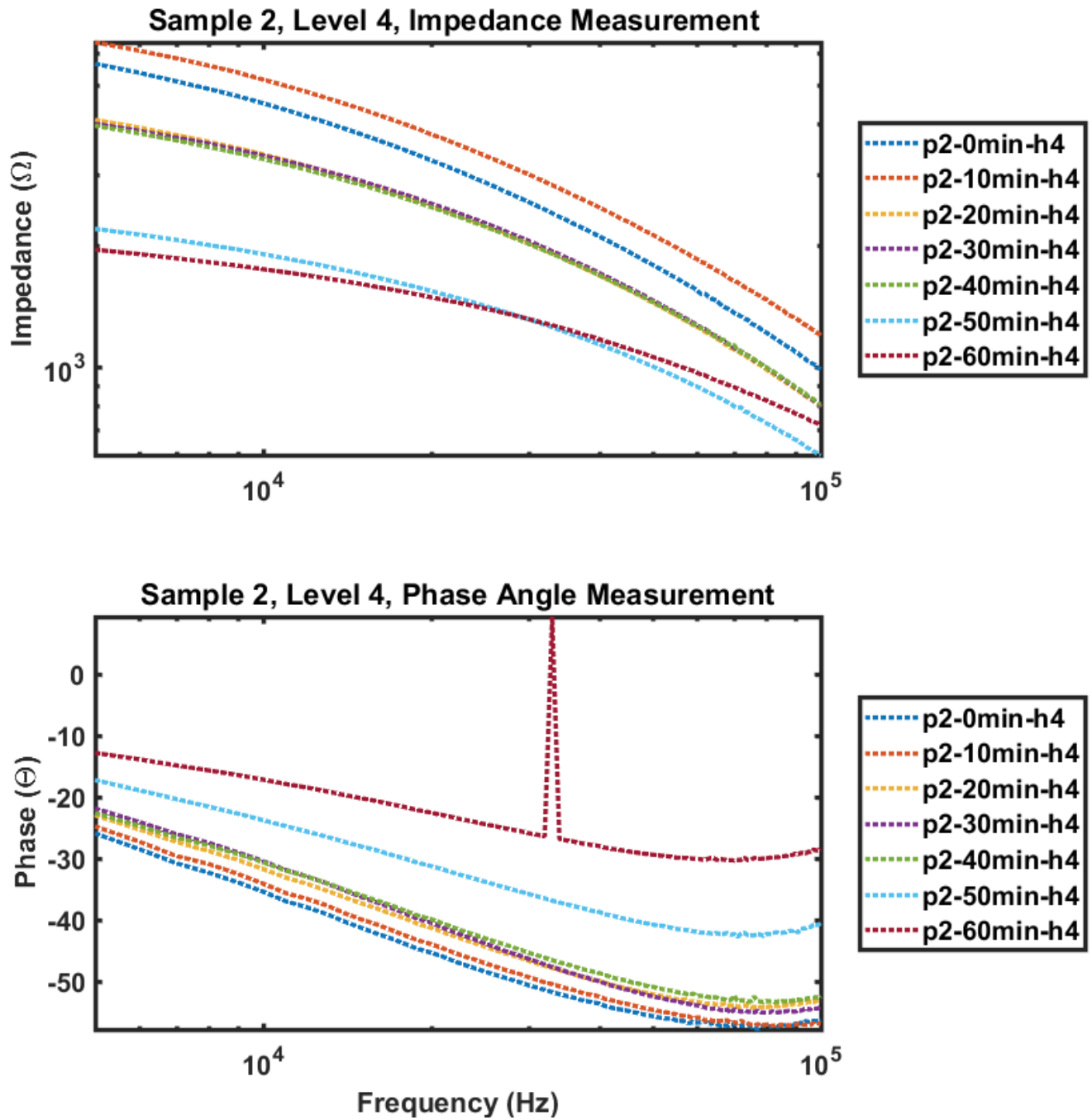


Figure C-7: Medium Heat Setting for Potato II

Level 6 Heat Setting (High)

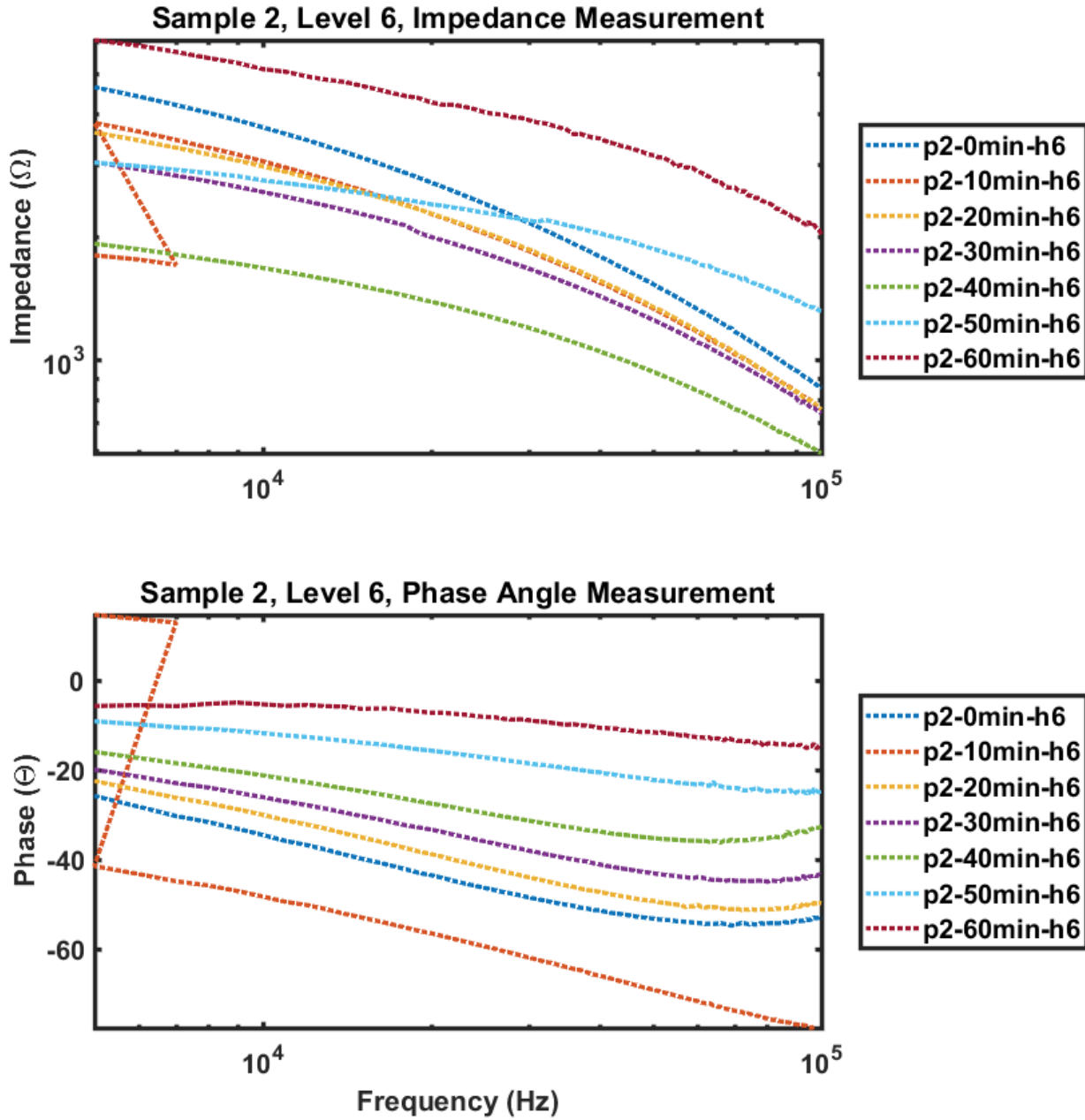


Figure C-8: High Heat Setting for Potato II

Potato Sample III

Control

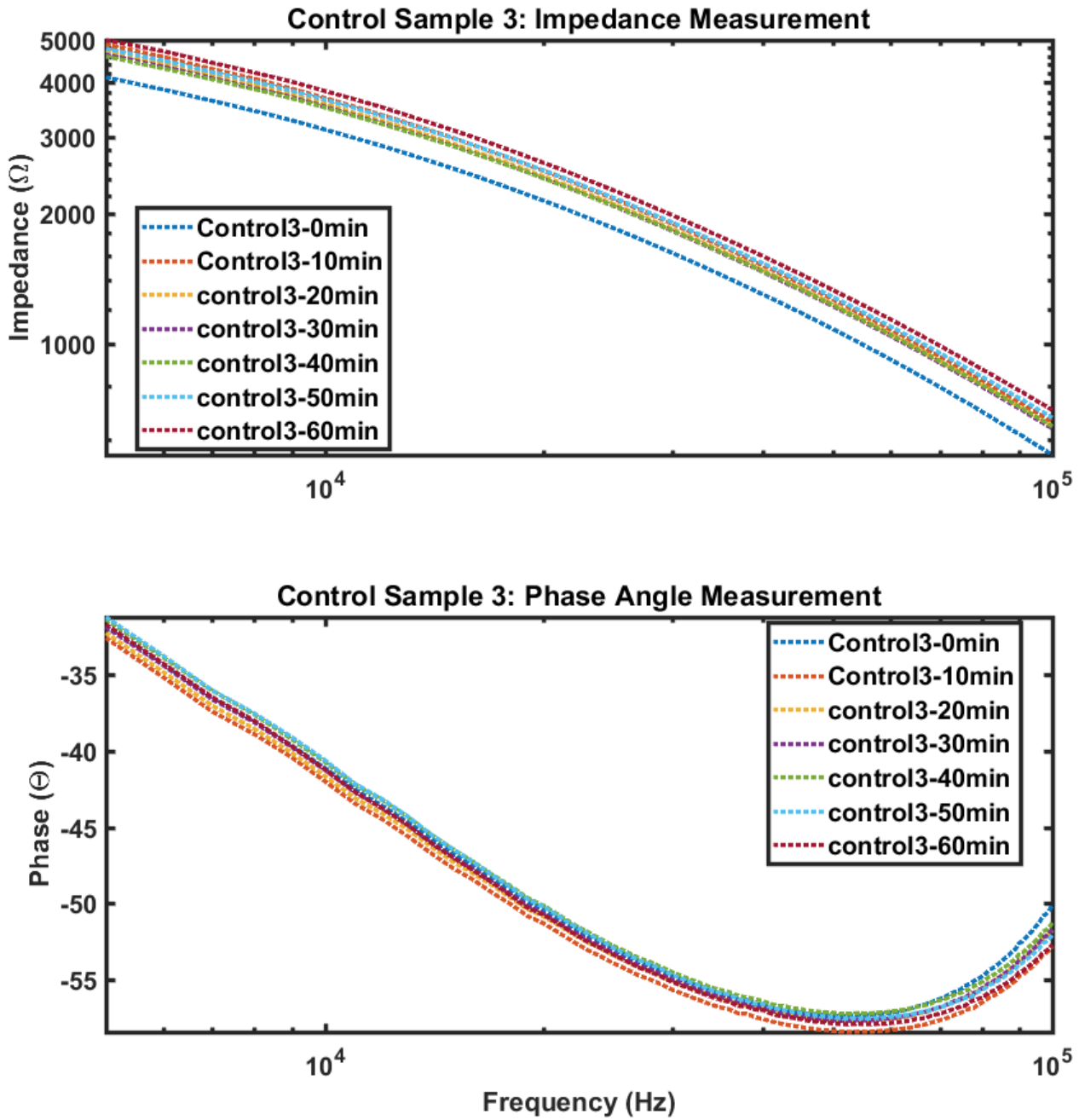


Figure C-9: Control Measurement of Potato Drying Sample III

Level 2 Heat Setting (Low)

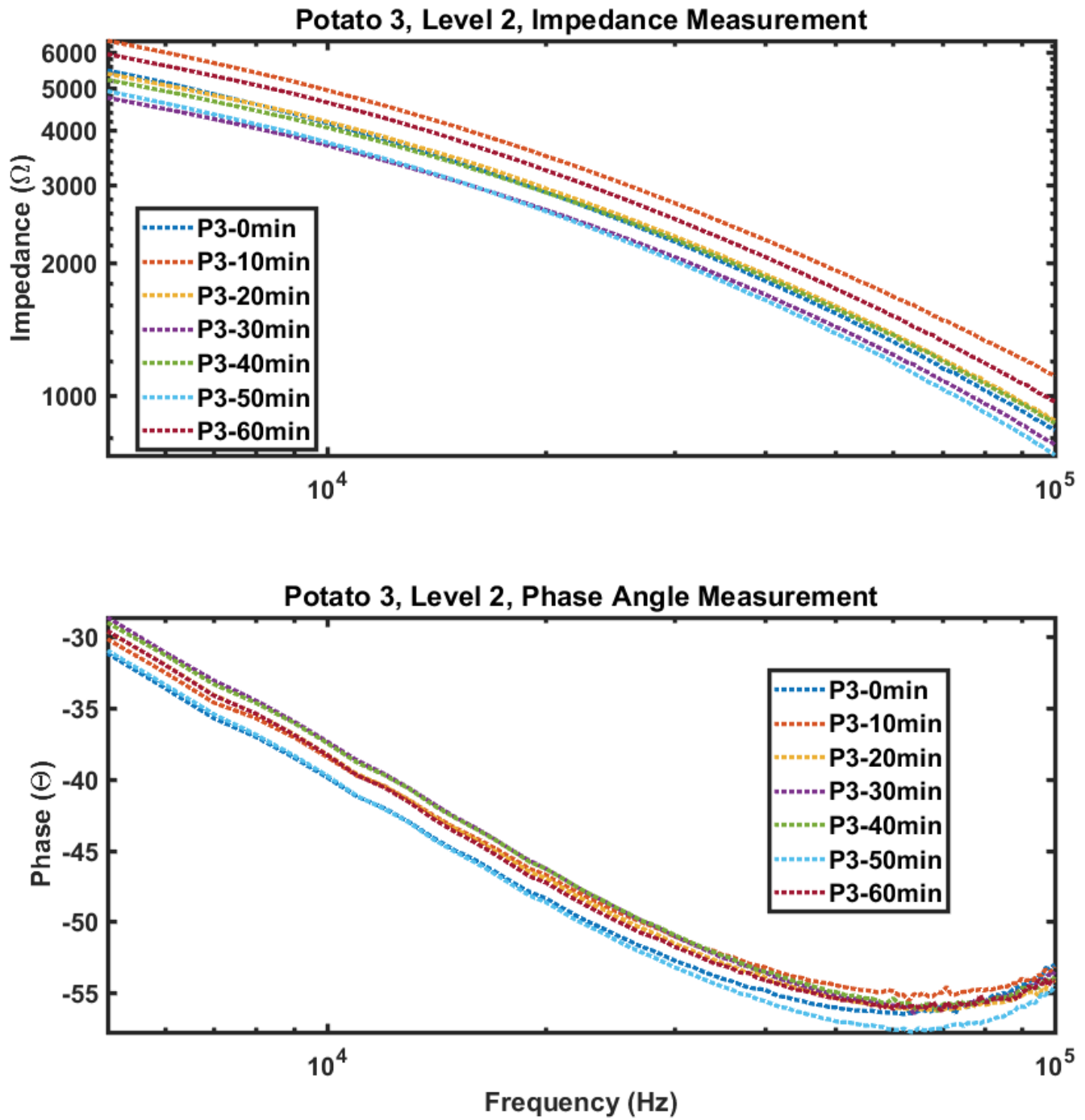
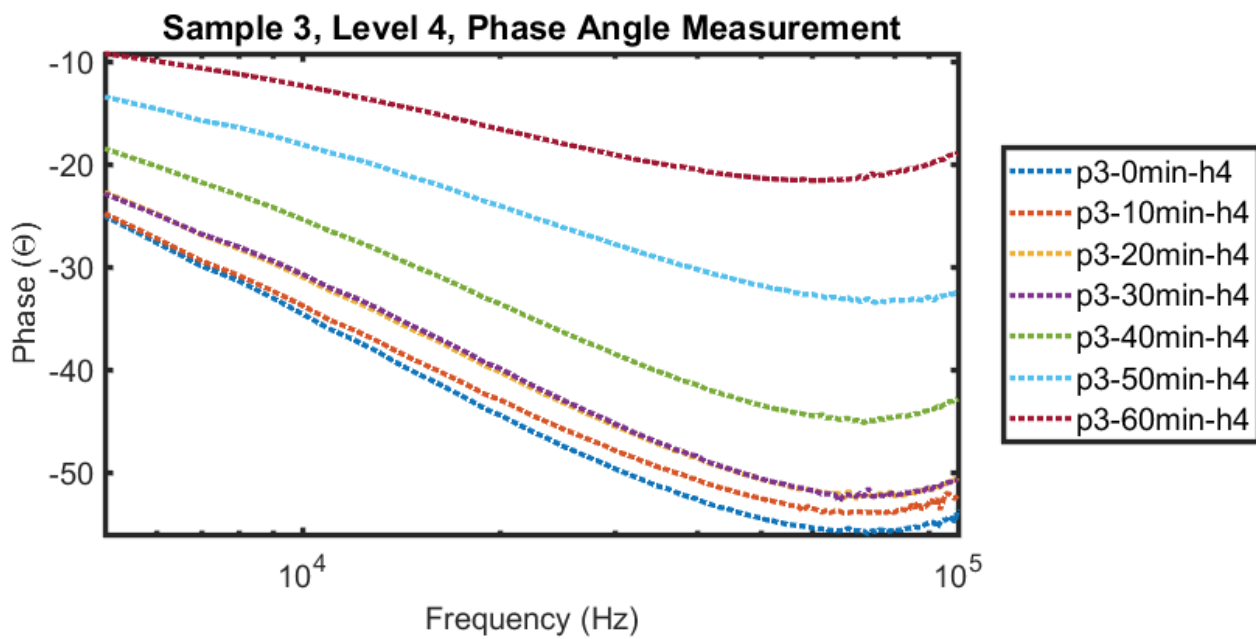
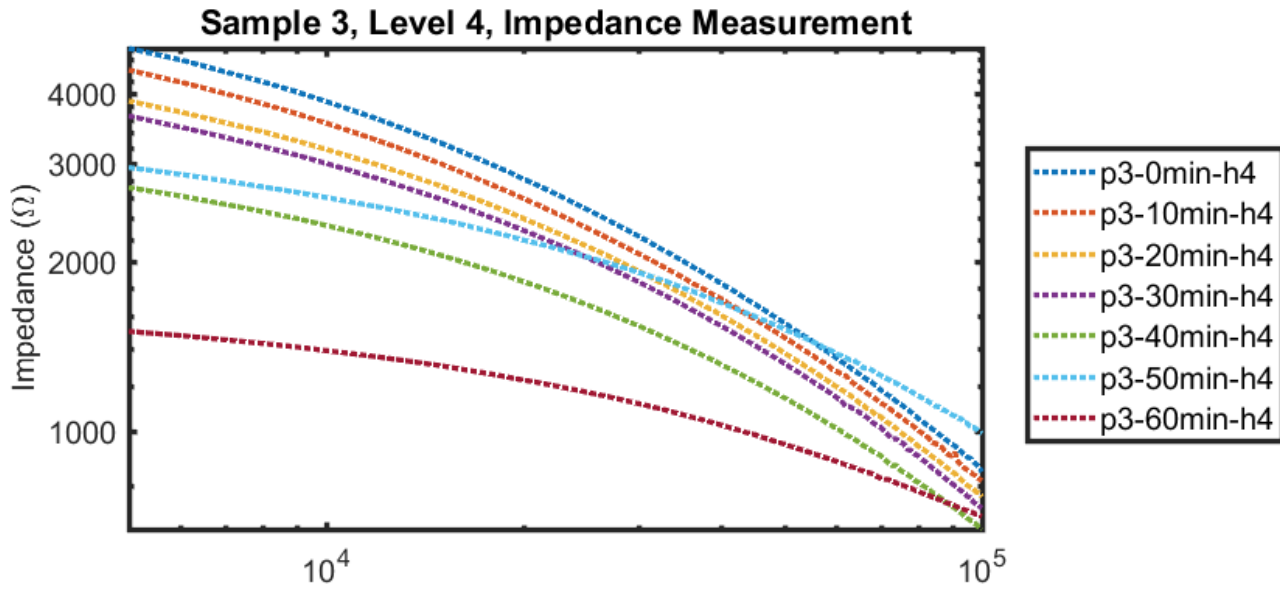


Figure C-10: Low Heat Setting for Potato III

Level 4 Heat Setting (Medium)



*Figure C-11: Medium Heat Setting for Potato III*

Level 6 Heat Setting (High)

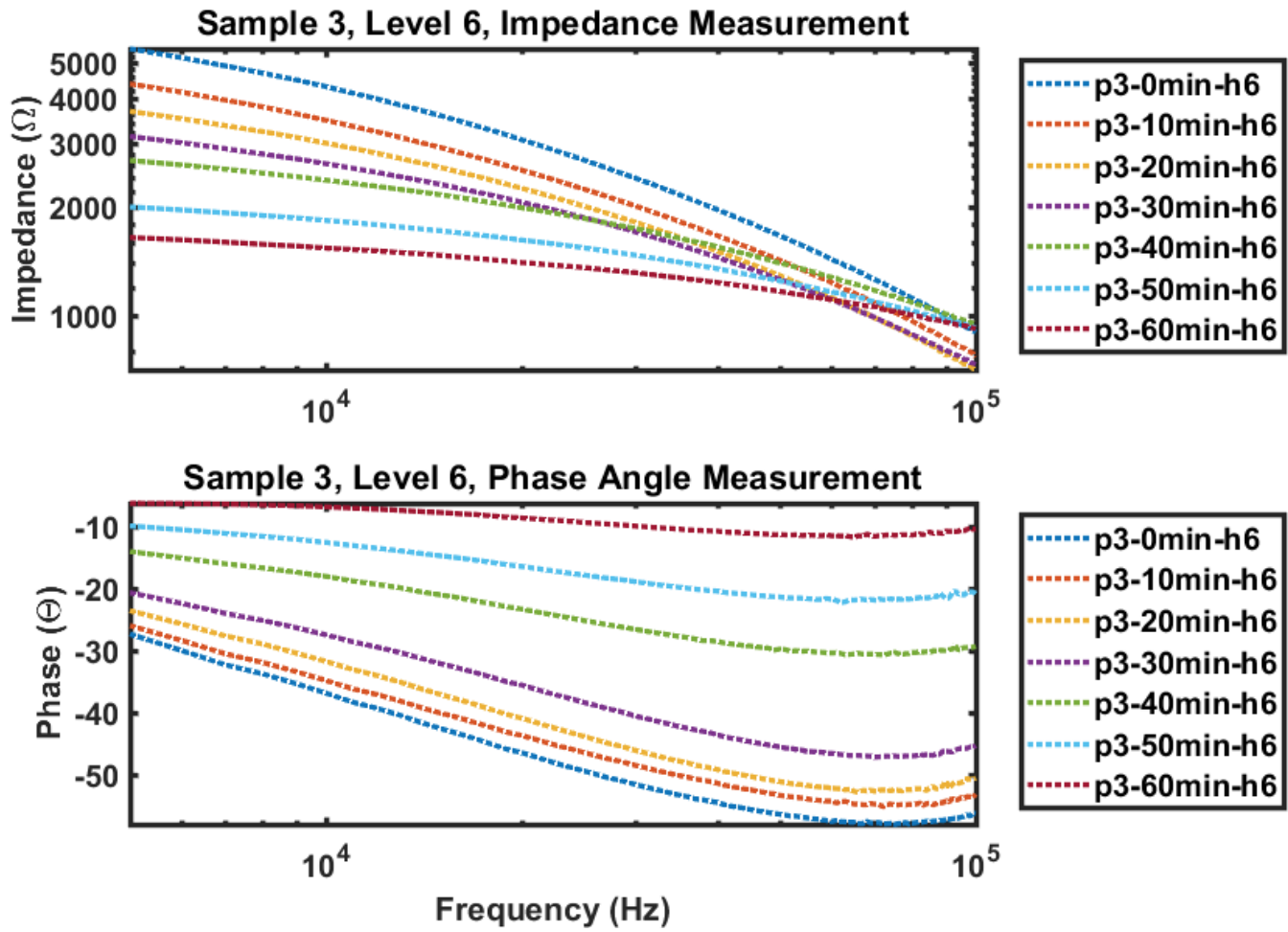


Figure C-12: High Heat Setting for Potato III

## ***Appendix D: MATLAB Code***

### ***MATLAB code to load data***

```
% Loads data from AFE4404EVM files (code or volts only)

% Does not work on xls files (which the TI GUI creates, re-save as.xlsx)

% Outputs:

% data_cell : imported data cell

% data      : data matrix (column vectors)

% PathName  : Path string

% FileName  : File Name String

% JRH 3_16_2017

function [data,PathName,FileName] = loadtxtdata(PathName,FileName)

%% Check Inputs

if ~exist('PathName') || ~exist('FileName') || isempty(FileName) || isempty(PathName)

    [FileName,PathName] = uigetfile('*.txt','Select txt file','MultiSelect','on');

end

%% Load Data

delimiterIn = ' ';

if iscell(FileName)

    [~,c] = size(FileName); % find number of columns (aka number of files)
```

```
data = cell(1,c); % Cell with 'c' entries
for i=1:c
    filedata = importdata([PathName,FileName{ 1,i}],delimiterIn);
    data{ 1,i}=filedata;
end
else
    data = importdata([PathName,FileName],delimiterIn);
end
end
```

### *MATLAB code to plot Bioimpedance Device data*

```
%% Load SEM Data

[data,PathName,FileName] = loadtxtdata();

addpath(PathName)

CalibFileName = '500_Ohm_40mV_Cal.mat';

GFCalFLAG = 1; % 1 for determining calibration, 0 for not calibrating

if iscell(data)==0

    F = data(:,1); % Frequency Vector

    R = data(:,2); % Real Vector

    I = data(:,3); % Imaginary Vector

    NAME = FileName(1:end-4);NAME(NAME=='_')=' '; % FileName for legend

    numincr = 96;          % Number of frequencies ( 5933 [inccrem+1] )

    numrep = length(R)/numincr; % Number of repetitions

    load(CalibFileName)

    try clear Imp Pha;catch;end

    if GFCalFLAG == 1; GF = 1*ones(96,1); end % turn on for calibration

    k = 1; % Column of Imp

    for i = 1:length(R)

        ind = i - numincr*(k-1);

        % Impedance Matrix [numincr,numrep]

        Imp(ind,k) = 1/(GF(ind)*sqrt(R(i).^2+I(i).^2)); % One Point Calibration

        % Phase Matrix
```

```

if R(i)>0 && I(i)>0
    Pha(ind,k) = atan(I(i)/R(i))*180/pi;
elseif R(i)>0 && I(i)<0
    Pha(ind,k) = 360 + atan(I(i)/R(i))*180/pi;
else
    Pha(ind,k) = 180 + atan(I(i)/R(i))*180/pi;
end

% Increment k (repetition number)
if mod(i,numincr)==0
    k = k+1;
end

end

F = F(1:numincr); % Adjust Frequency array to one run (for plotting)

meanImp = mean(Imp,2); % Mean of Impedance
stdImp = std(Imp,0,2); % Standard Deviation of Impedance
meanPha = mean(Pha,2); % Mean of Phase
stdPha = std(Pha,0,2); % Standard Deviation of Phase

figure(1)
subplot(2,1,1); ax1 = gca;
loglog(F.*1000,meanImp,'.-','DisplayName',NAME);hold
on;legend(gca,'show','location','best');axis('tight')

subplot(2,1,2); ax2 = gca;
semilogx(F.*1000,meanPha-PhaCal,'.-','DisplayName',NAME); hold
on;legend(gca,'show','location','best');axis('tight')

```

```

figure(2); ax3 = gca;
REAL = abs(abs(meanImp).*cos(pi/180*(meanPha-PhaCal)));
IMAG = abs(meanImp).*sin(pi/180*(meanPha-PhaCal));
plot(REAL,-IMAG,'o','DisplayName',NAME); hold on;legend(gca,'show','location','best');axis('tight')

else

[~,c] = size(data);
for j=1:c
    F = data{1,j}(:,1); % Frequency Vector
    R = data{1,j}(:,2); % Real Vector
    I = data{1,j}(:,3); % Imaginary Vector
    NAME = FileName{1,j}(1:end-4);NAME(NAME=='_')=' '; % FileName for legend
    numincr = 96;          % Number of frequencies ( 5933 [incrunum+1] )
    numrep = length(R)/numincr; % Number of repetitions
    load(CalibFileName)
    try clear Imp Pha;catch;end

    k = 1; % Column of Imp
    for i = 1:length(R)
        ind = i - numincr*(k-1);
        % Impedance Matrix [numincr,numrep]
        Imp(ind,k) = 1/(GF(ind)*sqrt(R(i).^2+I(i).^2)); % One Point Calibration
        % Phase Matrix
        if R(i)>0 && I(i)>0
            Pha(ind,k) = atan(I(i)/R(i))*180/pi;
        end
    end
end

```

```

elseif R(i)>0 && I(i)<0
    Pha(ind,k) = 360 + atan(I(i)/R(i))*180/pi;
else
    Pha(ind,k) = 180 + atan(I(i)/R(i))*180/pi;
end

% Increment k (repetition number)
if mod(i,numincr)==0
    k = k+1;
end

end

F = F(1:numincr); % Adjust Frequency array to one run (for plotting)

meanImp = mean(Imp,2); % Mean of Impedance
stdImp = std(Imp,0,2); % Standard Deviation of Impedance
meanPha = mean(Pha,2); % Mean of Phase
stdPha = std(Pha,0,2); % Standard Deviation of Phase

figure(1)
subplot(2,1,1); ax1 = gca;
loglog(F.*1000,meanImp,'.-','DisplayName',NAME);hold
on;legend(gca,'show','location','best');axis('tight')
subplot(2,1,2); ax2 = gca;
semilogx(F.*1000,meanPha-PhaCal,'.-','DisplayName',NAME); hold
on;legend(gca,'show','location','best');axis('tight')
figure(2); ax3 = gca;
REAL = abs(abs(meanImp).*cos(pi/180*(meanPha-PhaCal)));

```

```

    IMAG = abs(meanImp).*sin(pi/180*(meanPha-PhaCal));

    plot(REAL,-IMAG,'o','DisplayName',NAME); hold
on;legend(gca,'show','location','best');axis('tight')

    end

end

%% FOR CALIBRATION, set GF = 1 and set the DENOMINATOR to the resistor value

GF = meanImp./18000;

PhaCal = meanPha;

%% FOR SAVING CALIBRATION

save('500_Ohm_40mV_Cal','GF','PhaCal')

%% Load and Plot Keysight Data

[data,PathName,FileName] = loadKeySightdata(); %load data, from one or more files

LS = '-'; % LineStyle

CS = '*'; % Cole-Cole Style

KEYDATA = data;

ax1.ColorOrderIndex = 1; % Reset color order

ax2.ColorOrderIndex = 1;

ax3.ColorOrderIndex = 1;

if iscell(data)==0 % if single data loaded then plot it

    F = data(:,1); % Frequency Vector

    Z = data(:,2); % Impedance Vector

    Phase = data(:,3); % Phase Angle Vector

    Res = data(:,4);

    Reac = data(:,5);

    NAME = FileName(1:end-4);NAME(NAME=='_')=' '; % FileName for legend

```

```

figure(1)
subplot(2,1,1)
loglog(F,Z,LS,'DisplayName',NAME);ylabel('Impedance (\Omega)');hold on
subplot(2,1,2)
semilogx(F,Phase,LS,'DisplayName',NAME);xlabel('Frequency (Hz)');ylabel('Phase (\Theta)');hold
on
figure(2)
plot(Res,-Reac,CS,'DisplayName',NAME);xlabel('Resistance (\Omega)');ylabel('-Reactance
(\Omega)');hold on
else % if more than one data loaded
[~,c] = size(data);
for i=1:c
    F = data{1,i}(:,1); % Frequency Vector
    Z = data{1,i}(:,2); % Impedance Vector
    Phase = data{1,i}(:,3); % Phase Angle Vector
    Res = data{1,i}(:,4); % Resistance Vector
    Reac = data{1,i}(:,5); % Reactance Vector
    NAME = FileName{1,i}(1:end-4);NAME(NAME=='_')=' '; % FileName for legend

figure(1)
subplot(2,1,1)
loglog(F,Z,LS,'DisplayName',NAME);ylabel('Impedance (\Omega)');hold on
subplot(2,1,2)
semilogx(F,Phase,LS,'DisplayName',NAME);xlabel('Frequency (Hz)');ylabel('Phase
(\Theta)');hold on
figure(2)

```

```
plot(Res,-Reac,CS,'DisplayName',NAME);xlabel('\Omega');ylabel('-Reactance  
(\Omega)');hold on
```

```
end
```

```
end
```

```
figure(1);legend(gca,'show');axis('tight')
```

```
figure(2);legend(gca,'show');axis('tight')
```

```
%%
```

```
% THEORETICAL SIMULATIONS BELOW
```

```
%
```

```
%% 10 K res
```

```
F = [5e3:1e3:1e5]';
```

```
RESISTOR = 10000;
```

```
ResT = RESISTOR*ones(96,1);
```

```
ReacT = zeros(96,1);
```

```
%% 1 nF CAP
```

```
F = [5e3:1e3:1e5]';
```

```
ResT = 0*ones(96,1);
```

```
ReacT = 1/(2*pi*1e-9)./F;
```

```
%% 10 series with 39K and 1nF parallel
```

```
F = [5e3:1e3:1e5]';
```

```
Ztemp = 10000*ones(96,1)+1./((1./(39000*ones(96,1)))+(1i*2*pi*1e-9.*F));
```

```
ResT = real(Ztemp);
```

```
ReacT = -imag(Ztemp);
```

```
%% 50K parallel 10k 1nF
```

```
F = [5e3:1e3:1e5]';
```

```

Ztemp = 1./ ( (1./(50000*ones(96,1))) + 1./(10000 + 1./(1i*2*pi*1e-9*F)));
ResT = real(Ztemp);
ReacT = -imag(Ztemp);
%% 20K parallel 20k 5pF
F = [5e3:1e3:1e5]';
Ztemp = 1./ ( (1./(20000*ones(96,1))) + 1./(20000 + 1./(1i*2*pi*100e-12*F)));
ResT = real(Ztemp);
ReacT = -imag(Ztemp);
%% 50K parallel 39k 1nF
F = [5e3:1e3:1e5]';
Ztemp = 1./ ( (1./(50000*ones(96,1))) + 1./(39000 + 1./(1i*2*pi*1e-9*F)));
ResT = real(Ztemp);
ReacT = -imag(Ztemp);
%% Calc and plot theoretical
ZT = sqrt(ResT.^2+ReacT.^2);
PT = -atan(ReacT./ResT)*180/pi;
figure(1)
subplot(2,1,1)
plot(F,ZT,'k','DisplayName','Z theo');hold on
figure(1)
subplot(2,1,2)
plot(F,PT,'k','DisplayName','Phase theo');hold on
figure(2)
plot(ResT,ReacT,'k*','DisplayName','Theo');hold on

```



*MATLAB code to plot Keysight Impedance Analyzer data*

```
%[data,PathName,FileName] = loadDepthdata(); %load data, from one or  
more files
```

```
LS = ':' ; % LineStyle
```

```
if iscell(data)==0 % if single data loaded then plot it
```

```
F = data(:,1); % Frequency Vector
```

```
Z = data(:,2); % Impedance Vector
```

```
Phase = data(:,3); % Phase Angle Vector
```

```
figure(1)
```

```
loglog(F,Z,LS,'DisplayName',[FileName{1,i}(1:end-4)])
```

```
xlabel('Frequency (Hz)')
```

```
ylabel('Impedance (\Omega)')
```

```
legend(gca,'show');axis('tight')
```

```
hold all
```

```
figure(2)
```

```
semilogx(F,Phase,LS,'DisplayName',[FileName{1,i}(1:end-4)])
```

```
xlabel('Frequency (Hz)')
```

```
ylabel('Phase (\Theta)')
```

```
legend(gca,'show');axis('tight')
```

```
hold all
```

```
else % if more than one data loaded
```

```
[~,c] = size(data);
```

```

for i=1:c
F = data{1,i}(:,1); % Frequency Vector
Z = data{1,i}(:,2); % Impedance Vector
Phase = data{1,i}(:,3); % Phase Angle Vector
figure(1)
loglog(F,Z,LS,'DisplayName',[FileName{1,i}(1:end-4)])
xlabel('Frequency (Hz)')
ylabel('Impedance (\Omega)')
hold all
figure(2)
semilogx(F,Phase,LS,'DisplayName',[FileName{1,i}(1:end-4)])
xlabel('Frequency (Hz)')
ylabel('Phase (\Theta)')
hold all
end
figure(1);legend(gca,'show');axis('tight')
figure(2);legend(gca,'show');axis('tight')
end
%legend('Copper Short','1 Layer','2 Layers','3 Layers'); title('1.5 CM
Separation on Copper at 200uA')
%legend('Table Short','1 Layer','2 Layers','3 Layers'); title('1.5 CM
Separation on Table at 200uA')
legend('1 Layer','2 Layers','3 Layers','4 Layers','5 Layers','6

```

```
Layers' );title('3CM Spacing at 500uA and 200uA,No Pressure' )
```

```
1
```

```
%legend('1 Layer','2 Layers','3 Layers','4 Layers','5 Layers','6
```

```
Layers');title('8 CM Separation on Table at 200uA')
```

```
%clear;clc;close all
```

## *Appendix E: Arduino Code*

### *Arduino Code for one mode programming*

```
// Remember to Set the Proper compiler and COM Port as:  
  
// Tools -> Board: 2560 Mega -> COM Port  
  
////////////////////////////////////  
  
#include <Wire.h>  
  
//Register locations of AD5933  
  
#define SLAVEADDR 0x0D // default serial bus address, 0001101 (0x0D).  
  
#define ADDRPTR 0xB0 // address pointer, 1011 0000.  
  
#define CTRLREG 0x80  
  
#define CTRLREG2 0x81  
  
#define STARTFREQ_R1 0x82  
  
#define STARTFREQ_R2 0x83  
  
#define STARTFREQ_R3 0x84  
  
#define FREQINCRE_R1 0x85  
  
#define FREQINCRE_R2 0x86  
  
#define FREQINCRE_R3 0x87  
  
#define NUMINCRE_R1 0x88  
  
#define NUMINCRE_R2 0x89  
  
#define NUMSCYCLES_R1 0x8A  
  
#define NUMSCYCLES_R2 0x8B
```

```

#define REDATA_R1 0x94

#define REDATA_R2 0x95

#define IMGDATA_R1 0x96

#define IMGDATA_R2 0x97

#define TEMPR1 0x92

#define TEMPR2 0x93

#define STATUSREG 0x8F

const float MCLK = 16.776*pow(10,6); // AD5933 Internal Clock Speed 16.776 MHz

const float startfreq = 5*pow(10,3); // Set start freq;      < 100Khz

const float increfreq = 1*pow(10,3); // Set freq increment;  > 0.1 Hz

const int increnum = 95;      // Set number of increments; < 511

void setup() {

    Wire.begin();      // Start I2C to 5933

    Serial.begin(9600); // Start Serial to COM port to PC via USB

    while (!Serial) {} // Wait for serial port to connect. Needed for native USB

    Serial.println(); // Sets last data in buffer to "newline"

    Serial.flush();   // Waits for the transmission of outgoing serial data to complete

}

void loop() {

    delay(1000); // Wait before next loop.

    programReg(); // Program Device Registers

```

```

runSweep(); // Run Sweep
}

void programReg(){
    //Set Range, PGA gain 1 (0x00 = x5, 0x01 = x1)
    writeData(CTRLREG,0x01); // 2 V pk-pk and x1 gain
    //writeData(CTRLREG,0x07); // 1 V pk-pk and x1 gain
    //writeData(CTRLREG,0x05); // 400 mV pk-pk and x1 gain
    //writeData(CTRLREG,0x03); // 200 mV pk-pk and x1 gain

    // Set Start frequency
    writeData(STARTFREQ_R1, getFrequency(startfreq,1));
    writeData(STARTFREQ_R2, getFrequency(startfreq,2));
    writeData(STARTFREQ_R3, getFrequency(startfreq,3));

    // Set Increment frequency
    writeData(FREQINCRE_R1, getFrequency(incfreq,1));
    writeData(FREQINCRE_R2, getFrequency(incfreq,2));
    writeData(FREQINCRE_R3, getFrequency(incfreq,3));

    // Set Number of Points in frequency sweep, max 511
    writeData(NUMINCRE_R1, (incenum & 0x001F00)>>0x08 );
    writeData(NUMINCRE_R2, (incenum & 0x0000FF));

    // Set settling time cycle count
    writeData(NUMSCYCLES_R1, 0x07); // Max cycles x4
    writeData(NUMSCYCLES_R2, 0xFF); // Max lower register for number of settling time cycles (255)
}

```

```

}

void runSweep() {
    short re;
    short img;
    double freq;
    int i=0;
    float Vpk;
    byte R1,R2;

    // 1. Standby '10110000' Mask D8-10 to avoid tampering with gains and pk-pk voltage. Required for
    sweeps.

    writeData(CTRLREG,(readData(CTRLREG) & 0x07) | 0xB0);

    // 2. Initialize sweep

    writeData(CTRLREG,(readData(CTRLREG) & 0x07) | 0x10);

    // 3. Start sweep

    writeData(CTRLREG,(readData(CTRLREG) & 0x07) | 0x20);

    while((readData(STATUSREG) & 0x07) < 4 ) { // Check that status reg != 4, sweep not complete

        delay(100); // delay between measurements

        //reads imaginary and real data

        int flag = readData(STATUSREG)& 2; // Check for valid real/imaginary data from status register

        if (flag==2) {

            R1 = readData(REDATA_R1);

            R2 = readData(REDATA_R2);

            re = (R1 << 8) | R2;

```

```

R1 = readData(IMGDATA_R1);
R2 = readData(IMGDATA_R2);
img = (R1 << 8) | R2;
freq = startfreq + i*incrfreq;
Vpk = sqrt(pow(re,2)+pow(img,2))/4833; // voltage pk-pk at ADC
Serial.print(byte(freq/1000));
Serial.print(" ");
Serial.print(re);
Serial.print(" ");
Serial.print(img);
Serial.print(" ");
Serial.println(Vpk);

//Increment frequency, do not increment if beyond sweep
if((readData(STATUSREG) & 0x07) < 4 ){
    writeData(CTRLREG,(readData(CTRLREG) & 0x07) | 0x30);
    i++;
}
}
}

writeData(CTRLREG,(readData(CTRLREG) & 0x07) | 0xA0);
}

void writeData(int addr, int data) {

```

```
Wire.beginTransmission(SLAVEADDR);  
Wire.write(addr);  
Wire.write(data);  
Wire.endTransmission();  
delay(1);  
}
```

```
int readData(int addr){  
    int data;  
    Wire.beginTransmission(SLAVEADDR);  
    Wire.write(ADDRPTR);  
    Wire.write(addr);  
    Wire.endTransmission();  
    delay(1);  
    Wire.requestFrom(SLAVEADDR,1);  
    if (Wire.available() >= 1){  
        data = Wire.read();  
    }  
    else {  
        data = -1;  
    }  
    delay(1);  
    return data;  
}
```

```

}

byte getFrequency(float freq, int n){
    long val = long((freq/(MCLK/4)) * pow(2,27)); // AD5933 Start frequency code.
    byte code;          // Frequency code for each register.
    switch (n) {
        case 1:
            code = (val & 0xFF0000) >> 0x10;
            break;
        case 2:
            code = (val & 0x00FF00) >> 0x08;
            break;
        case 3:
            code = (val & 0x0000FF);
            break;
        default:
            code = 0;
    }
    return code;
}

```

## *Arduino Code for Automatic Switching of Modes*

```
// Remember to Set the Proper compiler and COM Port as:  
  
// Tools -> Board: 2560 Mega -> COM Port  
  
////////////////////////////////////  
  
#include <Wire.h>  
  
//Register locations of AD5933  
  
#define SLAVEADDR 0x0D // default serial bus address, 0001101 (0x0D).  
  
#define ADDRPTR 0xB0 // address pointer, 1011 0000.  
  
#define CTRLREG 0x80  
  
#define CTRLREG2 0x81  
  
#define STARTFREQ_R1 0x82  
  
#define STARTFREQ_R2 0x83  
  
#define STARTFREQ_R3 0x84  
  
#define FREQINCRE_R1 0x85  
  
#define FREQINCRE_R2 0x86  
  
#define FREQINCRE_R3 0x87  
  
#define NUMINCRE_R1 0x88  
  
#define NUMINCRE_R2 0x89  
  
#define NUMSCYCLES_R1 0x8A  
  
#define NUMSCYCLES_R2 0x8B  
  
#define REDATA_R1 0x94  
  
#define REDATA_R2 0x95
```

```

#define IMGDATA_R1 0x96

#define IMGDATA_R2 0x97

#define TEMPR1 0x92

#define TEMPR2 0x93

#define STATUSREG 0x8F

#define MX 52

const float MCLK = 16.776*pow(10,6); // AD5933 Internal Clock Speed 16.776 MHz

const float startfreq = 5*pow(10,3); // Set start freq; < 100Khz

const float increfreq = 1*pow(10,3); // Set freq increment; > 0.1 Hz

const int increnum = 95; // Set number of increments; < 511

const float LL = 0.05; // Lower limit of adc

const float UL = 2.95; // Upper limit of adc

void setup() {

  Wire.begin(); // Start I2C to 5933

  Serial.begin(9600); // Start Serial to COM port to PC via USB

  while (!Serial) {} // Wait for serial port to connect. Needed for native USB

  Serial.println(); // Sets last data in buffer to "newline"

  Serial.flush(); // Waits for the transmission of outgoing serial data to complete

  // Write Initial Parameters to 5933

  writeData(CTRLREG,0x03); // 200 mVpp and x1 gain, Set Vpp Range, PGA gain 1 (0x00 = x5, 0x01
= x1)

  writeData(FREQINCRE_R1, getFrequency(increfreq,1)); // Set Increment frequency

```

```

writeData(FREQINCRE_R2, getFrequency(incrfreq,2));
writeData(FREQINCRE_R3, getFrequency(incrfreq,3));
writeData(NUMSCYCLES_R1, 0x07); // Max cycles x4, Set settling time cycle count
writeData(NUMSCYCLES_R2, 0xFF); // Max lower register for number of settling time cycles (255).

//Multiplexer Pin From Arduino

pinMode(MX, OUTPUT);
}

void loop() {
  programReg(); // Program Device Registers
  runSweep(); // Run Sweep
  delay(100); // Wait before next loop.
}

void programReg(){
  writeData(STARTFREQ_R1, getFrequency(startfreq,1)); // Set Start frequency
  writeData(STARTFREQ_R2, getFrequency(startfreq,2));
  writeData(STARTFREQ_R3, getFrequency(startfreq,3));

  writeData(NUMINCRE_R1, (increnum & 0x001F00)>>0x08 ); // Set Number of Points in frequency
sweep, max 511

  writeData(NUMINCRE_R2, (increnum & 0x0000FF));
}

```

```

void runSweep() {
    short re;
    short img;
    double freq;
    int i=0;
    float Vpk;

    writeData(CTRLREG,(readData(CTRLREG) & 0x07) | 0xB0); // 1. Standby '10110000'. Required for
sweeps.

    writeData(CTRLREG,(readData(CTRLREG) & 0x07) | 0x10); // 2. Initialize sweep
    writeData(CTRLREG,(readData(CTRLREG) & 0x07) | 0x20); // 3. Start sweep

    while((readData(STATUSREG) & 0x07) < 4 ) { // Check that status reg != 4, sweep not complete

        delay(100); // delay between checks

        int flag = readData(STATUSREG)& 2; // Check for valid real/imaginary data
from status register

        if (flag==2) {

            byte R1 = readData(REDATA_R1);

            byte R2 = readData(REDATA_R2);

            re = (R1 << 8) | R2;

            R1 = readData(IMGDATA_R1);

            R2 = readData(IMGDATA_R2);

            img = (R1 << 8) | R2;

            freq = startfreq + i*incrfreq;

            Vpk = sqrt(pow(re,2)+pow(img,2))/4833; // Approximate voltage pk-pk
at ADC

```

```

        if (LL < Vpk < UL) {
            printData(freq, re, im, Vpk); //print Freq,Real and
Imaginary

            //Increment frequency

            if((readData(STATUSREG) & 0x07) < 4 ){

                writeData(CTRLREG,(readData(CTRLREG) &
0x07) | 0x30);

                i++;

            }

        }

    else {

        switch (readData(CTRLREG) & 0x07){

            case 0x01: // 2V out -----

                if (Vpk > UL) {

                    changeMode(0x07, freq, i);

                }

                else {

                    //Need to have MUX Switch Logic Here

                    printData(freq, re, im, Vpk); //print Freq,Real and Imaginary

                    //Increment frequency

                    if((readData(STATUSREG) & 0x07) < 4 ){

                        writeData(CTRLREG,(readData(CTRLREG) & 0x07) | 0x30);

                        i++;

```

```
}
```

```
}
```

```
break;
```

```
case 0x07: // 1V out -----
```

```
if (Vpk > 2.9){
```

```
    changeMode(0x05, freq, i);
```

```
}
```

```
else {
```

```
    changeMode(0x01, freq, i);
```

```
}
```

```
break;
```

```
case 0x05: // 400mV out -----
```

```
if (Vpk > 2.9){
```

```
    changeMode(0x03, freq, i);
```

```
}
```

```
else {
```

```
    changeMode(0x07, freq, i);
```

```
}
```

```
break;
```

```
case 0x03: // 200mV out -----
```

```
if (Vpk > 2.9){
```

```
    //Need to have MUX Switch Logic Here
```

```
printData(freq, re, im, Vpk); //print Freq, Real and Imaginary
```

```

//Increment frequency
if((readData(STATUSREG) & 0x07) < 4 ){
    writeData(CTRLREG,(readData(CTRLREG) & 0x07) | 0x30);
    i++;
}

    }

    else {
        changeMode(0x05, freq, i);
    }

    break;
}

}

}

}

    writeData(CTRLREG,(readData(CTRLREG) & 0x07) | 0xA0); // Power Down mode, retain
parameters
}

```

```

void printData(double freq, short re, short im, float Vpk){
    Serial.print(freq/1000);
    Serial.print(" ");
    Serial.print(re);
    Serial.print(" ");
    Serial.print(img);
}

```

```

Serial.print(" ");

Serial.println(Vpk);

}

void changeMode(int a, double freq, int i){

    writeData(CTRLREG2,0x10);        //Reset Sweep Command on Reg 0x81 D4

    writeData(CTRLREG,a);           //Change Vpk mode on Reg 0x80

    writeData(STARTFREQ_R1, getFrequency(freq,1)); //Update with the current frequency
    writeData(STARTFREQ_R2, getFrequency(freq,2));
    writeData(STARTFREQ_R3, getFrequency(freq,3));

    writeData(NUMINCRE_R1, ((incenum-i) & 0x001F00)>>0x08 ); //Set updated number of
increments

    writeData(NUMINCRE_R2, ((incenum-i) & 0x0000FF));

    writeData(CTRLREG,(readData(CTRLREG) & 0x07) | 0x10);// Initialize sweep
    writeData(CTRLREG,(readData(CTRLREG) & 0x07) | 0x20);// Start sweep

}

void writeData(int addr, int data) {

    Wire.beginTransmission(SLAVEADDR);

    Wire.write(addr);

    Wire.write(data);
}

```

```

Wire.endTransmission();

delay(1);
}

int readData(int addr){

int data;

Wire.beginTransmission(SLAVEADDR);

Wire.write(ADDRPTR);

Wire.write(addr);

Wire.endTransmission();

delay(1);

Wire.requestFrom(SLAVEADDR,1);

if (Wire.available() >= 1){

data = Wire.read();

}

else {

data = -1;

}

delay(1);

return data;

}

byte getFrequency(float freq, int n){

```

```

long val = long((freq/(MCLK/4)) * pow(2,27)); // AD5933 Start frequency code.
byte code;          // Frequency code for each register.
switch (n) {
    case 1:
        code = (val & 0xFF0000) >> 0x10;
        break;
    case 2:
        code = (val & 0x00FF00) >> 0x08;
        break;
    case 3:
        code = (val & 0x0000FF);
        break;
    default:
        code = 0;
}
return code;
}

// -----
// Extra Code, For Quick Reference
// -----

//writeData(CTRLREG,0x01); // 2 V pk-pk and x1 gain
//writeData(CTRLREG,0x07); // 1 V pk-pk and x1 gain

```

```
//writeData(CTRLREG,0x05); // 400 mV pk-pk and x1 gain
```

```
//writeData(CTRLREG,0x01); // Set Range 1, Programmable Gain Amplifier (PGA) gain 1.
```

```
//writeData(CTRLREG2,0x10);// Reset ctrl register, interrupts sweep.
```

```
//writeData(CTRLREG,(readData(CTRLREG) & 0x07) | 0xA0); // Power Down mode, retain parameters
```